THE UNIVERSITY OF QUEENSLAND

AUSTRALIA

Nonlinear vibro-ultrasonics for detection of damage and weak bonds in composites

Mitchell Dunn

B Engineering (Mechanical) (Hons)

A thesis submitted for the degree of Doctor of Philosophy at The University of Queensland in 2018

School of Mechanical and Mining Engineering

Abstract

Using composite materials in primary structures requires careful consideration of the ability of the material to withstand service loads, particularly the resistance to impact loads generated through contact with objects during flight or routine maintenance. While perhaps not causing immediate failure of the structure, even small, barely visible levels of damage can cause a decrease in stiffness or strength. It is important to detect this damage at an early stage, lest the damage grow and the strength of the structure be reduced to the level of service loading.

This thesis contributes to the use of nonlinear vibro-ultrasonic techniques for detection of damage in composite laminates. These techniques utilise measurements of frequency components of the received ultrasonic signal to identify defects; additional frequency components not present in the excitation signals are created when propagating waves interact nonlinearly due to damage or inherent material nonlinearity. This thesis aims to improve understanding of the influence of system parameters on the generation and detection of sideband frequency components in nonlinear vibro-ultrasonic testing of fibre-reinforced composite structures.

In order for nonlinear vibro-ultrasonics to be used reliably for the detection of damage in composite laminates, particularly the initial onset of damage, the measurement of sideband frequency components is of utmost importance. It is also essential that the experimental system does not introduce additional nonlinearity to the point of obscuring that which is present due to damage. It is therefore a focus of this thesis to analyse how various instrumentation components, as well as experimental procedures and analyses, affect the ability of the experimental system to detect sidebands. A comprehensive analysis of the excitation, acquisition and post-processing system used to collect data is presented and leads to an optimised set of parameters for discernment of sidebands. It is demonstrated that careful selection of experimental instrumentation and signal processing techniques leads to a lower noise floor and clearly defined sideband peaks.

Nonlinear vibro-ultrasonic testing is performed on composite laminate samples with artificial delamination damage, with results indicating a higher level of nonlinear response than beams without delamination. These results demonstrate that gross laminar defects cause an increase in nonlinearity as to be confidently differentiated from intact specimens. The work in this thesis extends on work from literature by analysing the relationship between excitation voltage and vibration amplitude and demonstrating a strong dependence of nonlinear wave interaction on the amplitude of the pumping wave in the presence of nonlinearity. Analysis of the vibration response of the composite laminate samples highlights that the dynamic nonlinearity of the system is likely to be maximal at resonance, leading to a recommendation that the pumping

frequency should be selected away from resonance for maximised sensitivity and robustness of nonlinear vibro-ultrasonic experiments.

Samples with laminar damage created from low-velocity impact tests are also studied. Similar to the artificial delamination damage, an increase in nonlinear response is observed for specimens with damage compared to pristine specimens. It is also confirmed that there is a strong dependence of nonlinear wave interaction on the amplitude of the pumping wave in the presence of the damage. It is also shown that for impact-induced damage, samples with a larger damage area (as measured by ultrasonic C-scan) exhibit greater nonlinearity.

This thesis also investigates the application of nonlinear vibro-ultrasonics to detecting interface damage in bonded composite and aluminium beams. Is it demonstrated that the typical methodology used for nonlinear vibro-ultrasonics, which is to select a single ultrasonic probing frequency and a single vibration excitation frequency for testing, is unable to confidently differentiate intact interfaces in the bonded composite beams from those with gross bondline defects. The findings of this analysis show instead that the relative nonlinearity measured between specimens depends on the ultrasonic probing frequency used; selection of a different frequency can change which specimen appears more nonlinear. The trial of a range of probing frequencies provides no clear evidence that nonlinear vibro-ultrasonic testing conducted in this manner is sensitive to gross bondline defects, in contrast to artificial delamination damage in composite laminates where a measured increase in nonlinearity (compared to pristine samples) was present for all tested probing frequencies.

Nonlinear vibro-ultrasonic testing of bonded aluminium beams was conducted with a single probing frequency per beam but over a wide range of vibration excitation frequencies. Measurements are made of the amplitude of the first five closest pairs of generated sideband frequency components and used for further analysis. The results of these analyses reveal that there is significant variation in the amplitude of the first pair of sidebands across excitation frequencies as well as between undamaged and damaged beams. When the amplitude of the first pair of sidebands is normalised by the sum of the remaining sideband amplitudes, however, the damaged specimens exhibit a large increase in nonlinearity within narrow frequency bands, an effect not seen in the undamaged specimens. This result highlights that specific combination of system parameters may lead to differentiation of bondline damage in bonded structures.

To summarise, this thesis makes the following important contributions to the use of nonlinear vibro-ultrasonics for detection of damage and weak bonds in composites:

1. Highlighting that deliberate selection of experimental instrumentation and signal processing parameters can increase discernibility of sideband frequency components.

2. Demonstration of the strong dependence of nonlinear wave interaction on the amplitude

of the pumping wave in the presence of nonlinearity.

3. Providing evidence that typical nonlinear vibro-ultrasonic methodology using a single probing frequency and single vibration excitation frequency is insufficient to characterise one specimen as more nonlinear than another; selection of different system parameters can change the relation.

4. Showing that advanced data analysis techniques are able to highlight specific combinations of system parameters which lead to a difference in measurement between undamaged and damaged bondlines in bonded aluminium specimens. This informs future work by demonstrating the requirement that a range of parameters must be explored in order to confidently assess damage in structures using nonlinear vibro-ultrasonics.

Declaration by author

This thesis is composed of my original work, and contains no material previously published or written by another person except where due reference has been made in the text. I have clearly stated the contribution by others to jointly-authored works that I have included in my thesis.

I have clearly stated the contribution of others to my thesis as a whole, including statistical assistance, survey design, data analysis, significant technical procedures, professional editorial advice, and any other original research work used or reported in my thesis. The content of my thesis is the result of work I have carried out since the commencement of my research higher degree candidature and does not include a substantial part of work that has been submitted to qualify for the award of any other degree or diploma in any university or other tertiary institution. I have clearly stated which parts of my thesis, if any, have been submitted to qualify for another award.

I acknowledge that an electronic copy of my thesis must be lodged with the University Library and, subject to the policy and procedures of The University of Queensland, the thesis be made available for research and study in accordance with the Copyright Act 1968 unless a period of embargo has been approved by the Dean of the Graduate School.

I acknowledge that copyright of all material contained in my thesis resides with the copyright holder(s) of that material. Where appropriate I have obtained copyright permission from the copyright holder to reproduce material in this thesis.

Publications during candidature

Peer-reviewed conference papers

1. **M. Dunn**, M. Veidt, P. Blanloeuil, A. Gunnion, C. H. Wang. Detection of laminar damage in composite beams using nonlinear ultrasonic modulation techniques. *Proceedings of the 8th Australasian Congress on Applied Mechanics 2014 (ACAM 8)*, pages 640-648, 2014.

2. **M. Dunn**, A. Carcione, P. Blanloeuil, M. Veidt. Critical Aspects of Experimental Damage Detection Methodologies Using Nonlinear Vibro-ultrasonics. *Procedia Engineering*, Volume 188, pages 133-140, 2017.

Conference abstracts

1. EAIT Postgraduate Conference. *Nonlinear Ultrasonic Modulation Technique for Damage Detection in Composite Laminates* . Brisbane, Australia, June 2013.

2. EAIT Postgraduate Conference. *Detection of laminar damage in composite beams using nonlinear ultrasonic modulation techniques*. Brisbane, Australia, June 2014.

Publications included in this thesis

- **M. Dunn**, A. Carcione, P. Blanloeuil, M. Veidt. Critical Aspects of Experimental Damage Detection Methodologies Using Nonlinear Vibro-ultrasonics. *Procedia Engineering*, Volume 188, pages 133-140, 2017.
  incorporated in parts of Chapters 3 and 4

Contributor	Statement of contribution
M. Dunn (Candidate)	Experiments (70%) Wrote and edited paper (50%)
A. Carcione	Experiments (30%)
P. Blanloeuil	Wrote and edited paper (20%)
M. Veidt	Wrote and edited paper (30%)

Contributions by others to the thesis

Chapter 3

Alessandro Carcione (undergraduate student, The University of Queensland) assisted with setup of the experimental system including developing LabVIEW software to automate data collection and design and construction of a custom differential amplifier. Parts of this chapter are related to Alessandro's Bachelor of Engineering thesis titled 'An Investigation into the Nonlinear Propagation of Acoustic Waves in Composite Beams' (2014), which he produced under my supervision.

Chapter 4

Alessandro Carcione (undergraduate student, The University of Queensland) assisted with instrumentation and preliminary data collection for the composite laminate beam specimens with artificial delamination damage. This data was collected under my supervision and using methodology which I developed; this data is not used in the main body of the thesis. It is used in Appendix A of this thesis as a comparison set of data labelled "repeat data". Parts of this chapter are related to Alessandro's Bachelor of Engineering thesis titled 'An Investigation into the Nonlinear Propagation of Acoustic Waves in Composite Beams' (2014).

Jesse Jackson (undergraduate student, The University of Queensland) assisted with data collection for the composite laminate beam specimens with impact damage. This data was collected under my supervision and using methodology which I developed; this data is presented in Section 4.5. Parts of this chapter are related to Jesse's Bachelor of Engineering thesis titled 'Impact Damage Detection in Composite Laminate Beams and Plates using Nonlinear Vibration Techniques' (2015).

Statement of parts of the thesis submitted to qualify for the award of another degree

None.

Acknowledgements

Firstly I would like to express my deep and sincere gratitude to my principal advisor A/Prof. Martin Veidt for his guidance and support throughout my MPhil and PhD candidature. His invaluable experience, knowledge and mentorship have been a great source of motivation. This thesis would not have been completed if not for his encouragment, endless patience and understanding.

My thanks also extends to Dr Edmund Liew, Dr Andrew Gunnion and Dr Philippe Blanloeuil who provided important input during discussions around the direction of the research, as well as contributing to and reviewing papers and thesis chapters.

I would like to thank the University of Queensland for funding my research in the form of a UQ Research Scholarship. I would also like to acknowledge financial support from the Cooperative Research Centre for Advanced Composite Structures.

To my many friends and colleagues at UQ and in the Composites group past and present: thank you all for your unwavering support, interesting and sometimes heated lunchtime discussions, and for making my time as a research student an experience never to be forgotten. Thanks to Hannes, Wouter, Simon, Alessandro and Jarrad for bringing these experiences well beyond research and for showing me the value of a healthy work-life balance, and thanks to Katrina for your unending encouragement, kindness and late night conversations.

To Mum, Dad, my brothers Jase and Adam, and aunty Mere: thank you for always supporting and encouraging my pursuits and teaching me to think carefully, critically and empathetically.

Above all, I thank my wonderful partner Charli who is an endless source of encouragement and motivation – thank you for supporting me every step of the way in the most caring way possible.

Keywords

Nondestructive testing, Nonlinear vibro-ultrasonics, Structural health monitoring, Delamination, Weak bonds

Australian and New Zealand Standard Research Classifications (ANZSRC)

ANZSRC code: 091304 Dynamics, Vibration and Vibration Control 60%
ANZSRC code: 091202 Composite and Hybrid Materials 30%
ANZSRC code: 091308 Solid Mechanics 10%

Fields of Research (FoR) Classification

FoR code: 0913, Mechanical Engineering 70%
FoR code: 0912, Materials Engineering 30%

Contents

List of Figures

List of Tables

Abbreviations and Nomenclature

Abbreviations

ADC	Analog-to-digital converter
AM	Amplitude modulation
CFRP	Carbon fibre-reinforced plastic
DANL	Displayed average noise level
DC	Direct current
DI	Damage index
FFT	Fast Fourier transform
FPGA	Field-programmable gate array
GFRP	Glass fibre-reinforced plastic
GFRPP	Glass fibre-reinforced polypropelene
HF	High frequency
IM	Impact modulation
LF	Low frequency
MDT	Modified diffraction tomography
NDT	Non-destructive testing
NRS	Nonlinear reverberation spectroscopy

NRUS	Nonlinear resonance ultrasound spectroscopy
PA	Phased array
PP	Polypropelene
PTFE	Polytetrafluoroethylene
PVC	Poly(vinyl chloride)
PZT	Lead zirconate titanate
RMS	Root mean square
SNR	Signal-to-noise ratio
THD	Total harmonic distortion
UNF	Unified fine thread
VM	Vibration modulation

Greek symbols

α	material hysteresis parameter
β	first-order nonlinearity parameter
β_m	mixed nonlinearity parameter
δ	second-order nonlinearity parameter
κ	curvature
λ	wavelength
ω	frequency
ρ	density
σ	stress
ε	strain

Roman symbols

$\bar{R}$	modulation index, ratio of sidebands
$\hat{R}$	modulation index, normalised
A_0	probing frequency amplitude
A_1	second harmonic amplitude
A_n^+	n^{th} sideband amplitude, upper side
A_n^-	n^{th} sideband amplitude, lower side
a_{base}	acceleration measured at the vibration shaker
c_0	acoustic wave velocity
E	Young's modulus
f_s	sampling rate
k	wave number
R	modulation index
r^2	regression fit coefficient
u	displacement
w	deflection
$Y(x)$	beam deflection curve

Chapter 1

Introduction

1.1 Background and motivation

Composite materials continue to see increasing use in the manufacture of high-performance structures such as aircraft, where they are valued for their high stiffness and strength-to-weight ratio. While traditionally limited to secondary and tertiary structures such as rudders and wing edge panels, fibre-reinforced plastics have recently seen deployment in primary load-carrying structures.

With use in primary structures comes careful consideration of the ability of the material to withstand service loads, particularly the resistance to impact loads generated through contact with objects during flight or routine maintenance. These low-velocity impact events are often caused by strikes from birds, hailstones, dropped tools or debris kicked up from runways. While perhaps not causing immediate failure of the structure, even small, barely visible levels of damage can cause a decrease in stiffness or strength. It is important to detect this damage at an early stage, lest the damage grow and the strength of the structure be reduced to the level of service loading.

Composite aircraft components can be difficult to inspect for damage, owing to their anisotropic and heterogenous properties. Complicating this further is the addition of sub-structural components such as stiffeners, doublers and other joints. Conventional non-destructive testing (NDT) techniques based on linear interaction of ultrasonic waves with damage rely on measurements of transmission, reflection or absorption of acoustic energy to identify defects. The presence of a defect changes the way that propagating ultrasonic waves are reflected back to a receiver. Greater complexity in these signals in composite materials due to their laminar or multi-material anisotropy and fibre reinforcement may mean that low levels of damage are difficult to detect, as they cause an indiscernible change to the received signal.

One approach to overcoming the NDT challenges of composite materials is to use nonlinear

ultrasonic techniques, which rely on nonlinear interaction of ultrasonic waves in the presence of defects. These methods utilise measurements of frequency components of the received ultrasonic signal to identify defects. Additional frequency components not present in the input ultrasonic excitations are created when propagating waves interact with damage. Depending on the excitations used, extra frequency components are created at the harmonics of a single input ultrasonic excitation, and at the sum and difference frequencies of multiple input excitations.

Figure 1.1 demonstrates this principle, comparing the response of a linear and nonlinear system to two excitations at dissimilar frequencies. The sideband frequency components, centred on the higher frequency at multiples of the lower frequency, are only present where nonlinear frequency mixing occurs.

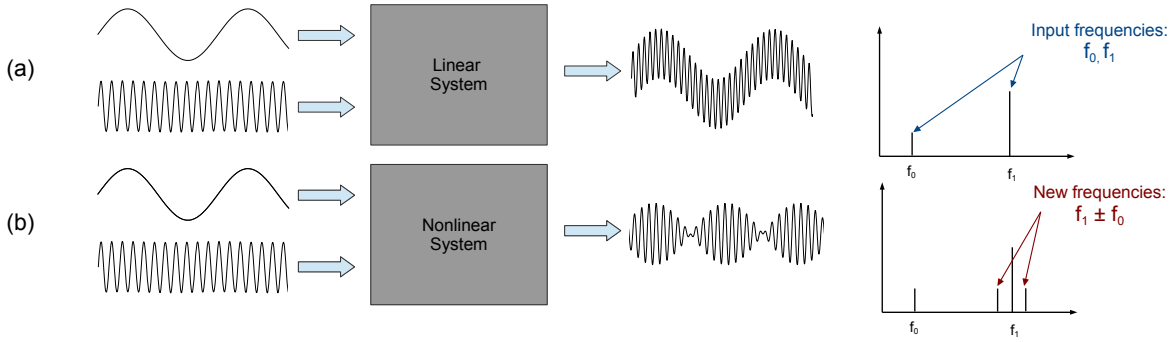

Figure 1.1: The response of (a) linear and (b) nonlinear systems to two excitations

Nonlinear ultrasonic techniques have seen use in a variety of applications, particularly for the detection of low levels of damage which could lead to catastrophic failure, and for which early detection is critical, such as fatigue crack growth in metals (e.g. Zaitsev and Sas, 2000) and laminar damage in composite laminates (e.g. Meo et al., 2008).

Compared to conventional ultrasonics which are sensitive to gross defects with a size on the order of excitation wavelength or larger, nonlinear techniques are often cited to be sensitive even to damage on a scale smaller than this wavelength (e.g. Kulkarni and Achenbach, 2008). The improvement in sensitivity over linear NDT is because the nonlinear distortion of the elastic wave which generates extra frequency components is sensitive to microstructural changes which cause anharmonicity in the volume of material through which the wave passes. Therefore nonlinear ultrasonic techniques provide an avenue for finding defects which do not cause changes necessary for detection by conventional ultrasonic techniques but which do introduce nonlinearity into the material's microstructure (Lissenden et al., 2015).

The use of a high-frequency, low-amplitude ultrasonic wave (a so-called *probing* wave) and a lower-frequency, high-amplitude wave (or *pumping* wave) forms the basis of a promising nonlinear NDT technique. Depending on the nature of pumping excitation, the technique has

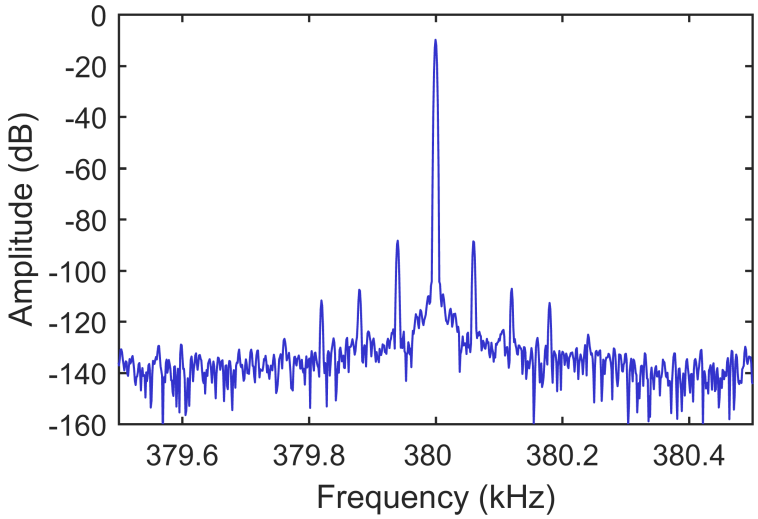

Figure 1.2: Typical spectrum of an ultrasonic probing wave modulated by vibration in the presence of nonlinearity.

been referred to by authors as vibro-acoustic modulation (e.g. Donskoy et al., 2001), nonlinear ultrasonic modulation (e.g. Sohn et al., 2013), and nonlinear wave modulation spectroscopy (e.g. Van Den Abeele et al., 2000). Throughout this thesis, this technique is referred to as *nonlinear vibro-ultrasonics*, in order to emphasize that it is a nonlinear ultrasonic technique which utilizes vibration excitation as the pumping wave.

The nonlinear distortion introduced to the ultrasonic carrier is quite small, and only detectable by observing the frequency spectrum carefully as the generated sideband frequencies are generally at amplitudes several orders of magnitude lower than the carrier wave. An example response spectrum from nonlinear vibro-ultrasonic experiments is shown in Figure 1.2. This data was collected using the experimental apparatus described later in this thesis, from a composite laminate beam excited by a probing frequency of 380 kHz and a vibration pumping frequency of 60 Hz. In the response six pairs of sidebands are visible at multiples of 60 Hz either side of the 380 kHz carrier. Subsequent pairs are not visible because their spectral amplitude is below that of the noise floor which is approximately between -135 dB and -125 dB.

Circumstances leading to lower spectral amplitude (e.g. lower amplitude or higher attenuation of excitations, less interaction of wave with nonlinear features) or a higher noise floor (e.g. electrical interference, influence of measurement components & signal processing) would lead to less visible sidebands. This means that the sensitivity of nonlinear ultrasonic methods is tied to the ability of the measurement system to resolve individual sidebands. Therefore, experimental methods which rely on the measurement of these spectral amplitudes should be carefully designed to maximise the amplitude of these sidebands relative to the noise floor.

In order for nonlinear vibro-ultrasonics to be used reliably for the detection of of damage in composite laminates, particularly the initial onset of damage, the measurement of sideband frequency components is of utmost importance. The focus of this thesis is thus the various aspects of nonlinear vibro-ultrasonics that influence the discernibility of these sidebands for damage in composite laminates. This includes a focus on the influence of system parameters and signal processing procedures on the capability of the excitation and measurement system to analyse signals generated through nonlinear system behaviour.

1.2 Thesis objectives

The aim of this thesis is to determine the influence of system parameters on the generation and detection of sideband frequency components in nonlinear vibro-ultrasonic testing of fibre-reinforced composite structures. The important parameters of most interest are the interaction of waves with the structure including any damage, selection of excitation frequencies, and the components of the instrumentation chain used for excitation and measurement. Hence, the key objectives of the thesis are to:

1. Investigate the influence of excitation, acquisition and post-processing system parameters on resolving sideband frequency components generated through nonlinear vibro-ultrasonics
2. Apply nonlinear vibro-ultrasonic techniques to composite laminates, to determine the influence of delamination and impact damage on generation of sidebands
3. Apply nonlinear vibro-ultrasonic techniques to bonded aluminium structures, to determine the influence of gross bond-line defects on generation of sidebands
4. Extend the application of nonlinear vibro-ultrasonic techniques to bonded composite laminates with gross defects at the interface

In particular the composite laminates investigated are carbon fibre/epoxy pre-preg systems typical of that used for aerospace applications.

1.3 Thesis outline

The remainder of the thesis is structured into six chapters. The outline of these chapters is as follows:

Chapter 2 summarises and critically discusses current approaches towards detecting damage in composite laminates using nonlinear ultrasonic techniques. This includes background on

nonlinear ultrasonics and a summary of existing gaps in literature.

Chapter 3 describes the experimental system and methodologies used, and provides a critical discussion of the instrumentation challenges related to discerning sideband frequency components generated by nonlinear vibro-ultrasonic techniques.

Chapter 4 describes investigation into the detection and characterisation of artificial delamination damage in composite laminate beams. Included in this chapter are details of particular experimental techniques and analysis which were developed through this investigation.

Chapter 5 builds on experimental and analysis techniques developed in the previous chapter to investigate the detection of gross bond-line defects in bonded composite laminates. Additional testing on bonded aluminium beams is presented, helping to provide understanding of results for the composite beams.

Chapter 6 pulls together important conclusions from the previous chapters and discusses them in context of nonlinear vibro-ultrasonics moving forward.

Chapter 2

Literature review

2.1 Introduction

This chapter introduces background information on nonlinear ultrasonic techniques and their use in detecting and characterising damage in engineering structures. A particular focus is given to the ability of these techniques to resolve damage in composite laminates and the potential to detect very small levels of damage which precede loss of integrity. The chapter is organised as follows:

- Section 2.2 provides background to ultrasonic nondestructive testing techniques, including basic principles and practicality considerations.
- Section 2.3 introduces nonlinear ultrasonics, including the underlying theory and concepts related to damage detection and characterisation based on nonlinear phenomena. Three important nonlinear phenomena are discussed, with examples of applications to damage detection.
- Section 2.4 is dedicated to one particular technique, nonlinear vibro-ultrasonics, which is the focus of this thesis.
- Section 2.5 critically analyses the conclusions of the previous sections by analysing the gaps in literature related to detection of defects in composite materials.

2.2 Ultrasonic nondestructive testing

Ultrasonics is a field of nondestructive testing (NDT) techniques used to detect and characterise defects in materials. The general principle of the field is the excitation of a structure by a low-energy, high-frequency stress pulse and observing the propagation and reflection of the resultant stress wave (e.g. Graff, 1975). The propagation, reflection and attenuation characteristics of a so-called *ultrasonic wave* is dependent on material properties and any boundaries or damage with which it interacts (e.g. Achenbach, 1973). These interactions cause various transmission and reflection of the wave, absorption of acoustic energy and other phenomena which can be measured by analysing variations in the amplitude and phase of the wave. Comprehensive information about the propagation and characteristics of ultrasonic waves can be found in fundamental textbooks on wave propagation in elastic solids such as those by Kolsky (1963), Dieulesaint and Royer (1980) and Rose (1999).

The generation and measurement of ultrasonic waves is most commonly achieved through use of piezoeletric elements in contact with the structure under inspection. The reverse form of the piezoelectric effect allows these elements to produce ultrasonic waves when pulsed with a voltage profile, and to convert a received ultrasonic wave to an electrical signal by the direct piezoelectric effect (Rose, 1999). Ultrasonic NDT methods vary in how they utilise the generated ultrasonic waves. The pulse-echo technique inspects the area under a transducer (or array of transducers), by sending pulses into the test sample and measuring ultrasonic waves reflected by defects, interfaces or from the back wall of the object. Figure 2.1 illustrates the principle of the pulse-echo technique; the arrival time of pulses can be used to detect the presence of flaws as well as the speed of wave propagation in the material.

Measurements of wavespeed and attenuation can be used to detect material defects and determine mechanical properties of the material under inspection (Kino, 1987). Other

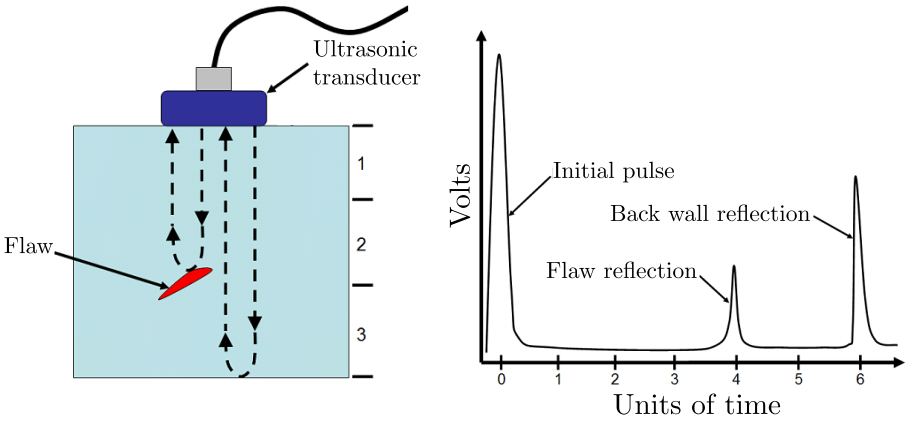

Figure 2.1: Principle of pulse-echo technique. Reflections from defects or back wall (left) arrive at different times (right). Adapted from National Instruments (2010)

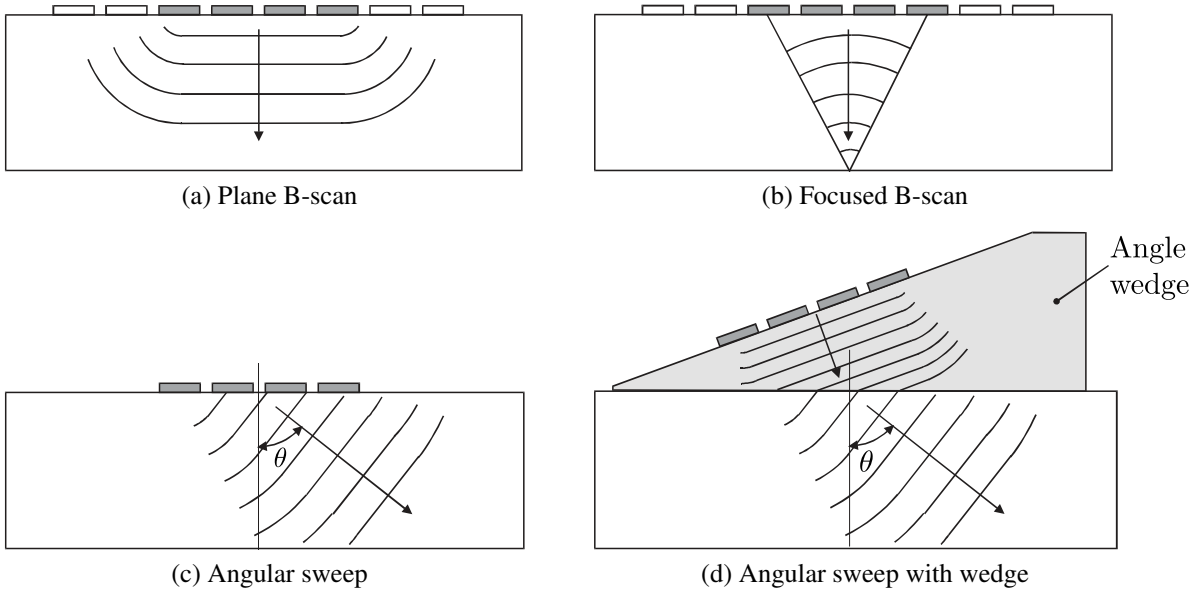

(a) Plane B-scan (b) Focused B-scan

(c) Angular sweep (d) Angular sweep with wedge

Figure 2.2: Common array inspection modalities, adapted from Drinkwater and Wilcox (2006).

techniques such as acousto-ultrasonic and guided wave methods are able to inspect a larger area by sending a pulse across the area of interest and measuring the response of the test sample at another location. These techniques allow for inspection over long distances or within complicated geometry. A good description of acousto-ultrasonic methods and their application is given by Vary (1990) and guided wave methods by Rose (2002).

Ultrasonic inspection of fibre-reinforced composite structures is a well-established field of research, with more than 40 years of development and evolution of techniques. Reviews such as those by Scott and Scala (1982), Reynolds (1984) and Adams and Cawley (1988) show that already by the 1980s a number of methodologies for detecting damage in composites had been developed. Measurement of attenuation through ultrasonic testing was commonly used at this time by manufacturers of composite components for detection and measurement of porosity and delamination as part of quality control. As noted by Adams and Cawley (1988), the more sensitive of these techniques involve sending an ultrasonic wave through the thickness of a structure, and require access to the structure directly on the defect location to send and receive the pulses. Use of these techniques is further limited due to detection difficulty increasing significantly near corners, edges and changes in geometry.

Some of the difficulties faced by ultrasonic inspection have been overcome by the use of phased array (PA) techniques where a number of individual elements within a single transducer are pulsed with carefully controlled timings. By changing the pulse timings, the ultrasonic beam can be focussed or scanned across the inspected material. Figure 2.2 shows common inspection modalities for a linear array of elements.

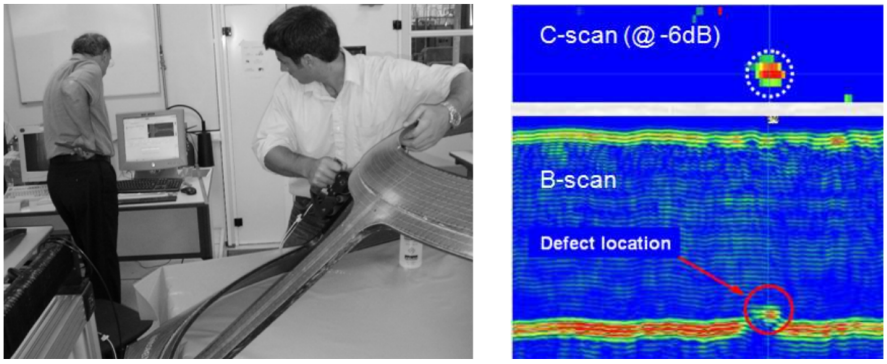

Figure 2.3: Composite frame under inspection (left) and results from using a multiplexed phased-array system (right). From Hopkins et al. (2011).

The fundamental principle for damage detection with PA is the same as for regular, single-element ultrasonic inspection, though the focusing or steering of the beam allows for better inspection performance and more flexibility in transducer placement (e.g. Drinkwater and Wilcox, 2006). There are two major methods for presenting the data obtained from a linear array of transducers: B-scan and C-scan. The B-scan shows a cross-sectional view of the test specimen, with time-of-flight information visualised across the length of the transducer (the axis along which the elements are positioned). An example B-scan is shown in Figure 2.3 (lower right), with the horizontal axis being position and vertical axis time, equivalent to depth. Colour repesents signal amplitude, with the lower part of the image in red and green indicating the back wall of the structure. In this example, a defect near the back wall results in an earlier arrival time.

The C-scan presentation results from the transducer being scanned across the specimen in the axis perpendicular to the element axis, and provides a top-down view visualisation of arrival time or signal amplitude. On the C-scan image shown in Figure 2.3 (upper right) the blue areas indicate regions of the specimen where the reflection comes from the back wall; the circled defect area appears in red and green because this signal arrives earlier.

Beam distortion and sensitivity loss around complex geometry profiles seen with single element techniques is improved using PA techniques (e.g. Mahaut et al., 2002). Holmes et al. (2008) have also demonstrated an advancement to the technique where every element is used as a transmitter and receiver individually and the full matrix of transmit-receive signals is used to construct a focused image of the entire inspection area in post-processing. The main improvement of this technique as with all PA techniques is an increased sensitivity to defects when inspecting near edges and changes in geometry (Holmes et al., 2008; Hopkins et al., 2011).

2.2.1 Guided Lamb wave-based damage detection

Guided waves are ultrasonic waves which propagate along a structure, guided by its boundaries. In the case of an elongated structure such as a beam or plate, the guided wave can travel for long distances with relatively low attenuation, making it useful for NDT purposes. The ultrasonic probing waves used in nonlinear vibro-ultrasonics are commonly guided waves, and hence the damage detecting capabilities of guided waves are relevant to this thesis.

Guided Lamb wave-based techniques for damage detection are particularly promising for inspection of difficult-to-access components or structures of a complex shape. These techniques utilise sensor arrays, where ultrasonic elements are placed on many different locations of the structure under inspection and transmit-receive signals are collected. As shown in Figure 2.4(a), interaction of the incident wave and damage generates a scattering wave, and measurements made will include both the incident and the scattering wave. To detect damage, the scattering wave information is extracted from the measurement signal, for example by subtracting away known damage-free reference data, which is known as baseline subtraction (Veidt et al., 2008; Ng and Veidt, 2009). Any additional signals present in the structure may be attributed to damage in the structure, and an image of the damage can be formed, for example as in Figure 2.4(b). Damage indices calculated from guided Lamb wave-based techniques have been shown to correlate with physical damage growth, for example fatigue crack growth in steel structures (e.g. Gresil et al., 2011). Detection and imaging of damage may be limited by noise in the signal, temperature variations or by features of the structure itself such as flanges and welds (Croxford et al., 2007).

Su et al. (2006) provide a good review of Lamb wave based-techniques for identifying damage in composites. For very simple structures, specimens with damage such as delamination, transverse ply cracks and through holes can be differentiated from intact samples

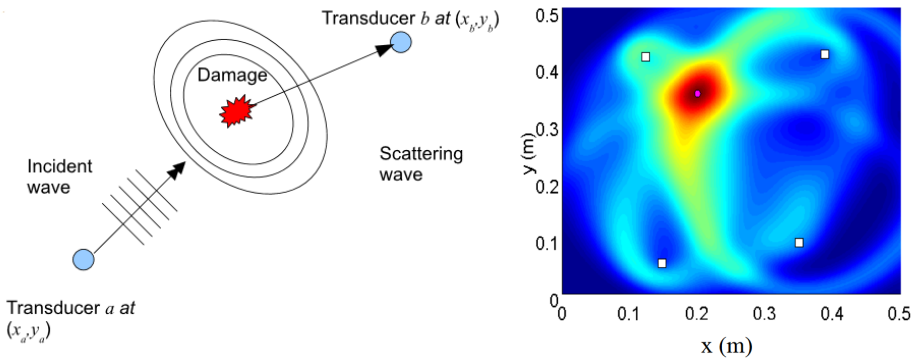

(a) Scattering of signal at damage (b) Image of through-hole defect

Figure 2.4: (a) Beamforming principle (Ng and Veidt, 2009), and (b) example beamforming image (Veidt et al., 2008). White squares are sensors, pink circle at centre of red area is a through-hole defect.

(e.g. Kessler et al., 2002). Very few studies have investigated structures more complex than a thin composite laminate beam or plate. One such study is by Yeum et al. (2012) who were able to detect the presence of delamination within a composite plate even with stiffeners, by sending a pulse through the damaged area in a so-called *pitch-catch* configuration.

An extension to damage detection is to locate and characterise the damage, i.e. the size and severity. Instead of simple subtraction of signals, it is possible to reconstruct wave propagation and interaction with damage from received signals and knowledge of propagation characteristics within the structure. Comparisons of various imaging algorithms are presented by Rose et al. (2015) and later Chan et al. (2016). The recommendation of these studies is that for correctly estimating damage location and size, beamforming and time reversal imaging algorithms should be used as they are robust to measurement error and noise. They note that while a modified diffraction tomography (MDT) technique is able to correctly estimate severity, it is sensitive to noise which leads to a requirement of a very large number of sensors (Chan et al., 2016).

The complex inverse problem of estimated damage type, location or severity is further complicated by composite materials due to their anisotropic viscoelastic nature. The context of the study by Chan et al. (2016) is that of an isotropic plate of simple geometry, such that analytical expressions exist for the Green's function which describes the wave propagation characteristics needed for reconstruction. To use the algorithms described for fibre-composite laminates or for a complex geometry, the Green's function would need to be calculated numerically or experimentally, as the analytical forms are unknown. Chan et al. (2014) present an extension to guided wave tomography where the Green's function for a composite laminate plate is numerically calculated, and the resulting guided wave tomography results in good prediction of damage size and shape.

Huthwaite and Simonetti (2013) describe an iterative technique for guided wave tomography where additional iterations of the reconstruction can be used, updating the estimate to Green's function every iteration. This combined with further work by Huthwaite (2014) demonstrates mapping the thickness of a corroded aluminium plate by reconstructing wavespeed, which is physically linked to the thickness of the plate. This method was able to detect with a resolution of around 2λ (twice the wavelength of the probing ultrasonic wave) and estimate the thickness loss within 10% accuracy.

Ultrasonic guided wave-based techniques are fit to the task of detecting the existence of damage, but are still mostly restricted to simple geometries and isotropic materials in the case of estimating damage size and severity. Progress in the field however looks promising and according to Chan et al. (2016) an extension of the quantitative characterisation to composite materials is feasible by accounting for structural complexities and improvement of image quality.

Recent investigations from Blanloeuil et al. (2016a, 2016b) have employed a variant of time reveral imaging based on nonlinear features of scattering signals, using data generated from a finite element model. The findings suggest that the nonlinear features allow for in-situ baseline-free detection and characterisation of a closed crack. While the study of nonlinear scattering and imaging algorithms is not particularly relevant to this thesis, the extraction of nonlinear features of a signal is an issue shared by nonlinear vibro-ultrasonics. The issues addressed in this thesis relating to detection of nonlinear components in measurement signals form the foundation for the successful development of experimental nonlinear guided wave imaging systems.

2.3 Nonlinear ultrasonics

As an excitation propagates through a structure, the majority of its energy remains at the same frequency or frequencies, even in a dispersive medium. Typical ultrasonic NDT techniques therefore involve analysis of system response at the same frequency as the input excitation frequency. Nonlinear ultrasonics is a branch of ultrasonic NDT which investigates additional frequency components in the system response which are different to those in the input excitation; it is nonlinearity encountered by the propagating excitation(s) that gives rise to these frequency components. The characteristics of the additional frequency components are diverse, as are the proposed mechanisms for their generation. This section provides a theoretical background to the field and a discussion of nonlinear ultrasonic NDT techniques as they relate to detecting and characterising damage in fibre-reinforced composites.

2.3.1 Theory and concept

Linear elastic wave propagation theory considers a proportional relation between stress and strain, governed by Hooke's Law, where restoring force to an excitation is proportional to displacement (e.g. Achenbach, 1973). The result of this is that an excitation with a single frequency component will cause oscillation of the system at only that frequency. In reality, a wave propagating through a material may encounter regions of the microstructure that contain anharmonicity, leading to nonlinear vibration and oscillation at multiple frequencies. This concept is discussed in greater detail by Lissenden et al. (2015).

When this anharmonicity is due to intrinsic imperfections in the material at the atomic scale, it is referred to as *inherent* or *material nonlinearity*. All materials have some level of inherent nonlinearity, and though it is generally small it causes distortion of a propagating elastic wave which can be measured by analysing generated frequency components. The basis of nonlinear ultrasonic methods is that damage within a structure can be detected by measuring an increase in nonlinearity above the level of inherent material nonlinearity. This requires that nonlinear ultrasonic techniques be able to effectively discern nonlinearity present due to damage, and necessarily that the defect has a nonlinear response to the interrogation excitation used.

Klepka (2013) provides a good review of the fundamental theory of nonlinear ultrasonics and its application to damage detection. This review also contains a summary of nonlinear mechanisms that authors have identified as related to cracks in solids. These mechanisms range from those at the macroscopic level (e.g. discontinuity due to closing-opening crack; Kim et al., 2003) to the mesoscopic level (e.g. local stiffness reduction or bilinear stiffness; Zaitsev and Sas, 2000) to the atomic level (e.g. stick-slip friction and adhesion hysteresis at crack surfaces; Woolfries, 1998).

The application of nonlinear ultrasonics to detecting fatigue cracks in metals has received considerable attention, and is an illustrative example of how measurements of nonlinearity can provide increased sensitivity over conventional NDT. The evolution of fatigue damage is very interesting from a nonlinear ultrasonics perspective, because it progresses from purely microstructural changes through to macroscales fracture surfaces. In the earlier stages, these changes are small enough to fall below the detection limits of conventional ultrasonics, whereas the later stages provide sufficient interruption to the propagating ultrasonic wave to be detectable. Authors such as Solodov (1998), Nagy (1998), and Donskoy et al. (2001) however have shown the capability of nonlinear ultrasonics to detect small cracks which were unable to be detected by conventional ultrasonic techniques. Several studies have also used nonlinear ultrasonic techniques to correlate an increase in dislocation density due to fatigue with material nonlinearity (Cantrell and Yost, 2001; Kim et al., 2006).

The use of these techniques effectively reduces the required severity for detection of fatigue damage in metals. It has been suggested by Kulkarni and Achenbach (2008) and Lissenden et al. (2015) among others that nonlinear ultrasonic techniques could be used to detect the microstructural changes that precede macroscale cracks. If the initiation of the crack is considered to be the onset of damage, then in some way one could consider that, using nonlinear ultrasonics, fatigue damage could be detected before it occurs. With these concepts in mind, the focus of much nonlinear ultrasonic research has been on detection of damage onset. Other forms of material degradation such as corrosion (e.g Van Den Abeele and Van de Velde, 2000), plastic strain (e.g. Pruell et al., 2009), creep (e.g. Baby et al., 2008; Xiang et al., 2012) and thermal degradation (e.g. Nucera and Lanza Di Scalea, 2014) have been investigated for the application of nonlinear ultrasonics to detect early onset of damage.

In recent years, research into nonlinear ultrasonic inspection of composite structures has gained popularity. The motivation to use nonlinear techniques for composites is much the same as for fatigue damage, which is the ability to detect damage earlier in its evolution, before the effect on structural integrity and safety is detrimental.

Jhang (2009) provides a good overview of the nonlinear phenomena that manifest in solids and which are useful for damage detection and characterisation. The following sections discuss three important nonlinear phenomena: the generation of higher harmonics (Section 2.3.2), shifting of resonance frequency (Section 2.3.3), and frequency mixing (Section 2.3.4) which describes the interaction of multiple waves in a nonlinear medium and is the basis for nonlinear vibro-ultrasonics.

2.3.2 Higher harmonic generation

2.3.2.1 Theory

The simplest phenomena resulting from distortion of a propagating wave is the generation of higher harmonic frequencies. Lord Rayleigh (1896) first pointed out that nonlinear terms in the wave equation cause a propagating sound wave to generate additional waves at frequencies which are multiples of its own - these frequency components are referred to as higher harmonics. To illustrate the generation of higher harmonic frequencies, we consider a simple one-dimensional case of wave propagation in a thin circular rod, governed by

$$\rho \frac{\partial^2 u}{\partial t^2} = \frac{\partial \sigma}{\partial x} \tag{2.1}$$

where u is axial displacement, ρ is density and σ is stress. We now presume that the material behaves nonlinear-elastically, following a modified Hooke's Law: where Young's Modulus (E) is a function of strain ($\varepsilon = \partial u/\partial x$)

$$\sigma = \varepsilon E(\varepsilon) \, , \qquad E(\varepsilon) = E_0(1+\beta\varepsilon) \tag{2.2}$$

where β is an elastic parameter referred to as a nonlinearity parameter. Substituting (2.2) into (2.1) yields the equation of motion

$$\rho \frac{\partial^2 u}{\partial t^2} = E_0 \frac{\partial^2 u}{\partial x^2} + 2\beta E_0 \frac{\partial u}{\partial x}\frac{\partial^2 u}{\partial x^2} \tag{2.3}$$

To obtain a solution to this, perturbation theory is applied with the displacement field u assumed to be of the form

$$u = u_0 + u' \tag{2.4}$$

where u_0 represents an initial excitation and u' the first order perturbation. If we select an initial excitation of a sinusoid with frequency ω,

$$u_0 = A_1 cos(kx - \omega t) \tag{2.5}$$

then the solution to this equation takes the following form:

$$u = u_0 + u' = A_1 cos(kx - \omega t) - \frac{1}{8}\,\beta A_1^2 k^2 x sin(2kx - 2\omega t) \tag{2.6}$$

The second term in equation (2.6) is the 2$^{\text{nd}}$ harmonic of the excitation wave, having frequency of 2ω. The amplitude of this second term depends not only on β but on propagation distance x, indicating that this is a cumulative effect. If the perturbation analysis were extended to higher

orders, it is found that additional higher harmonics are created at frequencies of 3ω, 4ω and so on. The addition of higher harmonic frequency components to an excitation signal may be referred to as *distortion* or simply *nonlinearity*.

Equation (2.2) includes only a first-order nonlinearity term, β, though it is possible to consider higher order terms:

$$\sigma = \varepsilon E(\varepsilon) \,, \qquad E(\varepsilon) = E_0(1 + \beta\varepsilon + \delta\varepsilon^2 + \dots) \tag{2.7}$$

Figure 2.5 shows stress-strain characteristics for first-order (β) and second-order (δ) nonlinearity as well as the accompanying strain spectra.

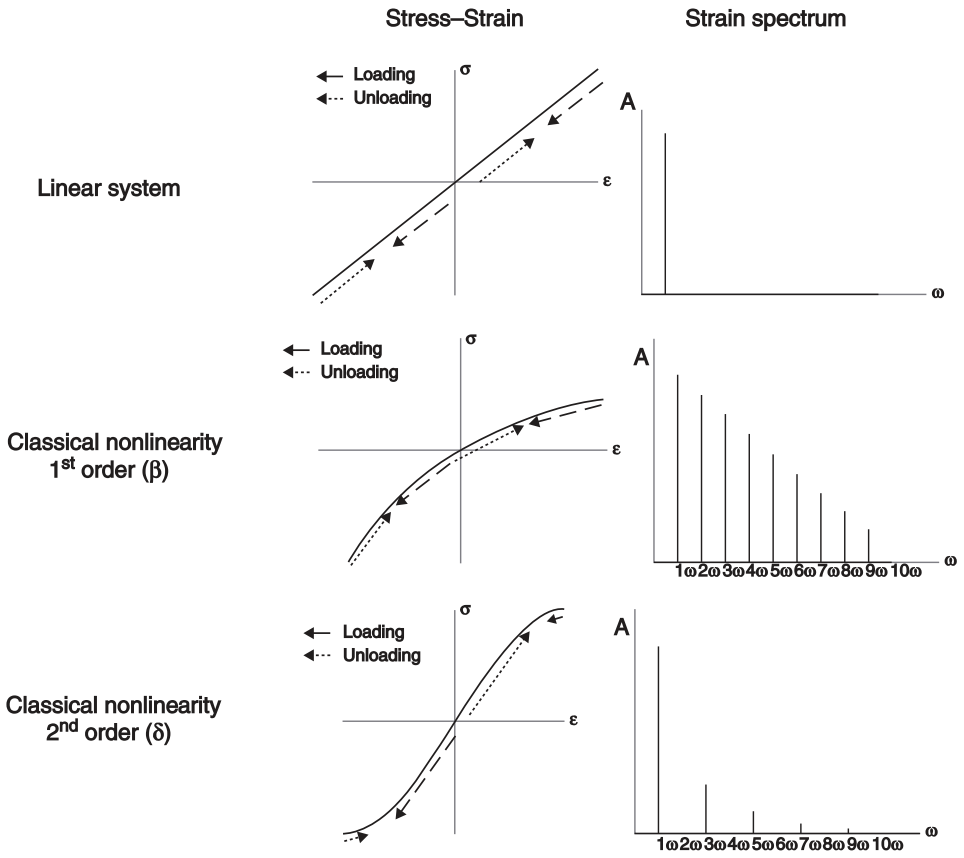

Figure 2.5: Typical stress-strain relations and frequency spectra for linear, 1st order classical nonlinearity and 2nd order classical nonlinearity, taken from Klepka (2013)

2.3.2.2 Application to damage detection

Figure 2.6 shows a simple illustration of higher harmonic-based nonlinear ultrasonic experiments. An initial sinusoidal ultrasonic pulse is sent across a sample, where it "accumulates" distortion as per equation (2.6). The receiving transducer hence receives a signal

made up not only of the initial excitation but also of higher frequency components due to the accumulated nonlinearity, clearly visible in the spectra of the signal.

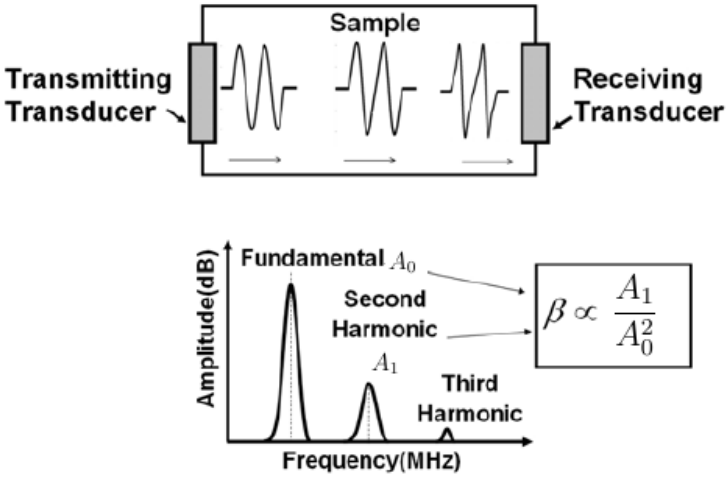

Figure 2.6: Schematic showing distortion of initially sinusoidal ultrasonic wave propagating in sectioned sample of specimen (top), the resulting Fourier spectrum of received signal (bottom), and relation to measurement of nonlinearity parameter (bottom). Adapted from Cantrell and Yost (2001)

The relative amplitudes of the fundamental frequency and second harmonic are related by the nonlinear parameter β, though studies differ in how this parameter is calculated. The two most common methods normalise second harmonic amplitude by fundamental amplitude (($\beta = A_1/A_0$, e.g. Mattei and Marty, 2003) and by the square of fundamental amplitude ($\beta = A_1/A_0^2$, e.g. Cantrell and Yost, 2001). Based on equation (2.6) an approximation to β can be determined from:

$$\beta = \frac{8}{k^2 x}\frac{A_1}{A_0^2} \tag{2.8}$$

This approximation to β includes a term for distance travelled by the excitation x and wavenumber k. It is common for these parameters to be constant for a given set of experiments and hence the comparison of nonlinear parameters between samples reduces to $\beta = A_1/A_0^2$.

Cantrell and Yost (2001) have shown that this nonlinearity parameter β can be an indicator of early fatigue damage in aluminium 2024-T4 'dogbone' specimens subjected to cyclic loading. Figure 2.7 shows their major finding, that the nonlinearity parameter monotonically increases with number of fatigue cycles. Cracks of size up to $40\mu m$ were reported as being present in the samples, though no information is provided as to how this varied with number of fatigue cycles. The authors argue that cracks of this size do not contribute sufficiently to the nonlinear parameter so as to explain their results. No justification is given for this argument, though theoretical calculations are briefly mentioned. The authors conclude that the increase in β for specimens with higher number of fatigue cycles is probably associated with dislocation dipole structures formed in the material during fatigue, and not cracks. This builds on previous work

(Cantrell and Yost, 1994) which suggested that dislocation dipoles contribute significantly to the generation of second harmonics. Within each sample, a variation of β was found for different measurement locations, suggesting the microstructural changes in the material were localised.

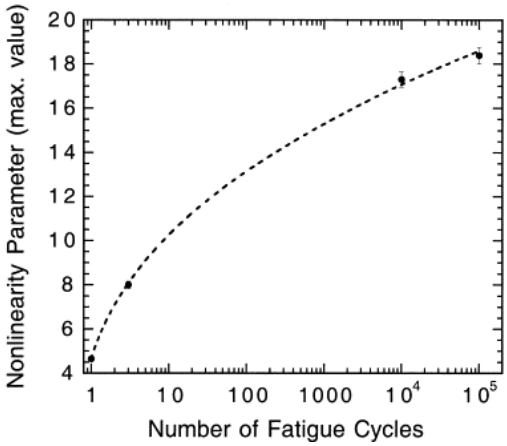

Figure 2.7: Graph of maximum measured value of nonlinearity parameter as function of number of fatigue cycles for aluminum alloy 2024-T4 (Cantrell & Yost 2001)

The studies by Cantrell and Yost (1994) and Cantrell and Yost (2001) concerned the contribution of fatigue-induced microstructural features to nonlinearity, but did not attempt to compare the nonlinear parameter with other techniques for detecting the onset of fatigue damage. Nagy (1998) builds on this work by comparing nonlinear parameters to linear parameters (sound velocity, ultrasonic attenuation and static modulus) for detecting onset of fatigue damage. It was found that shortly before failure, the nonlinear parameter increases by up to an order of magnitude compared to the inherent material nonlinearity prior to fatigue cycling. Figure 2.8 shows results obtained for (a) aluminium alloy and (b) titanium matrix composite specimens, with similar trends exhibited for plastics (PVC, polycarbonate, nylon, and epoxy adhesives). In all materials tested, the nonlinear parameter was found to increase earlier in testing and be more sensitive than the linear parameters to the onset of fatigue damage.

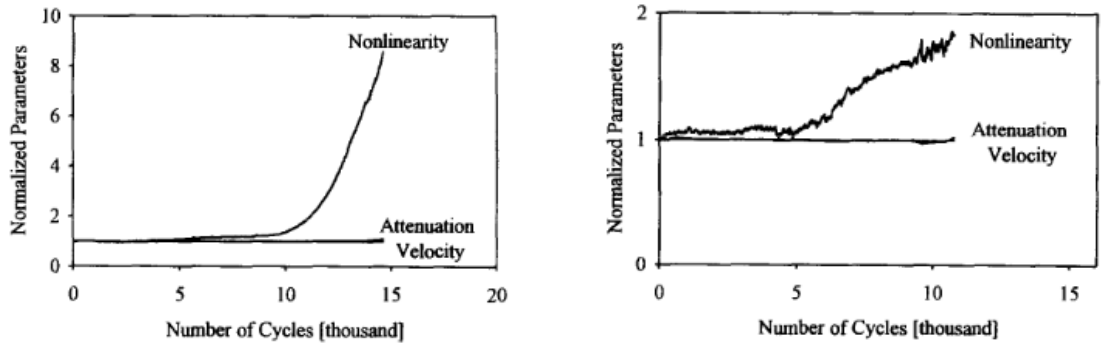

(a) Aluminium 2090 alloy

(b) Titanium matrix composite

Figure 2.8: Comparison of nonlinear and linear parameters from Nagy (1998) for (a) aluminium 2090 and (b) titanium matrix composite specimens undergoing fatigue cycling

While no fibre-reinforced plastics were tested by Nagy (1998), all plastics which were tested showed higher inherent nonlinearity than metals and metal matrix composites as well as more sensitivity to temperature changes. These findings agree with earlier work (Adler and Nagy, 1991; Nagy and Adler, 1992) which suggest that nonlinear parameters measured from local acoustic wave velocity (and not from higher harmonics) are sensitive to degradation of strength of plastics during long-term fatigue loads. In these cases the nonlinear parameter is calculated from an alternative rearrangement of (2.7) substituted into (2.1) which yields:

$$\frac{\partial^2 u}{\partial t^2} = c_0^2(1+2\beta\varepsilon+3\delta\varepsilon^2+\dots)\frac{\partial^2 u}{\partial x^2} \tag{2.9}$$

where $c_0^2 = E_0/\rho$ is the acoustic wave velocity for an unstrained body. The effective acoustic wave velocity as a function of strain is hence

$$c(\varepsilon) = c_0(1+\beta\varepsilon+\frac{3}{2}\delta\varepsilon^2+\dots) \tag{2.10}$$

This formulation is used by Solodov et al. (2004) and a "mixed" nonlinearity parameter β_m is defined as

$$\beta_m = \frac{\partial c(\varepsilon)}{\partial \varepsilon}\frac{1}{c_0} \tag{2.11}$$

and is calculated by taking measurements of local acoustic wave velocity as a function of applied static strain. Though this parameter is not calculated by measurement of higher harmonic frequency components of an ultrasonic signal, it is based on the same underlying equations of nonlinear elasticity. Studies which investigate nonlinearity through acoustic wave velocity measurements are closely related to and important to the study of application of higher harmonic nonlinear ultrasonic techniques.

2.3.2.3 Application to damage detection in composites

Though fatigue damage in metals and plastics has received significant attention, fewer studies have shown results for the application of higher harmonic generation for nondestructive detection of damage in fibre-reinforced composite materials.

Using measurements of wave velocity to determine nonlinearity, a study by Solodov et al. (2004) reported on nonlinearity of polypropelene (PP) and glass fibre-reinforced polypropelene (GFRPP) specimens during tensile testing. The nonlinearity calculated

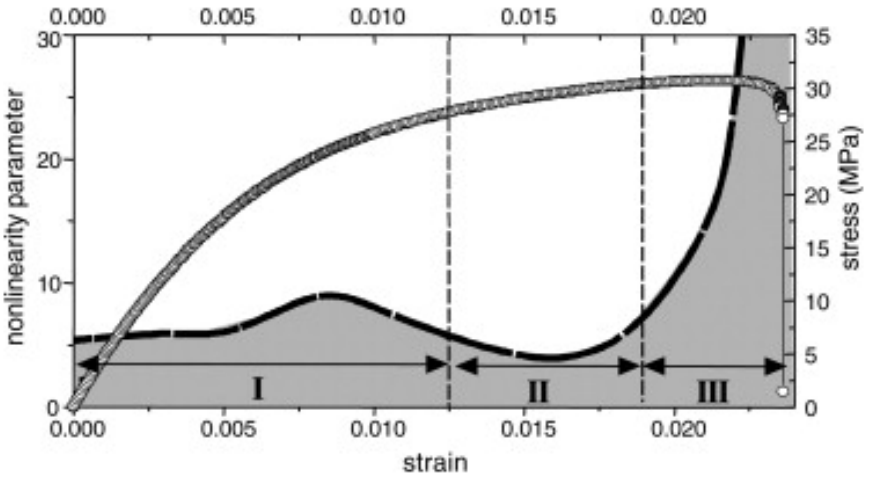

Figure 2.9: Nonlinearity parameter β (black line with grey area under curve shaded) and stress (hashed line) plotted as functions of strain for a 30% GFRPP tensile test specimen (Solodov et al., 2004)

for a 30% GFRPP tensile test specimen is shown in Figure 2.9, along with a stress-strain curve. Three regions are marked, where the authors point out regimes where nonlinearity remains mostly constant at low strains (I), slightly decreases during plastic deformation (II) and sharply increases before failure (III). The authors conclude that micro-cracks develop within the matrix between longitudinally oriented fibres during regions I and II, and that increased fibre tension and gradual pull-out bridges these cracks during region III. Importantly, the sharp rise in nonlinearity precedes the eventual fibre fracture and unstable growth of cracks which leads to material failure.

Li et al. (2012) considered second harmonic-based nonlinear methods for detecting thermal degradation in carbon/epoxy composite laminates. Figure 2.10 demonstrates their finding, that the nonlinear acoustic parameter is more sensitive to thermal fatigue cycling than group velocity or attenuation. Over the span of 1000 cycles, the nonlinear parameter increased by more than three times, while the relative changes in linear parameters was less than 10%. These results are reminiscent of those for fatigue damage cycling in metals described in Section 2.3.2.2.

Similar findings have been obtained by Rauter and Lammering (2015) for impact damage

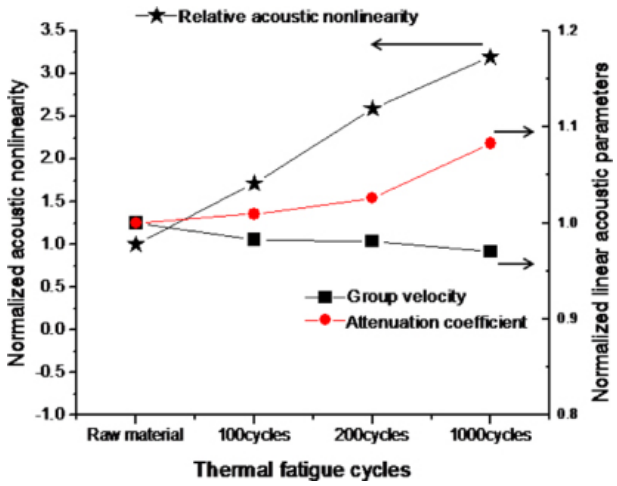

Figure 2.10: Comparison of nonlinear and linear acoustic parameters for thermal fatigue cycles in carbon/epoxy (Li et al., 2012).

in carbon/epoxy composite laminates. Their results also show a change of less than 10% in group velocity while the nonlinear parameter increased more than seven-fold, for three samples impacted at different energy levels, compared to an intact sample. Microscopy on the sample with the highest impact energy indicates the development of fibre and matrix cracking as well as delaminations.

An experimental investigation by Mattei and Marty (2003) showed evidence of the sensitivity of higher harmonic measurements to micro-damage in carbon-fibre reinforced composite laminates. Their experiments compared a conventional amplitude C-scan performed using an 18 MHz tone-burst signal to a harmonic imaging technique where a 9 MHz tone-burst was used and the amplitude of the second harmonic (at 18 MHz) used to compute nonlinearity at each scan location. Scanning was performed on laminates before and after fatigue cycling performed using a four-point bending apparatus, and a set of results for a single laminate is shown in Figure 2.11. The conventional C-scan shows no discernible discontinuity or change in attenuation in this laminate before or after the fatigue cycling (at 15000 or 17000 cycles), though the fatigue test was concluded based on the recording of an acoustic emission from the sample. In contrast, the harmonic imaging shows development of the nonlinearity, evidenced by an increase in nonlinear parameter calculated from the ratio of second harmonic and fundamental amplitudes ($\beta = A_1/A_0$).

To understand the mechanism behind observed increases in nonlinearity, Mattei and Marty (2003) cut and polished samples post-fatigue cycling, finding micro-delaminations and matrix cracks. Regions of the laminates where harmonic imaging measured a larger nonlinearity (white zones in figure 2.11) were found to have higher crack density. Matrix cracks were measured to be on the order of 200 μm long and up to 20 μm "open". The results of these experiments indicate that the development of small matrix cracks during fatigue of CFRP are detectable

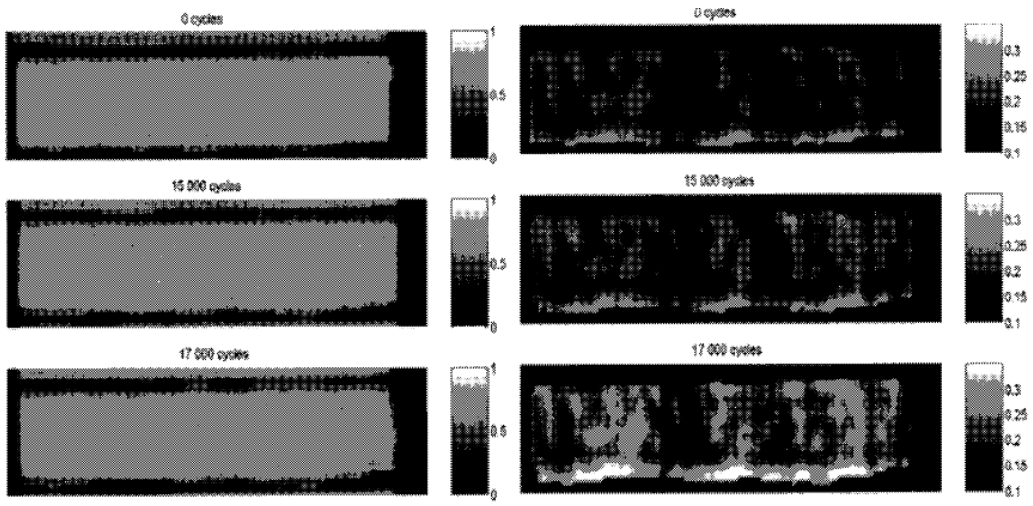

Figure 2.11: Imaging of CFRP laminates before (top) and after (middle, 15000 cycles; bottom, 17000 cycles) fatigue cycling, obtained using (a) conventional C-scan & (b) second harmonic (Mattei and Marty, 2003)

through second harmonic analysis. Although the study stopped short of inducing more severe fatigue damage which would be detectable by the linear C-scan or cause material failure, the results show the nonlinear parameter to be more sensitive than linear amplitude-based methods to detecting microstructural changes which precede fatigue failure in fibre-reinforced composites.

More recent work by Rauter and Lammering (2014) does not strongly confirm these findings, providing evidence that second harmonic generation may not be a good predictive indicator for fatigue damage in fibre-reinforced composite samples. Unidirectional carbon fibre/epoxy composite laminates were subjected to cycling tensile loading, with both C-scan and second harmonic generation of Lamb waves used to assess damage of the samples. Results in the form of nonlinear parameter for a number of samples pre- and post-cycling are shown in Figure 2.12(a). These results show that for 5 of the 8 specimens tested (corresponding to 0, 5000, 10000 and 15000 loading cycles) the nonlinearity parameter shows no convincing trend.

In fact, three of the specimens which underwent fatigue loading cycles exhibited lower nonlinearity than the pristine reference sample. Only the two 20000 cycle specimens and one of the two 15000 cycle specimens showed a definitive increase in nonlinearity after testing.

The reference specimen and the 15000-cycle specimen that exhibited greatest nonlinearity were inspected using C-scan, and the total attenuation over the specimen area used to calculate a damage index. Figure 2.12(b) shows these two data points, with the 15000-cycle specimen having a higher damage index. No information was provided regarding the damage state of the other 6 specimens. These results show that the nonlinear parameter β is no more sensitive than linear parameters to detect tensile fatigue damage in carbon-fibre reinforced composite laminates. The second harmonic generation was not found to be significant until after the onset

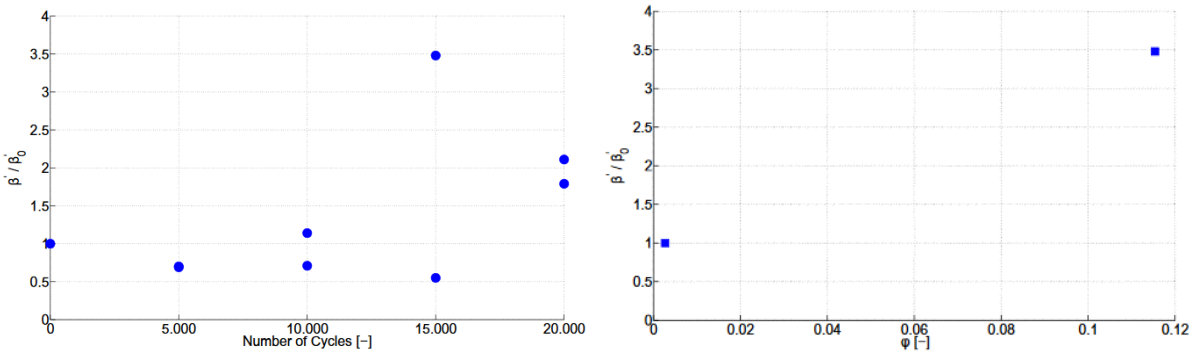

(a) β against cycles (b) β against observed damage (C-scan)

Figure 2.12: Results from second harmonic generation experiments using Lamb waves, carbon/epoxy composite laminates undergoing tensile loading cycles (Rauter and Lammering, 2014)

of macroscale damage, such as was easily detectable by C-scan. The findings suggest that the fatigue damage is not preceded by microstructural changes which generate significant second harmonics.

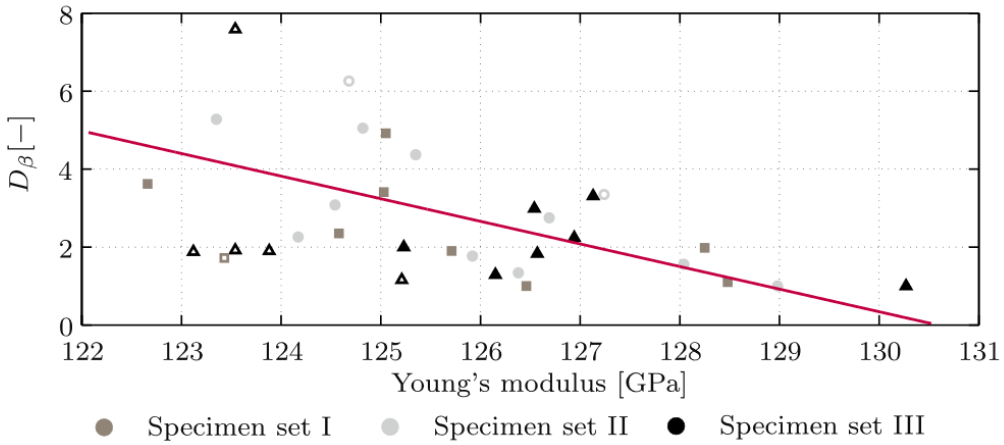

Figure 2.13: Nonlinear parameter D_β against Young's modulus for CFRP laminates. Symbols represent number of cycles, colour indicates specimen set (Rauter et al., 2016)

An extension to Rauter and Lammering (2014) study was performed by Rauter et al. (2016), and testing was performed on an additional 6 specimens per cycling duration (5000, 10000, 15000 and 20000 cycles). The focus of these results is the correlation between Young's modulus and an acoustic nonlinearity parameter D_β derived from β but normalised by the smallest exhibited β within each set of specimens. Figure 2.13 shows that a higher nonlinearity indicates lower Young's modulus, with a large spread in the data as for the previous study. The authors conclude that the high variability in the results of this study and of Rauter and Lammering (2014) is due to the manufacturing process of the laminates, specifically supporting threads that hold pre-preg fibres in place during curing. These threads are the first point of failure during tensile testing, which initiates micro-damage in the epoxy matrix of the material. The authors

suggest that it is the breakage of these threads which is highly variable, and therefore the damage present in each specimen within an ”identical” testing set can vary from other members.

Rauter et al. (2016) conclude that material degradation in CFRP laminates due to cyclic tensile load damage can be detected using an acoustical nonlinear parameter calculated from second harmonic measurements. This conclusion appears to be at odds with their results, which instead indicate no definitive increase in nonlinearity during onset of fatigue damage. While it does appear that the loading cycles introduce micro-damage, it is not conclusive that this damage causes significant harmonic generation, that an increase in nonlinear parameter precedes onset of macroscale damage, or that the nonlinear parameter is more sensitive than a linear parameter, e.g. Young’s modulus at detecting damage. These results are interesting, because as stated previously, Mattei and Marty (2003) have shown sensitivty of the second harmonic to fatigue damage in CFRP laminates, though for damage induced by cyling bending rather than tensile loading.

2.3.3 Nonlinear resonance

Nonlinear resonance techniques rely on the phenomenon of shifting resonance frequencies in nonlinear structures where resonance frequency is dependent on strain amplitude (Jhang, 2009).

2.3.3.1 Theory

Consider again a modified Hooke's Law with higher-order terms:

$$\sigma = \varepsilon E(\varepsilon, \dot{\varepsilon}) \,, \qquad E(\varepsilon, \dot{\varepsilon}) = E_0(1 + \beta\varepsilon + \delta\varepsilon^2 + \alpha\left[\Delta\varepsilon + \varepsilon(t)\text{sign}(\dot{\varepsilon}) + \ldots\right]) \tag{2.12}$$

As in equation (2.7) this Hooke's Law contains a first-order nonlinearity parameter β and second-order nonlinearity parameter δ. In addition to these, a material hysteresis parameter α takes into account stress history of the material, using the sign (positive or negative) of strain rate $\dot{\varepsilon}$. A typical, ideal stress-strain relation and frequency spectrum for hysteretic nonlinearity is shown in Figure 2.14.

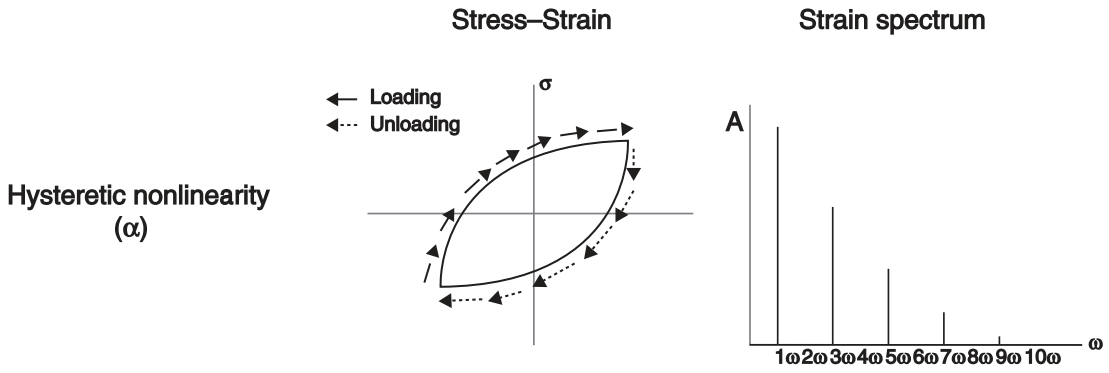

Figure 2.14: Typical stress-strain relatios and frequency spectrum for hysteretic nonlinearity, adapted from Klepka (2013)

Consider then a material behaving under this modified Hooke's Law (equation 2.12), excited by a sine wave with amplitude A_1 as in Figure 2.15(a). The stress-strain curve of the loading and unloading is shown in Figure 2.15(b), with an average modulus K_1 (analog to E_1) indicated by the slope of the dashed line, and the energy dissipated by the shaded region within the loop. Compare this to an excitation of larger amplitude A_2, which shows a reduction in average modulus and an increase in the energy dissipation. This is an illustration of a set of parameters β, δ and α such that the material softens as excitation amplitude is increased. The combined effect is that the material exhibits an amplitude-dependent resonant frequency, one which decreases with increasing excitation amplitude.

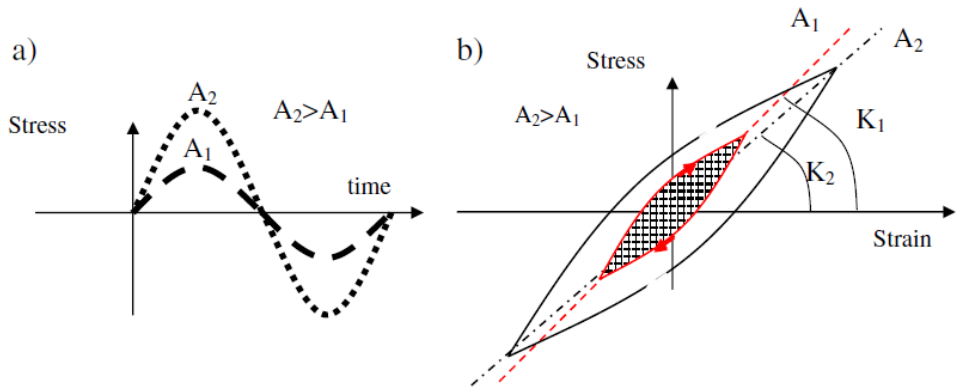

Figure 2.15: (a) excitation profile and (b) stress-strain relation, for a material exhibiting softening with increased amplitude, adapted from Meo et al. (2008)

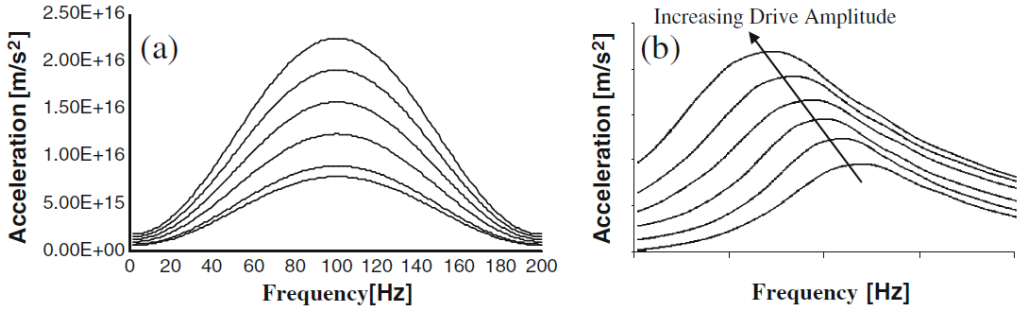

Figure 2.16: Frequency response curves for varying drive amplitudes for (a) an intact CFRP sample and (b) CFRP sample damaged by impact (Meo et al., 2008)

2.3.3.2 Application to damage detection

The effect of an amplitude-dependent resonant frequency arising from hysteretic nonlinearity allows for a technique to experimentally determine α. The method, known as nonlinear resonance ultrasonic spectroscopy (NRUS) involves measuring the frequency shift occurring for an increased excitation amplitude. An example of NRUS data from Meo et al. (2008) is shown in Figure 2.16 demonstrates the principle well, with little to no shift observed for an intact carbon-fibre reinforced plate but a large shift seen in a plate with barely visible impact damage.

The shift of resonant frequency with increasing drive amplitude can be quantified to resolve nonlinearity parameters, for example as Meo et al. (2008) have done, by assuming hysteretic effects dominate at large amplitudes and calculating α from:

$$\alpha \Delta\varepsilon = \frac{f_0 - f_1}{f_0} \tag{2.13}$$

where $\Delta\varepsilon$ is average strain amplitude, f_0 is resonant frequency for the lowest amplitude used,

and f_1 is resonant frequency measured for each drive amplitude.

A very similar technique is described by Van Den Abeele et al. (2009) as nonlinear reverberation spectroscopy (NRS). The slight change in name reflects the slight variation in methodology: an excitation at a single amplitude and frequency (close to a known resonance) is applied for a continuous period and abruptly turned off, allowing vibration within the material to decay (or reverberate, hence the name). Measuring the frequency components present in small packets of the signal and their rate of decay is equivalent to the frequency-domain analysis of NRUS. Again, variation of the resonant frequency with amplitude indicates nonlinearity, and can be quantified simple as a ratio of change of frequency to change of amplitude.

2.3.3.3 Application to damage detection in composites

Van Den Abeele and Van de Velde (2000) have reported the success of resonant techniques for inspection of E-glass reinforced polyester composites, for the detection of degradation caused by exposure to chemical treatments. NRUS was used to quantify corrosion and compare the results to measurements of mechanical properties. The authors found that nonlinearity parameter measured by NRUS showed a similar trend with increasing chemical exposure time to static mechanical properties measured through flexural and tensile tests. A follow-up study by Van Den Abeele et al. (2001a) using the same specimen type and damage case explicitly compared flexural modulus and tensile strength of the specimens, with their results reproduced here in Figure 2.17. These results show excellent correlation between an increase in nonlinearity parameter and decrease in mechanical properties for two different chemical treatments.

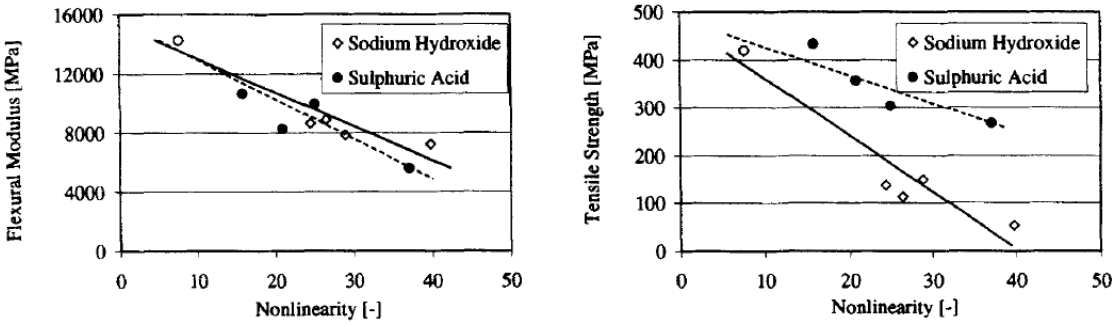

Figure 2.17: Nonlinearity measured by NRUS, against flexural modulus and tensile strength for E-glass reinforced polyester specimens (Van Den Abeele et al., 2001a)

A study by Van Den Abeele et al. (2001b) investigated the use of NRUS to measure nonlinearity of artificial slate tiles used as roofing material. Samples were subjected to cyclic fatigue loading, and multiple measurements taken of both linear and nonlinear parameters after a number of cycles. The linear parameters measured were wavespeed and wave dissipation (damping ratio) while the nonlinear parameter was equivalent to α in (2.13). As each measurement was taken, the static Young's modulus E was also measured, and the stiffness degradation was used as a damage factor D. The findings of this study were that the nonlinear parameter measured by NRUS is much more sensitive than linear parameters (Figure 2.18).

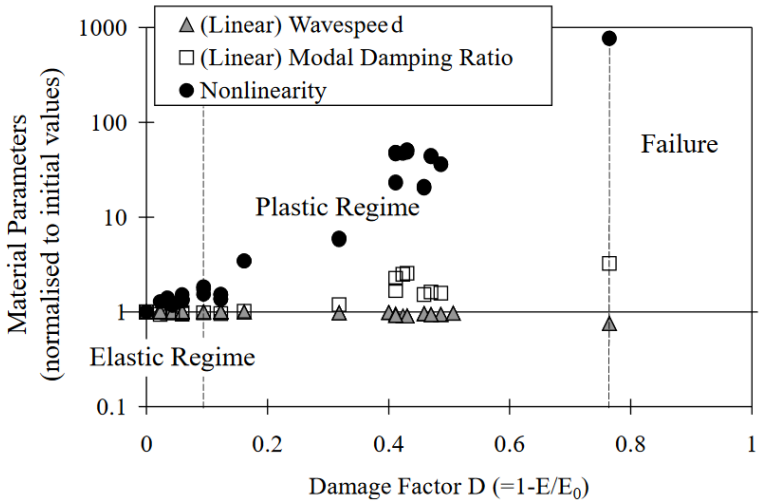

Figure 2.18: Evolution of linear and nonlinear parameters with reduction in static modulus, of artifical slate tiles subjected to fatigue loading (Van Den Abeele et al., 2001b)

The studies described until this point have correlated nonlinearity parameter measured through resonant techniques with material properties, but have not attempted to investigate the mechanism behind the nonlinearity, for example by imaging the damage and measuring crack growth. A more recent study by Van Den Abeele et al. (2009) set about to do just this, by imaging microcracks in CFRP caused by thermal degradation and correlating this to nonlinearity measured by NRS. The results from this work are shown in Figure 2.19.

These results may be interpreted by considering an entirely linear material, where the resonant frequency measurement would not vary with strain amplitude, and on Figure 2.19 would be represented by a horizontal line of slope 0. A decrease in resonant frequency with increasing strain amplitude is represented by a downward slope, with gradient equivalent to nonlinearity parameter α. These gradients are shown on the figure, with values of -1092, -2480, -7610 and -9163 for the four damage cases listed. The undamaged reference sample shows a non-zero value of nonlinearity, though this is consistent with other nonlinear ultrasonic studies where inherent material nonlinearity is present. A clear trend is present, with increased exposure to thermal loads (and at higher temperatures) leading to larger shifts in resonant frequency.

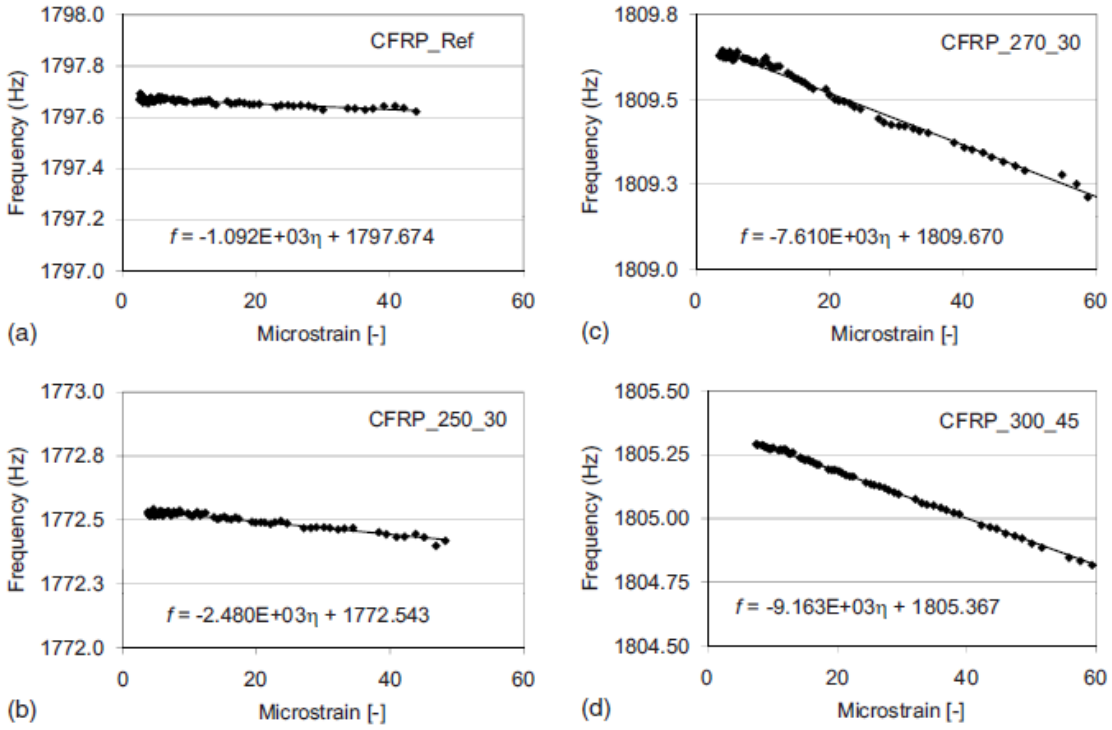

Figure 2.19: Resonant frequency as a function of strain amplitude, for a reference undamaged sample of CFRP and samples subjected to (b) 250°C for 30 mins, (c) 270°C for 30 mins, (d) 300°C for 45 mins (Van Den Abeele et al., 2009)

The authors then performed optical measurements of crack density in different parts of the thermally damaged CFRP by cross-sectioning through the specimens. Individual measurements of crack density are shown on Figure 2.20 as white diamonds, with black solid circles representing an average of these measurements per sample. The general observed trend is that increased nonlinearity correlates well with increased crack density. A very large spread in crack density data is observed, which the authors attribute to non-homogenous distribution of the micro-cracks within the sample. No further insight is provided, for example what the distribution of the cracks is within each sample, or exactly what was being measured when the reference sample was said to have non-zero crack density. The authors suggest that the observed similarity in crack density of the reference sample to the sample treated at 250°C for 60 minutes may indicate that the optical measurement is incapable of resolving the microstructural changes which precede macro-scale fracture surfaces. There is an increase in nonlinearity of almost 200% between the samples, indicating that some change has taken place.

Other studies have investigated nonlinear resonance for detection of fatigue damage in steel and delamination damage in composite laminates (Van Damme and Van Den Abeele, 2014) and accumulated micro-cracks in human bone (Muller et al., 2005; Muller et al., 2008). The technique has been shown to be capable of predicting a degradation of mechanical properties

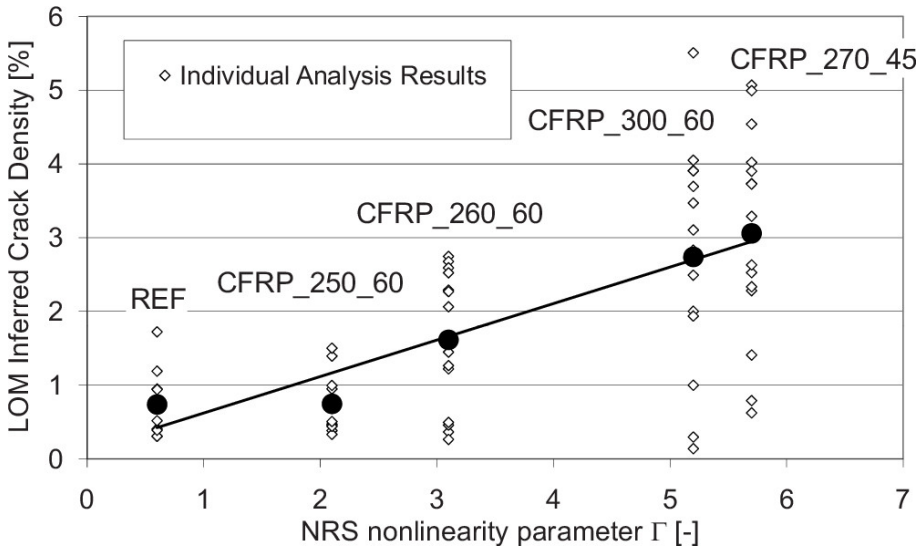

Figure 2.20: Crack density vs nonlinearity parameter for temperature loaded CFRP samples. White diamonds are obtained for individual parts of each image, solid black circles are averaged results per sample (Van Den Abeele et al., 2009)

for a variety of composite materials and damage types by an increase in nonlinearity, though the only data which attempts to match this to a physical mechanism is not definitive (Van Den Abeele et al., 2009). As pointed out by Muller et al. (2008) in their in-depth study on bone micro-damage, more work is required to combine the nonlinear resonant measurements with proper micro-damage quantification and characterisation. Even so, the technique appears to have good sensitivity and broad applicability as a measure of nonlinearity.

2.3.4 Frequency mixing

Frequency mixing is a nonlinear phenomenon occuring when two waves interact in a nonlinear medium. The result of this interaction is the generation of multiple new frequency components which can then be used to detect and characterise damage. Nonlinear vibro-ultrasonics is an example of a technique based on frequency mixing.

2.3.4.1 Theory

The simple one-dimensional case of nonlinear-elastic wave propagation, originally presented in Section 2.3.2, is now revisited for a case where two excitations are present. For a thin, circular rod the modified Hooke's Law behaviour is given by

$$\rho \frac{\partial^2 u}{\partial t^2} = E_0 \frac{\partial^2 u}{\partial x^2} + 2\beta E_0 \frac{\partial u}{\partial x} \frac{\partial^2 u}{\partial x^2} \tag{2.3}$$

where u is displacement, ρ is density and σ is stress, β is the first-order nonlinearity parameter. To obtain a solution to this, perturbation theory is applied with the displacement field u now containing two terms, corresponding to two excitations:

$$u = u_0 + u' \,, \qquad u_0 = A_1 cos(k_1 x - \omega_1 t) + A_2 cos(k_2 x - \omega_2 t) \tag{2.14}$$

where u_0 represents an initial excitation and u' the first order perturbation. This differs from the previous analysis where the initial excitation was a single sinusoid. In this case, the excitation is the linear combination of two waves, each with its own amplitude and frequency. An example solution to equations (2.3) and (2.14) is shown in Figure 2.21, for two sinusoidal excitations with frequencies ω_1 and ω_2. The solution in the time domain shows a wave of frequency ω_2, amplitude-modulated by the lower frequency ω_1. The frequency domain of this solution reveals multiple terms, corresponding to:

(i) original excitation terms, with frequencies ω_1 and ω_2

(ii) higher harmonic terms of excitations, with frequencies $2\omega_1$ and $2\omega_2$

(iii) mixed terms, with sum and difference frequencies $\omega_2 - \omega_1$ and $\omega_2 + \omega_1$, referred to as *sideband frequency components*

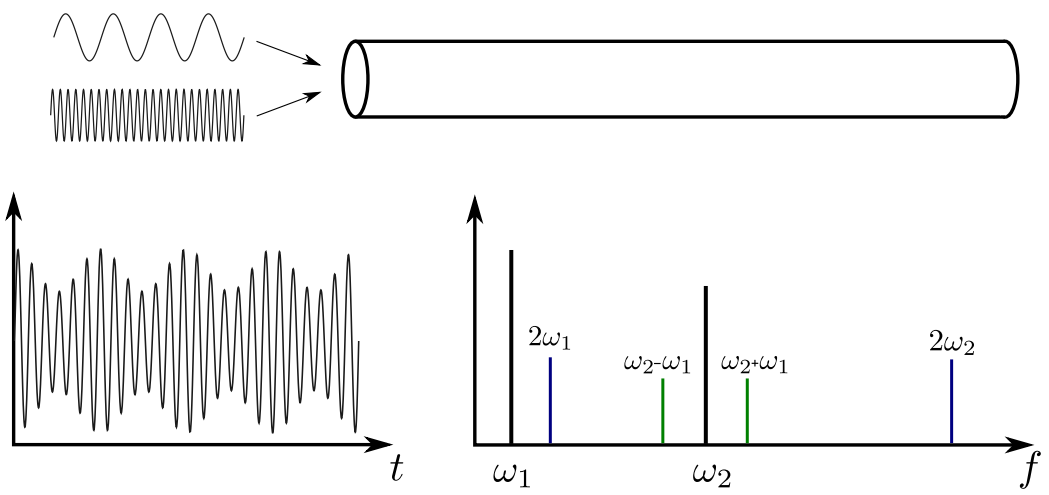

Figure 2.21: Frequency mixing solution in first-order-nonlinear medium, using first-order perturbation analysis. Original excitations (black), higher harmonics (blue) and sidebands (green) are present.

The amplitude of each of these terms is a function of the original amplitudes and the nonlinearity parameter, for example the mixed terms have amplitude proportional to $\beta A_1 A_2$.

Just as for the higher harmonics analysis presented in 2.3.2, if the perturbation analysis were extended to higher orders, it is found that additional higher order terms are also created. In the case of higher harmonic terms, these are frequencies of 3ω, 4ω and so on, while the mixed terms have frequencies of $\omega_2 \pm 2\omega_1$, $\omega_2 \pm 3\omega_1$ and so on.

Figure 2.22 shows strain spectra for the frequency mixing phenomenon, zoomed around the higher frequency ω_2, for a linear case and for 1$^{\text{st}}$-order (β) and 2$^{\text{nd}}$-order (δ) nonlinearity. This shows that for the purely 2$^{\text{nd}}$ order nonlinearity (δ) the sidebands are limited to the "even" terms $\omega_2 \pm 2\omega_1$, $\omega_2 \pm 4\omega_1$ and so on. This demonstrates that the spectrum contains information about the nature of the nonlinearity. For waves interacting in real structures, this is equivalent to containing information about the physical nonlinear mechanism.

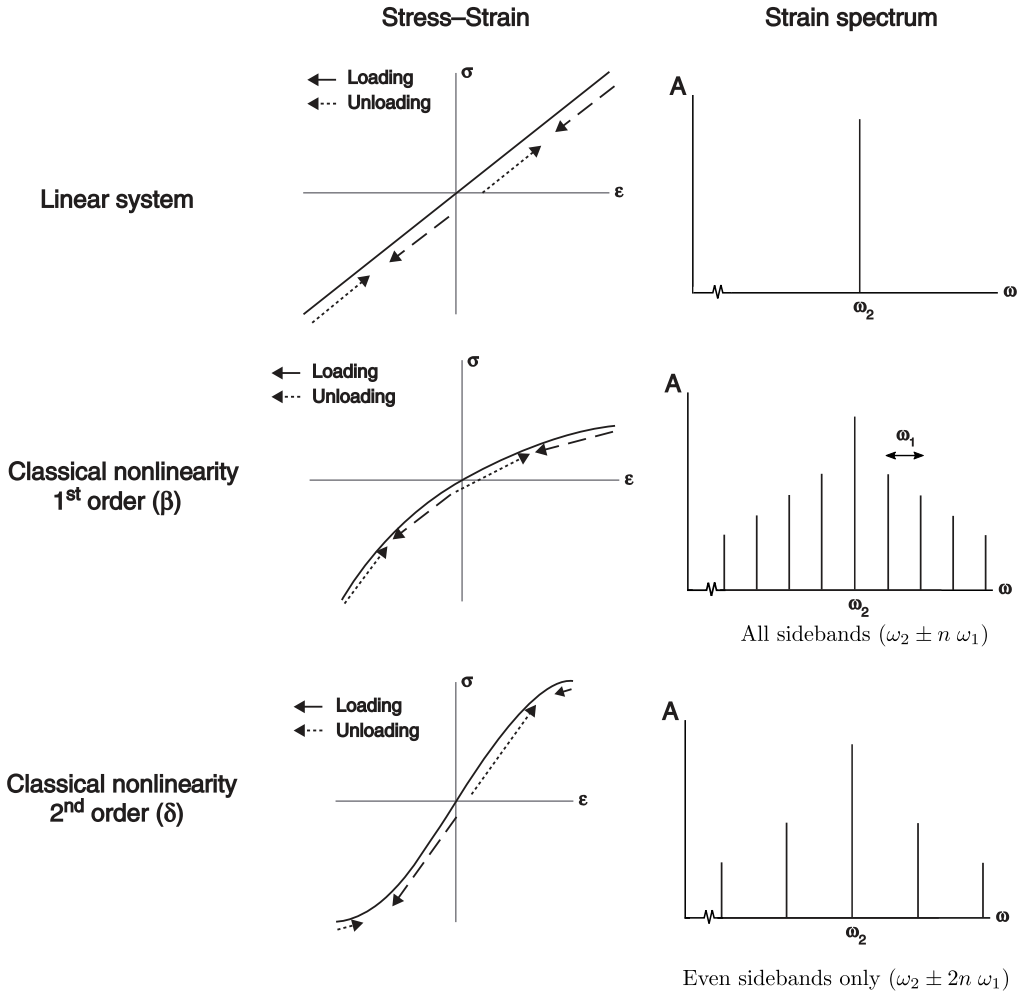

Figure 2.22: Stress-strain relations and strain spectra for frequency mixing, adapted from Klepka (2013)

2.3.4.2 Application to damage detection

The phenomenon of nonlinear frequency mixing has lead to the development of a number of experimental ultrasonic techniques for damage detection and characterisation. The basic principle of the techniques is the same as for higher harmonic ultrasonic techniques, which is to use generated frequency components as a measurement of nonlinearity, and correlate this nonlinearity parameter to material degradation or the presence of damage. While frequency mixing occurs no matter the relative frequency of the two waves, typically the technique involves the mixing of a high-frequency, low-amplitude ultrasonic wave (a so-called *probing* wave) and a low-frequency, high-amplitude vibration wave (or *pumping* wave).

For example, consider the case where a structure with first-order nonlinearity is excited simultaneously by signals of amplitude A_1 and A_2, and that the sideband frequency components

have amplitude proportional to $\beta A_1 A_2$

$$A_{sideband} \propto \beta A_1 A_2 \qquad \therefore \beta \propto \frac{A_{sideband}}{A_1 A_2} \tag{2.15}$$

In this case the nonlinearity of a structure may be calculated by measuring the amplitude of the sideband frequency component (or taking an average of the pair of sidebands) and normalising by the input amplitudes. Because the sidebands represent amplitude- or frequency-modulation of the probing wave by the pumping wave, this calculated parameter is often referred to as modulation index (Donskoy et al., 2001; Sutin and Johnson, 2005; Amerini and Meo, 2011) or modulation intensity (Parsons and Staszewski, 2006; Klepka et al., 2012).

Techniques making use of nonlinear modulation phenomena have been investigated for detecting a variety of structural defects. Early work in the field by Korotkov et al. (1994) showed sensitivity of the method to detecting small cracks in metal, and subsequent work by Sutin and Nazarov (1995) showed applicability to fatigue cracks in graphite electrodes. The technique has since been demonstrated for detection of fatigue cracking in steel pipe welds (e.g. Sutin and Donskoy, 1998) and aluminium plates (e.g. Zaitsev and Sas, 2000), as well as cracks in non-metallic structures such as plexiglas and sandstone (e.g. Van Den Abeele et al., 2000).

In recent years, research into the application of these techniques to inspect composite structures has gained popularity. The majority of research concerns detection of low-velocity impact damage, including barely-visible impact damage, in fibre-reinforced composite laminates (e.g. Meo et al., 2008; Aymerich and Staszewski, 2010a; Chrysochoidis et al., 2011b) and composite sandwich panels (e.g. Meo and Zumpano, 2005; Klepka et al., 2013; Pieczonka et al., 2014). Other studies have also investigated frequency mixing phenomena for the detection of artificial delamination damage (Chrysochoidis et al., 2011a) and matrix cracking (Chrysochoidis et al., 2015) in composite laminates.

2.3.4.3 Advantages over higher harmonic techniques

There are a number of commonly cited advantages of techniques which exploit frequency mixing over the higher harmonic techniques. A modified version of the previous solution to frequency mixing is shown in Figure 2.23 to help to illustrate some of these advantages, considering a case of a probing wave of frequency ω_2 modulated by a pumping wave of frequency ω_1.

Recall that when two waves interact, higher harmonic terms are generated in addition to sideband frequency components. In Figure 2.23 three higher harmonics of the ultrasonic probing wave are shown. An NDT technique using higher harmonic response for damage

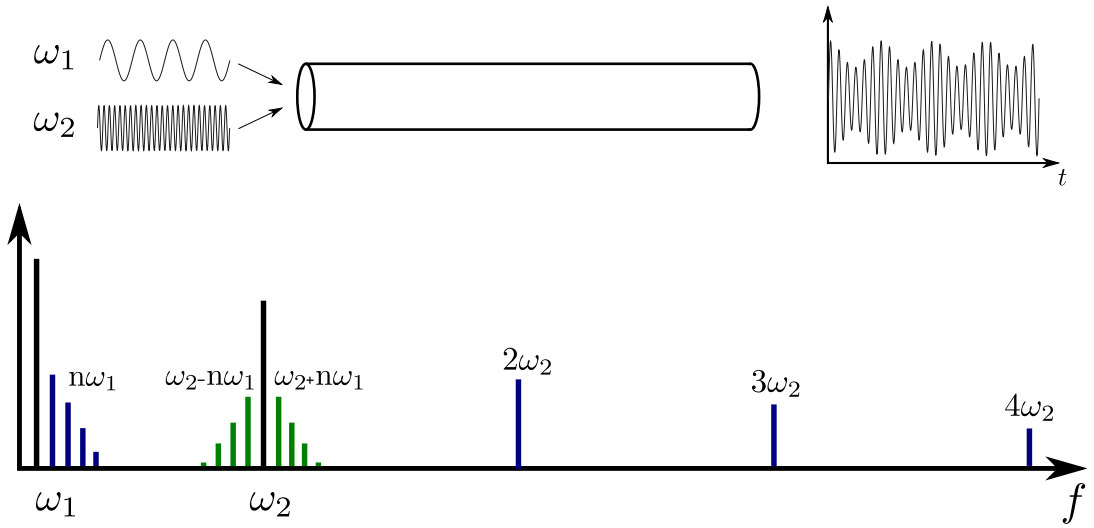

Figure 2.23: Frequency mixing solution in first-order-nonlinear medium. Original excitations (black), higher harmonics (blue) and sidebands (green) are present.

detection would probe the structure with a frequency of ω_2 and measure response at $2\omega_2$, $3\omega_2$, $4\omega_2$. A technique utilising frequency mixing phenomena however would probe the structure with the same frequency ω_2 but measure response at $\omega_2 \pm n\omega_1$, which are frequencies much closer to the probing frequency than the higher harmonics. This is an advantage due to two practical considerations. The first is that higher frequencies attenuate much more rapidly, as noted by Donskoy et al. (2006). The second consideration is that measurement equipment such as piezotransducers and signal digitizers may have a limited measurement range prohibiting them from detecting such higher frequencies. It is likely that instrumentation systems used to excite and measure ultrasonic waves at the probing frequency are capable of taking measurements at the similar sideband frequencies, while for example response curves of measurement transducers and sample rates of digitizers can limit measurements.

The most commonly cited advantage to measuring sidebands rather than higher harmonics however is related to the nonlinearity of instrumentation systems. Zaitsev and Sas (2000) note that nonlinear distortions in electrical circuits, actuators used to provide excitation and sensors used to measure response can mask nonlinear response of structures. Donskoy et al. (2001) state that practical implementation of a system to measure higher harmonics for damage detection requires careful minimisation of these nonlinear distortions. These authors are referring to harmonic distortion, where an electrical signal acquires overtones of its frequencies, i.e. higher harmonics. Instrumentation producing excitation signals inherently create this distortion, which will be carried through actuators into the structure under inspection. Figure 2.24 shows diagrammatic example spectra of a case with instrumentation distortion, where the contribution of nonlinearity from the structure may be masked, particularly if it is small relative to harmonic distortion effects.

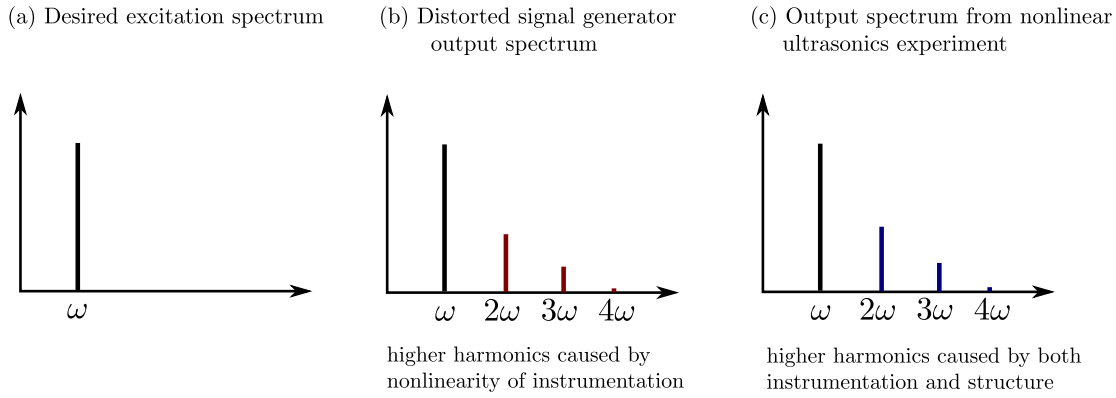

Figure 2.24: Example spectra of (a) desired excitation signal, (b) signal generator construction of this signal and (c) an example output from a nonlinear structure.

According to Solodov et al. (2010) this distortion is inevitable and unavoidable in a practical implementation, and describe an illustrative example where the background noise of a second-harmonic imaging method rendered it incapable of discerning a defect. Figure 2.25 shows this image, as well as sideband-based imaging of the same plate which shows improved noise levels.

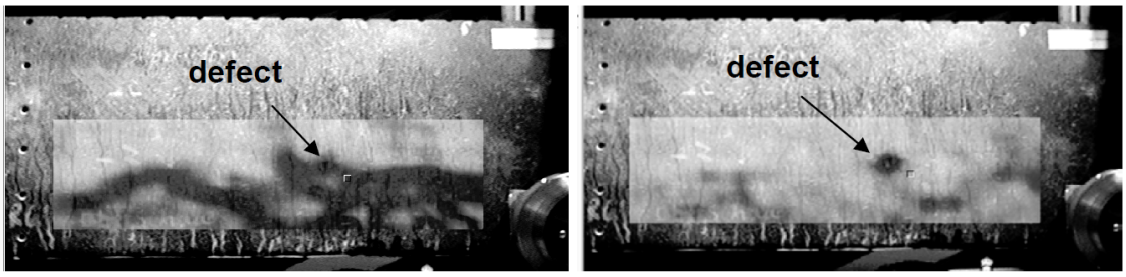

Figure 2.25: Background noise in second-harmonic imaging of a stringer debond (left). Sideband-based imaging of the same plate (right) shows improved noise levels. (Solodov et al., 2010)

That the experimental instrumentation nonlinearity typically appears at the same frequencies as material and defect nonlinearity necessitates the use of expensive hardware designed to minimise nonlinearity (Zagrai et al., 2008). Eliminating this need means that frequency mixing techniques are relatively simpler to implement.

2.3.4.4 Variations of techniques

Techniques making use of frequency mixing phenomena must necessarily excite the structure at two frequencies, in order to observe and measure sideband frequency components. How this is achieved varies from study to study, particularly where the low-frequency pumping wave is concerned.

Many important early studies into frequency mixing phenomena (e.g. Sutin and Donskoy, 1998; Van Den Abeele et al., 2000; Donskoy et al., 2001) showed results for two techniques, referred to as *impact modulation* and *vibration modulation*. In the impact modulation technique, an instrumented impact hammer is used to excite low-frequency modes of a structure while an ultrasonic wave is used to probe. A commonly cited advantage of the method is that the vibrations will occur at structural resonances, which according to Zaitsev et al. (2006) creates the best conditions for measuring sidebands as the pumping excitation amplitude is maximised. As illustrated by Sutin and Johnson (2005) the convenience of the impact hammer excitation allows for inspection of parts of varying shapes, sizes and materials.

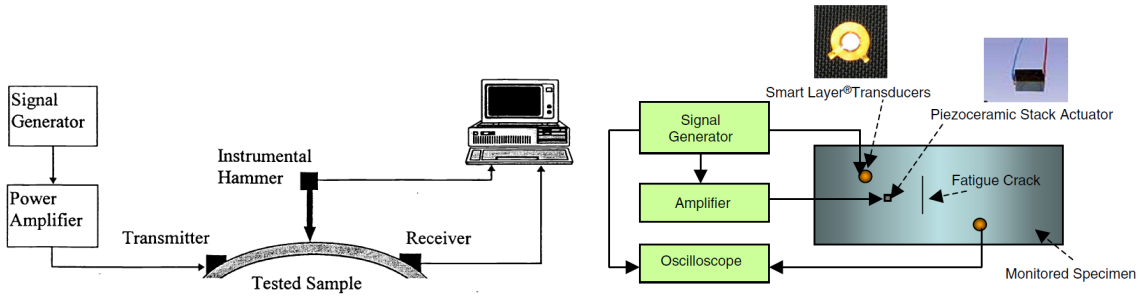

(a) impact modulation (b) vibration modulation

Figure 2.26: Example system configurations for (a) impact modulation (taken from Sutin and Donskoy, 1998) and (b) vibration modulation (taken from Parsons and Staszewski, 2006)

Vibration modulation on the other hand employs forced harmonic vibration of a structure at a particular frequency. The major differences to impact modulation are that the pumping frequency can be chosen arbitrarily rather than only at structural resonances, and that the vibration is typically continuous, exciting a steady-state standing wave rather than a transient, decaying wave. The vibration excitation is commonly provided by an electromagnetic vibration shaker (e.g Kazakov et al., 2002) or by piezoceramic transducers (e.g. Van Den Abeele et al., 2000). In some cases, the technique has shown to work with vibration provided by non-contact (air-coupled) transducers (Lim et al., 2014b) or a speaker (Polimeno and Meo, 2008).

Studies by Kim et al. (2003, 2004) used a 5 MHz ultrasonic wave to probe aluminium samples during different stages of fatigue testing. The samples were not removed from the cyclic tensile fatigue loading machine for this testing, meaning the 10 Hz cyclic tensile load acted as a pumping wave on the samples, modulating the probing wave. The applied tensile load also had a static component, meaning tests could be performed on the sample under different stress states. A similar technique was used by Zagrai et al. (2008), except that the fatigue test was under three-point bending rather than axial load. The use of such a technique is useful for collecting experimental data for a range of damage states, starting with an intact sample progressing through microstructural changes and developing meso- and macroscale damage.

A slight modification to these modulation techniques is described by Zaitsev et al. (2002). Their method, referred to as *cross-modulation*, involves exciting a structure by a pumping wave which itself is amplitude modulated, as in Figure 2.27. The result of this method is that the amplitude modulation is tranferred to the probing wave. The resultant, generated sideband components are then at the original probing frequency plus-and-minus the modulating frequency of the pumping wave, rather than the central pumping frequency.

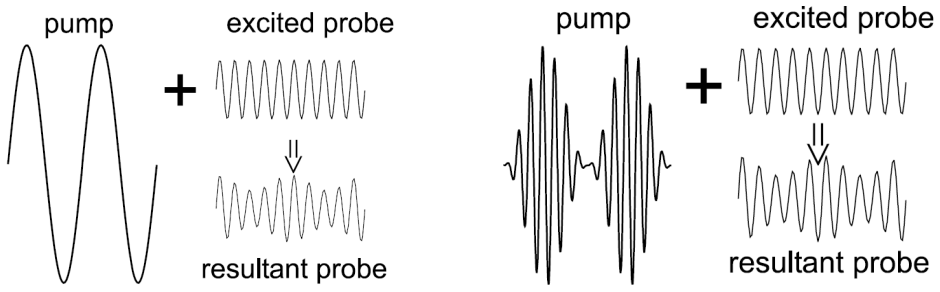

(a) conventional modulation (b) cross-modulation

Figure 2.27: Schematic of pump and probe excitations and resultant (measured) signal, comparing (a) conventional modulation and (b) cross-modulation. (Zaitsev et al., 2002)

Frequency mixing techniques have been referred to by authors by many names, such as vibro-acoustic modulation (e.g. Donskoy et al., 2001), nonlinear ultrasonic modulation (e.g. Sohn et al., 2013), and nonlinear wave modulation spectroscopy (e.g. Van Den Abeele et al., 2000). In this thesis, particular focus is given to nonlinear ultrasonic techniques where vibration pumping excitation is used. For this reason, the terminology nonlinear vibro-ultrasonics is used. The next section provides more detailed background information to these methods in particular.

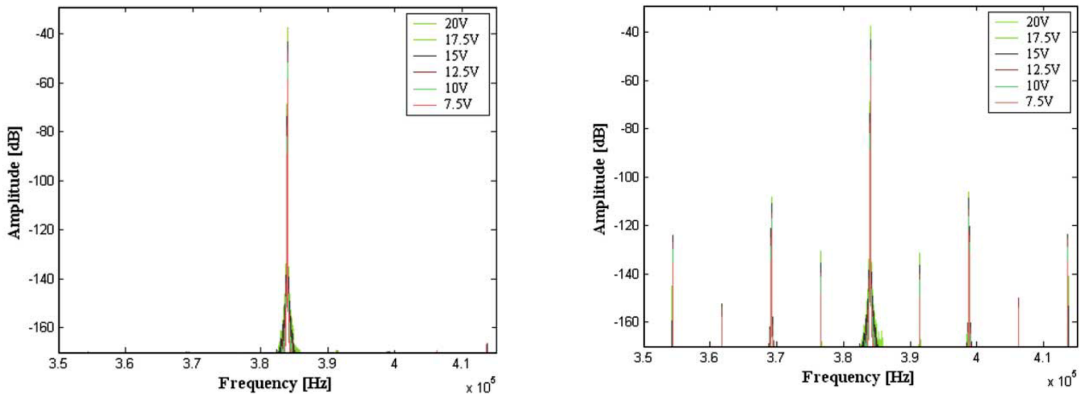

(a) intact panel (b) panel after impact test

Figure 2.28: Nonlinear vibro-ultraonic spectra of sandwich panels from firewall of a helicopter. (Meo and Zumpano, 2005)

2.4 Nonlinear vibro-ultrasonics

This section provides detailed information on previous studies of nonlinear vibro-ultrasonics, with particular attention given to investigating effectiveness at detecting defects in composite materials.

2.4.1 Application to damage detection in composites

As with other nonlinear ultrasonic techniques, much study of nonlinear vibro-ultrasonics is for the purpose of detecting damage in metal structures, particularly the progression of fatigue damage. While the application to composite materials has been studied in less detail, there exists promising research in the area.

Important early work in the field of nonlinear vibro-ultrasonics by Sutin and Donskoy (1998) and Donskoy et al. (2001) described the technique and results for metallic structures, and both works remark that the technique can also be applied to composite materials. Neither of these papers demonstrate results for composite materials nor go into further detail about applicability, though Donskoy et al. (2001) comment that composite parts used in the aerospace industry, with and without defects, have been examined.

2.4.1.1 Impact damage detection

The first study appearing to contain experimental detail and experimental results for the technique applied to composite parts was from Meo and Zumpano (2005). In this work, a sandwich panel from the firewall of a helicopter was examined, consisting of a 6.35 mm thick honeycomb core with 2 mm thick laminate face sheets. Piezoceramic transducers were used to

produce both a 7.4 kHz pumping wave and a 384 kHz probing wave. While the plate was intact, no sideband frequency components were observed. After a 1 mm diameter, 5 mm deep hole was formed through an impact test, sidebands were visible in the frequency spectrum. These spectra are shown in Figure 2.28, with the test repeated for pumping wave amplitudes from 7.5 V to 20 V. The authors conclude that these spectra alone are a ”clear indication” of the presense of damage including fibre breakage and matrix cracking in the face sheets, as well as crushing of the core. No mention of visual or other inspection of the plates to characterise this damage appeared in the paper. Nevertheless, these results at least show that a greater degree of nonlinearity was observed for the sample after impact testing.

A similar study by Meo et al. (2008) compared three measures of nonlinearity, including nonlinear vibro-ultrasonics, for impact damage in composite laminate plates. Two plates were impacted by a 9 J and 10 J impact respectively, to create areas of delamination. These areas were quantified using C-scan ultrasound. The results of their nonlinear vibro-ultrasonic testing are shown in Figure 2.29, with the plate with larger delamination area (red triangles) producing larger sidebands in general.

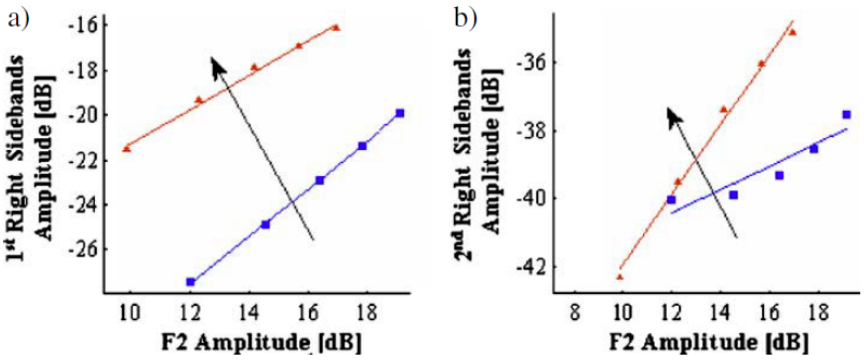

Figure 2.29: Results from nonlinear vibro-ultrasonic inspection of impacted composite laminate plates. Red triangle data points are for the plate with the larger delamination area. F2 Amplitude refers to probing wave amplitude. (Meo et al., 2008)

Many details of the investigation are missing from the paper including how the low- and high-frequency excitations were applied, which frequencies were used for testing, how signals were measured and what the resulting areas of delamination were for each impact energy. The conclusion of the paper is that nonlinear vibro-ultrasonics can be used to assess damage magnitude, agreeing with their results for a higher-harmonic method and a nonlinear resonance method (shown earlier in Figure 2.16). Interestingly in Figure 2.29(b) the data points for both panels at a probe wave amplitude of 12 dB are very close, while for higher probe wave amplitudes the trends separate. Compare this to the results for second- and third-harmonic from the same paper in Figure 2.30, which show consistent, parallel trends for the two plates. These results indicate variation in the ability of particular system parameters to predict nonlinearity measurements.

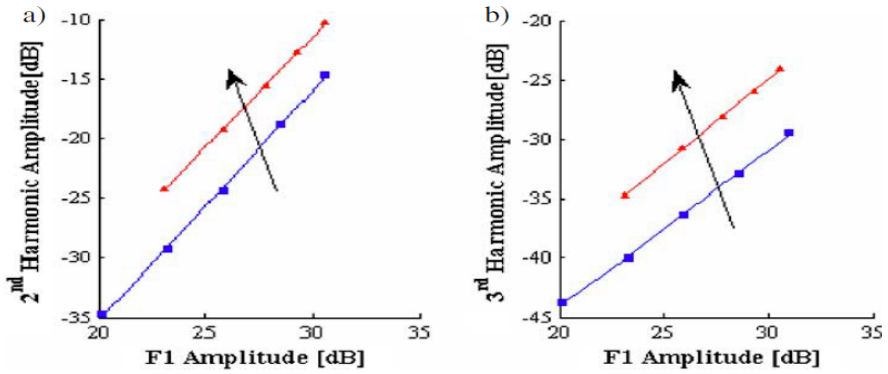

Figure 2.30: (a) 2nd harmonic and (b) 3rd harmonic amplitude from inspection of impacted composite laminate plates. Red triangle data points are for the plate with the larger delamination area. F1 Amplitude refers to pumping wave amplitude. (Meo et al., 2008)

Two studies by Aymerich and Staszewski (2010a, 2010b) also investigate nonlinear vibro-ultrasonics for detection of impact damage. A carbon/epoxy composite laminate of 2 mm thickness was impacted twice by a drop-weight apparatus to induce progressive damage. The panel was inspected by nonlinear vibro-ultrasonics in the intact state as well as after each impact, to observe the growth of sideband frequency components. The authors give good detail of their experimental setup, which saw the panel supported at one end by a clamp using a servo-electric testing machine (allowing for control of clamping force), with the other end left free to create clamped-free boundary conditions. Piezoceramic transducers were used to excite and measure the probing wave, and an electromagnetic vibration shaker provided pumping excitation.

In their first study Aymerich and Staszewski perform multiple nonlinear vibro-ultrasonic tests, with pumping frequencies of 77 Hz, 262 Hz and 2934 Hz used, determined through earlier modal analysis of the plate. The results of this testing for the 77 Hz pumping frequency case is shown in Figure 2.31. Importantly, the frequency spectrum for the damage before impact testing (damage-free state) contains sideband frequency components, indicating the presence of inherent nonlinearity. After each impact, the amplitude of these sidebands grows, with the second pair of sidebands (located 144 Hz from the central frequency) exhibiting largest growth.

Figure 2.32 shows the average increase in sideband amplitude compared to the damage-free case for both impact energy levels and all three pumping frequencies. Particularly interesting in these results is that for a pumping frequency of 2934 Hz, the 2.04 J impact energy case actually caused a decrease in average sideband amplitude. These results highlight the dependence of sideband amplitude not only on the level of nonlinearity in the specimen but also of system parameters selected.

The second study of interest by Aymerich and Staszewski (2010b) instead used the cross-modulation variation of nonlinear vibro-ultrasonics to inspect similar carbon/epoxy

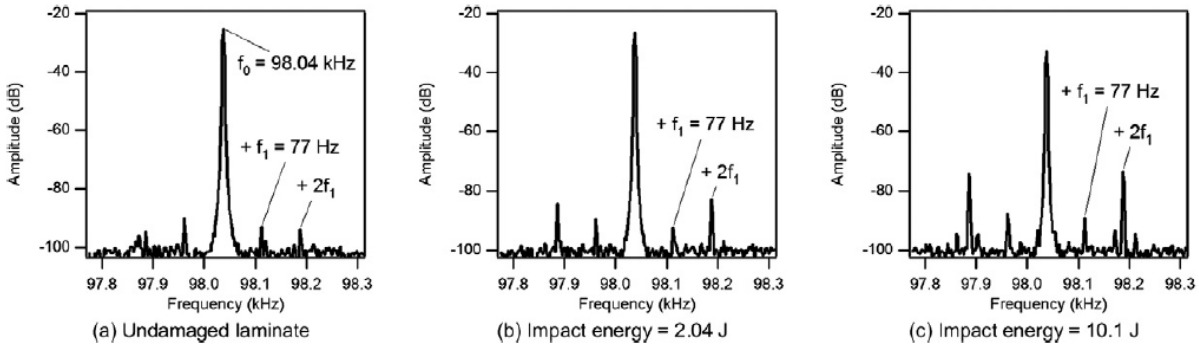

Figure 2.31: Spectra from nonlinear vibro-ultrasonic inspection of composite panels with impact damage. (Aymerich and Staszewski, 2010a)

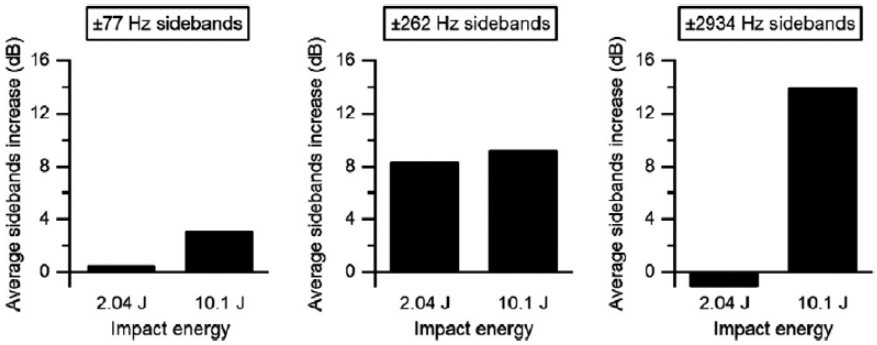

Figure 2.32: Average increase in sideband amplitude compared to damage-free case for composite panels with intact damage, various frequencies. (Aymerich and Staszewski, 2010a)

composite laminates, though this time with five increasing energy levels. They used amplitude measurements of the fundamental frequency of the probing wave and of generated sidebands to calculate the following damage indices (DI) for comparison:

$$\mathrm{DI}_1(\mathrm{dB}) = \left|A_{f_0} - A_{sb}\right|_{undamaged} - \left|A_{f_0} - A_{sb}\right|_{damaged} \tag{2.16}$$

$$\mathrm{DI}_2 = \frac{(V_{sb}/V_{f_0})_{damaged}}{(V_{sb}/V_{f_0})_{undamaged}} - 1 \tag{2.17}$$

where A_{f_0} and V_{f_0} are the amplitude of the fundamental frequency of the probing wave, in dB and volts respectively, and A_{sb} and V_{sb} are the average amplitude of the first pair of sidebands, in dB and volts respectively. These damage indices were compared by observing their trends with impact energy, projected delamination area and cumulative dissipated energy, with results shown in Figure 2.33. The authors interpret these results to indicate the indices are sensitive to initial damage in the panels (the increase in nonlinearity between intact and 2.04 J impact energy) as well as initiation of local crushing and penetration (the increase between 6.97 J and 10.1 J energy levels). It appears from these results that DI_1 shows greater sensitivity to the initial damage due to the log scale of dB.

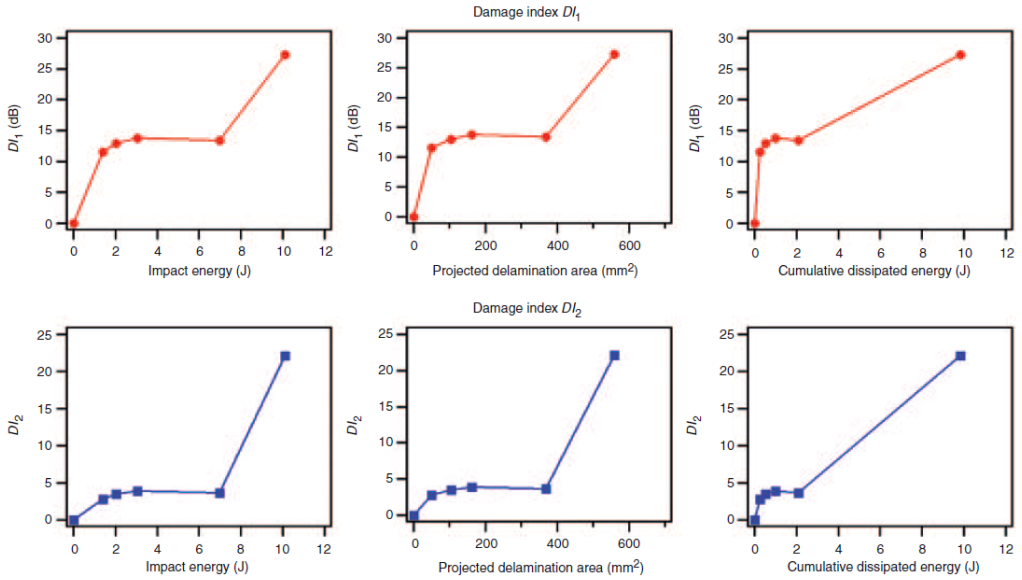

Figure 2.33: Comparison of two damage indices calculated from nonlinear vibro-ultrasonic testing. (Aymerich and Staszewski, 2010b)

2.4.1.2 Other damage types

Very few studies have been conducted to investigate the application of nonlinear vibro-ultrasonics to detect non-impact induced damage in composites.

One such study, by Chrysochoidis et al. (2011a), looked at detection of an artificial delamination in a composite laminate, created by insertion of a PTFE film during curing. Using piezos for both the low- and high-frequency excitations, they provide results for a number of tests where a beam with artificial delamination exhibits a greater degree of nonlinearity than the pristine specimen. They also provide results for some combinations of input parameters (low, high frequencies) where no sidebands are present, even in the specimens with artificial delamination damage.

Another study, by Chrysochoidis et al. (2015), looked at matrix cracks in composite laminate beams that were induced through three-point bending. Their findings show that the nonlinearity of samples with matrix cracks is higher than a pristine specimen, with a trend of greater nonlinearity for samples which registered more acoustic emission during three-point bending. Their results also highlight that probing frequencies exist for which a higher amplitude is present in the output signal for samples with damage. The authors attribute this result to modified linear propagation of ultrasonic Lamb waves due to matrix cracks in the outer plies.

2.4.2 Influence of frequency selection

Some studies present results which indicate that selection of excitation frequency, both for pumping and probing wave, may be an important influence in the results of nonlinear vibro-ultrasonic testing.

Klepka et al. (2013) present results for impact-damaged chiral-core composite sandwich structures, which are shown in Figure 2.34. In this study, two selections for the frequency of the pumping wave were compared: Figure 2.34(a) shows results using the first mode of vibration of the panel, 2.34(b) shows second mode of vibration.

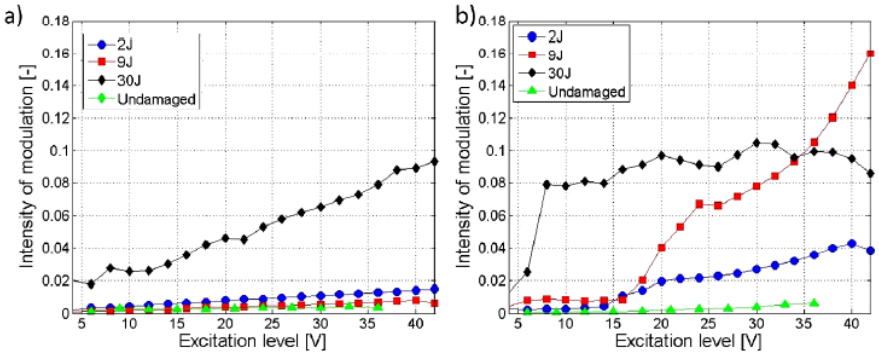

Figure 2.34: Intensity of modulation as function of excitation level, for (a) first mode and (b) second mode of vibration (Klepka et al., 2013).

These results show that the second mode of vibration produces greater differentiation of the undamaged, 2 J and 9 J impact energy cases, with a larger variation between them compared to using the first mode, for large excitation voltages. Though the magnitude of modulation intensity is similar for the 30 J impact energy case, the trend is much more clear and monotonic for the first mode.

A study from Klepka et al. (2014) investigates the effect of varying not only the low-frequency excitation but also the high-frequency. Figure 2.35 shows results using pumping excitation frequencies corresponding to the 5th modal frequency (left) and 7th modal frequency (right). Tests were conducted using a probing frequency of 43 kHz (top row) and 30.095 kHz (bottom row) - corresponding to a frequency where the defect responded maximally to vibration, which they term a local defect resonance.

These results show that the level of nonlinearity (modulation index, R) observed can vary significantly with either a change of low- or high-frequency selection. In addition, the relationship of modulation index with LF voltage is more monotonic for the 30.095 kHz case.

A study by Lim et al. (2014a) looked at two mock-up specimens, made of aluminium alloy 6061-T6 and representing aircraft wing fitting-lug connectors. One of the specimens had a 40 mm long fatigue crack, introduced by cyclic loading. A nonlinearity index was calculated

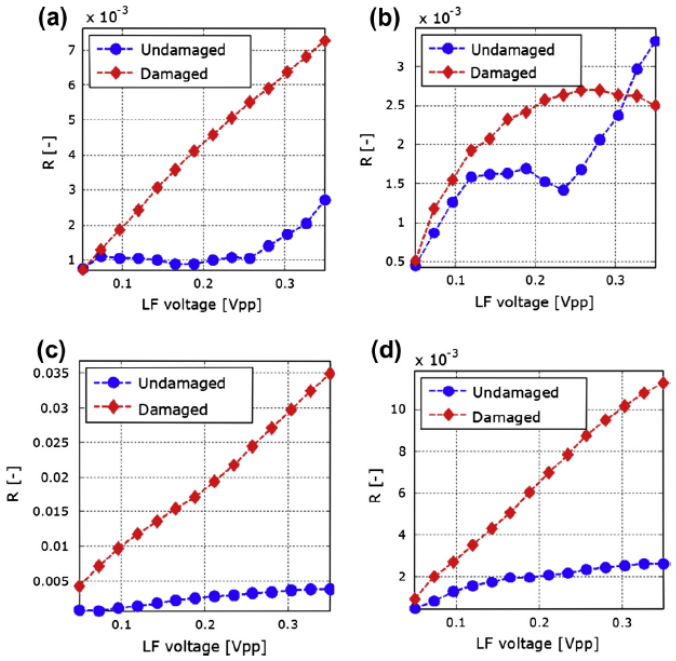

Figure 2.35: Effect of varying low-frequency and high-frequency input parameters in nonlinear vibro-ultrasonic inspection of composite panels with impact damage. (Klepka et al., 2014)

for a series of nonlinear vibro-ultrasonics experiments performed on the specimens where the low-frequency was varied. The results (Figure 2.36) show that the variation in nonlinear index is very small for the undamaged sample, but very large for the sample with the fatigue crack.

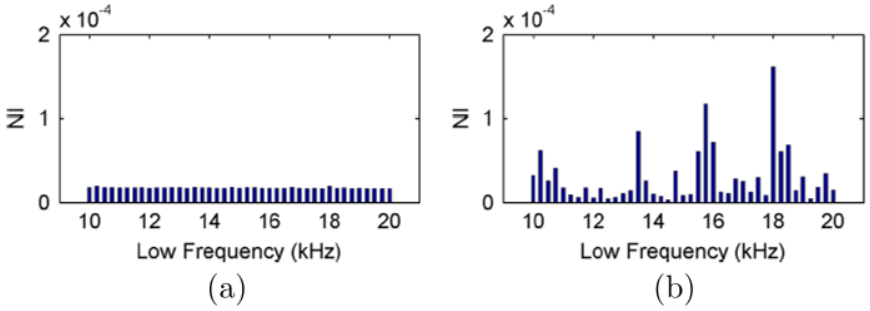

Figure 2.36: Nonlinearity index results for an intact (a) and damaged (b) specimens (Lim et al., 2014a).

While the nonlinear index does not exceed 2×10^{-5} for the intact specimen, many of the results for the damaged specimen exceed 5×10^{-5}. Interestingly, at some frequencies the nonlinear index appears to be smaller for the damaged sample than the undamaged. The authors of this study suggest using an outlier analysis of samples collected at a range of input frequencies (both for the pumping and the probing wave). These results show the importance of system parameters on the results of nonlinear vibro-ultrasonic experiments.

2.4.3 Influence of boundary conditions

Within a complex structure, joints and fixtures may act as sources of nonlinearity, which together with material nonlinearity can obscure nonlinearity caused by damage. Experimental investigations of nonlinear vibro-ultrasonics typically study a clamped-clamped or clamped-free structure, without mechanical fixtures or joints. The clamped boundary condition and the attachment of instrumentation to the test specimen are the only boundary conditions which could influence the result of testing.

Both studies by Aymerich and Staszewski (2010a, 2010b) include an investigation into the influences of clamping force on the nonlinearity present in the measured signal. Figure 2.37 shows the results for their vibration modulation experiments for two different clamping forces, 0.7 kN and 3.7 kN. The 3.7 kN clamping force results in a visible decrease in the amplitude of sideband frequency components.

Aymerich and Staszewski (2010b) varied the clamping force in their cross-modulation experiment between 500 N and 5000 N and observed changes in the fundamental (central) frequency amplitude as well as the average sideband amplitude (Figure 2.38). For both an undamaged and damaged specimen, average sideband amplitude decreases with increasing clamping force. The effect is more striking for the undamaged specimen as the results are

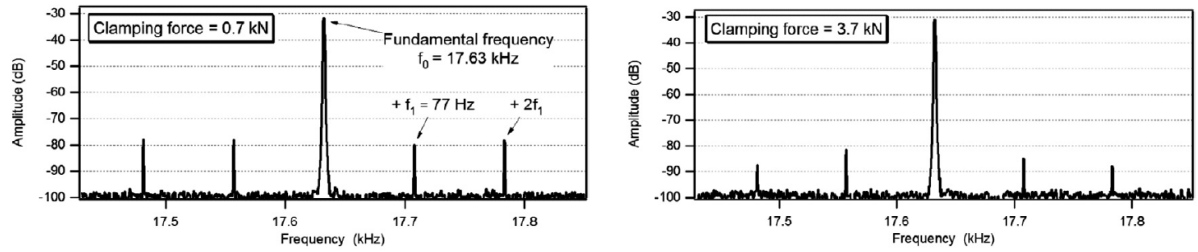

(a) (b)

Figure 2.37: Dependence of sideband amplitude on clamping force at end of specimen. (Aymerich and Staszewski, 2010a).

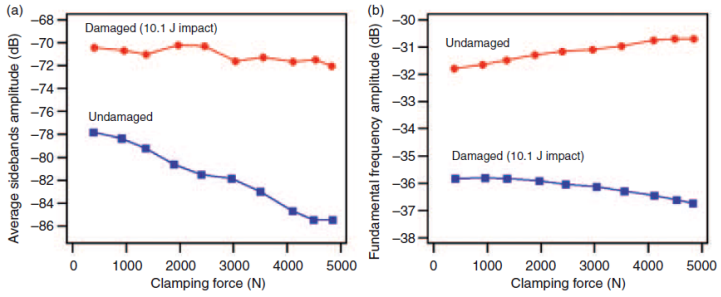

Figure 2.38: Fundamental frequency amplitude (left) and average sideband amplitude (right) from nonlinear vibro-ultrasonic testing of composite laminates. (Aymerich and Staszewski, 2010b)

presented on a log scale; in linear terms these results show an equal decrease in sideband amplitude for both specimens. The results for probing frequency amplitude show an increase for increasing clamping force for the undamaged specimen, but an accompanying decrease in amplitude for the damaged specimen.

The mechanism for decreased nonlinearity for increased clamping force is likely related to contact at the clamp-specimen interface, especially motion/friction at the boundary. As the clamping force increases, relative motion of the contact surfaces is restricted and less nonlinear dissipation of energy due to friction occurs.

The results of these studies demonstrate the influence of boundary conditions on measured nonlinearity, and highlight the importance of ensuring that nonlinearity does not occur at joints and fixtures of the apparatus.

2.5 Summary of gaps in literatures

Nonlinear vibro-ultrasonic testing is an emerging technique when it comes to inspection of composite materials. The review of literature provided here has highlighted the following important points:

- There is evidence that damage in composite materials is sensitive to nonlinear ultrasonics techniques, and that the use of such techniques can provide greater sensitivity than traditional, linear ultrasonic techniques.
- Nonlinear distortions in electrical circuits, actuators used to provide excitation and sensors used to measure response can mask nonlinear response of materials under inspection. It is therefore important to consider methodologies, instrumentation and experimental parameters which aim to minimise systemic nonlinearity.
- Experimental parameters such as selection of excitation frequencies are important, and the measurement of nonlinearity can vary depending on this selection. It is therefore important to develop a methodology where a range of parameters are investigated.
- The influence of boundary conditions on measured nonlinearity needs to be taken into consideration, and it is important to ensure that nonlinearity of joints and fixtures of the testing apparatus does not obscure nonlinearity due to damage in the material under inspection.

The review of literature has also revealed in addition that the following points have not been discussed in great detail, to the knowledge of the author, and must be brought to attention:

- There exist very limited studies which investigate the application of nonlinear vibro-ultrasonic techniques to non-impact induced damage in fibre-reinforced composites. In particular few studies have investigated adhesive joints in composite structures, and very few have investigated delamination damage other than those caused by impact.
- Resonant frequencies of the system are often selected for low-frequency vibration excitation, with little to no reasoning provided. There are very limited examples of tests performed with frequencies that do not correspond to resonant frequencies, and it is therefore important to understand what effect on results this choice has.
- Most studies do not pay regard to the boundary conditions of the experimental apparatus and those that do mainly discuss the clamping and support fixtures with no mention of

instrumentation which is attached to the specimen, which together with instrumentation cabling could be either a source of nonlinearity or have an influence on the vibration response of the system.

- In many cases, no details are provided on the electronic instrumentation used to acquire measurement samples. All electronic components have inherent nonlinearity, and some of these components may influence the detectability of damage in samples by providing additional nonlinearity to measurements. It is therefore important not only to understand the nonlinear behaviour of instrumentation but also to minimise it.

- The vast majority of studies report spectra for pristine specimens containing no sidebands whatsoever, though no mention of limiting noise floor is made. If less noise were present in the signal, the spectrum could well reveal the presence of sidebands.

  In addition, very little information is reported on the signal processing methods used to obtain results in nonlinear vibro-ultrasonic testing; signal processing is also a big factor on discernibility of sidebands above background noise level.

- Few studies attempt to correlate the growth of damage in a specimen with nonlinearity parameters. For example, microscopic imaging of the defect could be used to measure cracks in the composite matrix or the region at the edge of delaminations, and compare this between specimens.

Chapter 3

Experimental system and analysis

3.1 Introduction

3.1.1 Chapter outline

This chapter provides detailed information on the experimental system used to perform nonlinear vibro-ultrasonic testing in this thesis. Particular attention is paid to how various system components, as well as experimental procedures and analyses, affect the ability of the experimental system to discern generated nonlinear frequency components within resulting spectra. The chapter is organised as follows:

- Section 3.1.2 describes the experimental methodology of the thesis
- Section 3.2 describes the mechanical apparatus for nonlinear vibro-ultrasonic testing, including details of the sensors, actuators and boundary conditions.
- Section 3.3 contains details of the instrumentation chain used to provide excitation and measurement for experiments, including considerations to detection capabilities and limits.
- Section 3.4 introduces concepts of signal processing and describes the signal processing procedures used for experimental work.
- Section 3.5 provides details of the analysis performed using the experimental system. This includes data collection and examples of analyses which are used in Chapters 4 and 5.

3.1.2 Experimental methodology

To fulfil the objectives outlined in Section 1.2, nonlinear vibro-ultrasonic experiments are performed. The fundamental experimental steps are outlined as follows:

1. Input signal parameter selection
2. Signal generation
3. Input amplification stage
4. Excitation of specimen
5. Measurement of response
6. Output amplification stage
7. Signal processing
8. Analysis of frequency spectrum

At each of these steps, system parameters are chosen: what frequencies and amplitudes of excitation to use, how to apply these excitations, how the response is measured, and what signal processing is used. Recall from Section 1.2 that it is the aim of this thesis to determine the influence of these system parameters on the generation and detection of sideband frequency components in the final frequency spectrum.

If nonlinearity is to be used as a measure of damage, it is essential that the experimental system does not introduce additional nonlinearity to the point of obscuring that which is present due to damage. It is therefore a focus of this work to minimise (and quantify where possible) additional nonlinearity added to the input excitation signals by generation or amplification (Steps 2 and 3), or to the response signal by measuring and amplifying (Steps 5 and 6). It is also essential that signal processing performed on the measured signals (Step 7) results in a good signal-to-noise ratio, such that at an accurate frequency spectrum is obtained.

In the remainder of this chapter, a comprehensive analysis of the excitation, acquisition and post-processing system used to conduct the experimental work of this thesis is performed. Using optimised parameters determined from this analysis, focus can then shift to understanding the influence of system parameters in Steps 1 and 8, as well as the parameters of the specimen itself.

The influence of input frequency and amplitude selections (Step 1) is studied by varying these parameters and observing trends of sideband amplitudes, similar to existing work in the field described in Section 2.4. The analysis of sideband amplitudes (Step 8) is also further developed, to explore trends against system variables other than input parameters. The influence

of damage type and severity on the generation of sidebands is included in this analysis, using test specimens manufactured with varied levels of damage.

3.2 Experimental apparatus

Figure 3.1 shows a diagram of the experimental apparatus used in this thesis. The apparatus provides a clamped-end boundary condition to one end of a beam specimen, where a *The Modal Shop 2007E* electromagnetic vibration shaker is attached to provide low-frequency pumping vibration excitation. The other end of the beam is left free to create clamped-free boundary conditions. On both ends of the beam, *PCB Piezotronics 353B18* accelerometers are mounted using beeswax couplant to provide measurement of vibration of the beam. Two *Ferroperm Pz27* piezoceramic transducers are used to provide excitation and measurement of ultrasonic probing waves.

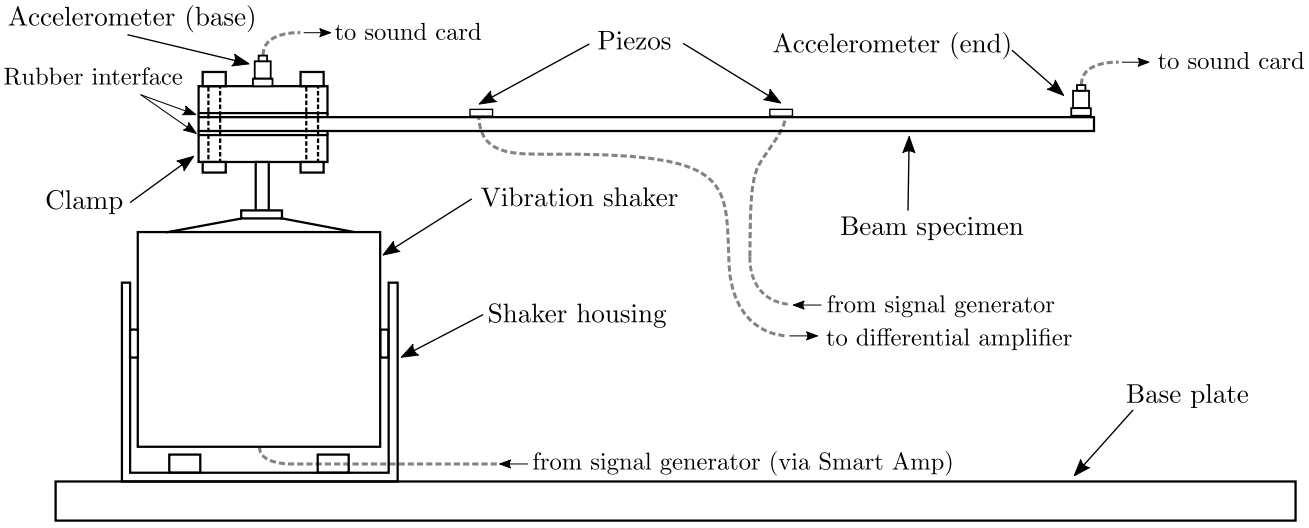

Figure 3.1: Experimental apparatus for vibro-ultrasonic testing of beams

Table 3.1: Details of sensing and actuating system components

Item	Model	Details
Accelerometers	*PCB Piezotronics* 353B18	Operating frequency: 1 - 10000 Hz Broadband resolution: 0.05 m/s^2 rms Nominal nonlinearity: $< 1\%$
Piezoelectric transducers	*Ferroperm* PZ27	Disc elements 5 mm (radius) x 2 mm (thickness)
Vibration shaker	*The Modal Shop* 2007E	Operating frequency: DC - 9 kHz Output force peak: 31 N

Table 3.1 provides relevant specifications on the sensing and actuation elements of the apparatus, which attach directly to the specimen. Details of attachment of these elements to specimens is provided in Sections 3.2.1 and 3.2.2.

3.2.1 Transducers and accelerometers

Piezoceramic transducers (from here referred to as *piezos*) are permanently bonded to each specimen, while accelerometers are temporarily coupled to each specimen undergoing testing using beeswax as a couplant. Figure 3.2 shows a detailed diagram of the attachment of piezoceramic transducers and accelerometers to specimens.

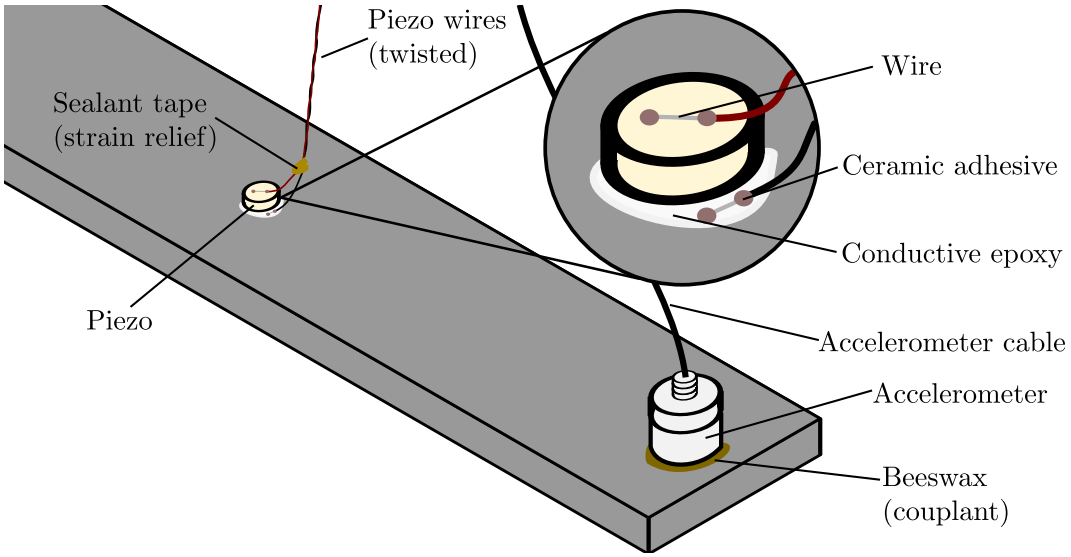

Figure 3.2: Attachment of piezo and accelerometer to specimen, showing adhesives and couplant used, as well as strain relief of wires. Inset: detailed view of piezo and wire bonding.

HBM X60 ceramic strain gauge adhesive was used to fix a wire to the top face of the piezo, with a small amount of *Electrolube* silver conductive paint used to ensure good electrical contact between piezo and wire. *Loctite Mix & Fix* epoxy was used to bond the piezo to the specimen, with a small amount of silver conductive paint mixed into the epoxy to provide electrical conduction. A second wire was attached directly to the specimen, next to the piezo, with silver conductive paint used to ensure electrical connection to the face of the piezo which was bonded to the specimen.

The two piezo wires are twisted together and secured to the specimen using sealant tape as a form of strain relief. Using sealant tape also avoids unwanted vibration of the wires against the specimen surface during experimentation, which in preliminary experiments was found to occur with other strain relief options such as epoxy, adhesive tape or ceramic strain gauge adhesive. This clapping vibration of the wires against the specimen is a possible source of nonlinearity.

The *PCB Piezotronics 353B18* accelerometers are attached to the specimen using beeswax, which is a convenient couplant as attachment is simple and positioning can easily be adjusted by hand. A microdot coaxial cable connects to the top of the accelerometer. Unlike the piezo wires, this cable is not attached to the specimen – due to the weight of this cable being comparable to that of the specimen, its weight is supported above the specimen. Care is taken to ensure the

cable does not interfere with vibration characteristics of the specimen, either through its weight or tension in the cable. The boundary conditions of the specimen are discussed in Section 3.2.2.

3.2.2 Vibration shaker and boundary conditions

As shown in Figure 3.1, the electromagnetic vibration shaker is bolted securely to an aluminium base plate and supports the remainder of the apparatus. The base plate is used to provide a stable foundation for the apparatus and to avoid unwanted vibration of the shaker housing, particularly ”clapping” vibration between shaker housing and laboratory workbench. A foam standoff is placed between the base plate and workbench to further isolate vibration of the system.

The specimen is attached to the vibration shaker through a clamping assembly shown in Figure 3.3. The vibration shaker mounting platform contains a #10-32 UNF thread, through which an aluminium threaded rod connects the first half of an aluminium clamp body. The bottom half of the clamp body has a channel in which the specimen sits, so that lateral movement is restricted. The two halves of the body are clamped by use of four M4 bolts.

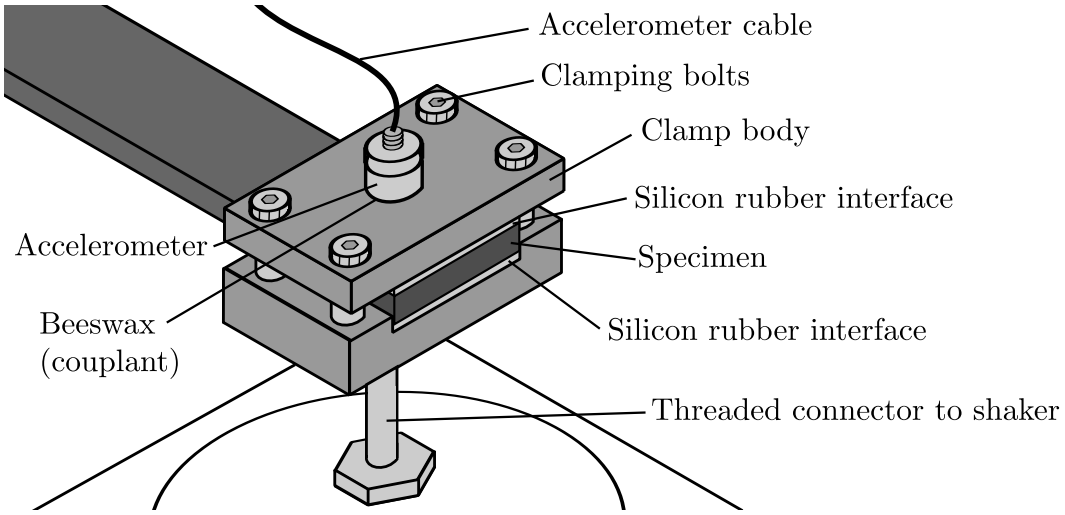

Figure 3.3: Attachment of specimen to vibration shaker, showing clamp assembly.

Layers of silicone rubber roughly 0.5 mm in thickness are placed either side of the specimen, in the area that makes contact with the clamp. The silicone rubber is compressed under the clamping force of the assembly, filling any gap between the surfaces of the specimen and clamp. This interface is important to ensuring there is no rubbing between the specimen and the clamp, which can be a source of nonlinearity.

The boundary conditions of the apparatus influence the response of the specimen to excitation. Of particular consideration is that low-frequency response of the beams is influenced by addition of mass, stiffness and support added to the apparatus. Due to the effect of accelerometers, cables, piezos and wires on the vibration response of the beam, setup is kept the

same during all experimentation. All specimens within an experimental set are kept the same length, with piezos bonded at the same locations along the length of the beam. Accelerometers at both ends of the apparatus are placed in the same locations between tests, and as explained in Section 3.2.1 accelerometer cables are carefully supported so that their weight and stiffness do not affect vibrational characteristics of the system.

The clamp assembly provides a secondary purpose, of avoiding unwanted rocking and shaking modes of the apparatus by increasing moment of inertia around the excitation axis. This increase causes resonance frequencies of these unwanted modes to be reduced below operational frequencies of interest.

3.3 Instrumentation chain

The sensing and actuating elements of the apparatus are connected to instrumentation which generate excitation signals and acquire measurements from the measurement piezo and accelerometers. A block diagram of the complete instrumentation chain, from specimen to control application, is shown in Figure 3.4.

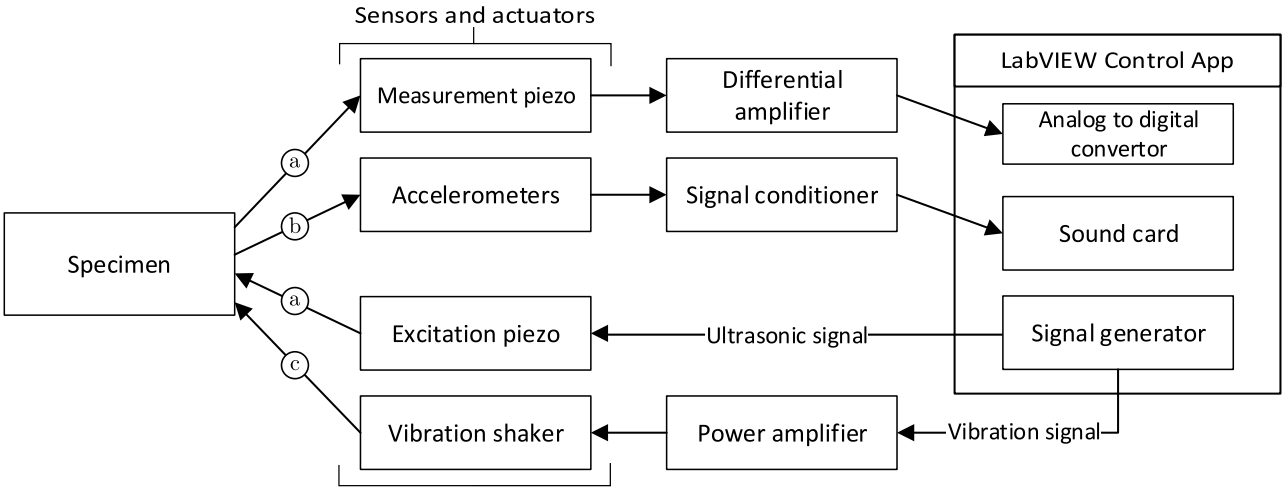

Figure 3.4: Overview of instrumentation chain for vibro-ultrasonic testing

Table 3.2 provides relevant details and specifications for the components of the instrumentation chain, including nonlinearity characteristics where appropriate.

The excitation and measurement tasks are controlled through a *LabVIEW* application

Table 3.2: Details of instrumentation system components (unfinished)

Item	Model	Details
Sound card	*Intel* HD Audio	Input impedance: >20 kΩ Frequency response: 20 Hz to 20 kHz Signal-to-noise ratio (SNR): >90 dB Channel separation: >80 dB Total harmonic distortion: < -75 dB (0.02%)
Signal conditioner (for accelerometers)	*PCB Piezotronics* 480C02	
Power amplifier (for vibration shaker)	*The Modal Shop* 2100E21-100	Total harmonic distortion: < 0.1%
Signal generator	*Rigol* DG1032Z	Vertical resolution: 14 bits Max frequency: 30 MHz Phase noise (@ 10MHz): <-125 dB/Hz Harmonic distortion (DC-10MHz): <-65 dB Spurious noise (≤ 10 MHz): < -70 dB
Differential amplifier	N/A	Max sample rate: 2.5 MHz Vertical resolution: 24-bit Memory depth: 1,048,576 samples Noise floor (DANL): >140 dB
Analog-to-digital interface	*Analog Devices* AD7760 *Analog Devices* CED1Z	

running on a desktop computer which is connected via USB interface to data acquisition and signal generating equipment. This LabVIEW application is discussed in more detail in Section 3.5.1. This includes low- and high-frequency excitation signals which are generated by a two-channel *Rigol DG1032Z* signal generator. The low-frequency pumping signal then passes through a *The Modal Shop 2100E21-100 Smart Amp* power amplifier which powers the vibration shaker, while the high-frequency signal directly powers the excitation piezo. The parameters of these excitation signals such as amplitude and frequency are controlled by the application, and these parameters are varied dynamically during experimentation by control commands sent to the signal generator via USB interface.

Accelerometers mounted to the beam are connected to *PCB Piezotronics 480C02 ICP* signal conditioners, with measurements acquired using a desktop PC with onboard *Intel HD Audio* sound card. The specifications for this sound card are listed in Table 3.2. This card has good signal-to-noise ratio (SNR), channel separation and total harmonic distortion (THD) characteristics, such that the vibration of the beam can be quantified during experiments.

Signals from the measurement piezo are amplified using a custom built ultrasonic preamplifier. This preamplifier is designed based on differential amplification whereby ground referenced noise in the system is greatly reduced. This differential amplifier is described in more detail in Section 3.3.1. The amplified piezo measurement signal is then captured using an analog-to-digital interface which is described in detail in Section 3.3.2. This arrangement

allows sampling of waveforms at 24-bit vertical resolution at 2.5 MSamples per second, while maximising SNR of the final measurement signal.

3.3.1 Differential preamplifier

Measurement of ultrasonic signals often requires handling of a signal of small amplitude due to attenuation through the structure, particularly if there is a large distance between transmitting and receiving transducers. This becomes especially problematic when external electrical noise is coupled into the measurement system when unshielded wires attached to the piezo act as antennas to receive noise. Due to the low voltage ranges of received ultrasonic signals, this noise can easily obscure relevant measurement information.

The experimental system used in this thesis utilises a custom built ultrasonic preamplifier. A circuit board containing *Analog Devices AD5253* and *AD8250* digitally controllable gain instrumentation amplifiers was built for this purpose. Also included is a supporting circuit board for basic microprocessor control and power, as well as internal shielding for further noise reduction. This preamplifier is designed based on differential amplification, which minimises the coupling of external electrical noise into the measurement system. This is achieved by amplifying the difference in voltage between the two wires attached to the piezo, causing any induced electrical noise common to both wires to destructively interfere, greatly reducing the magnitude of induced noise.

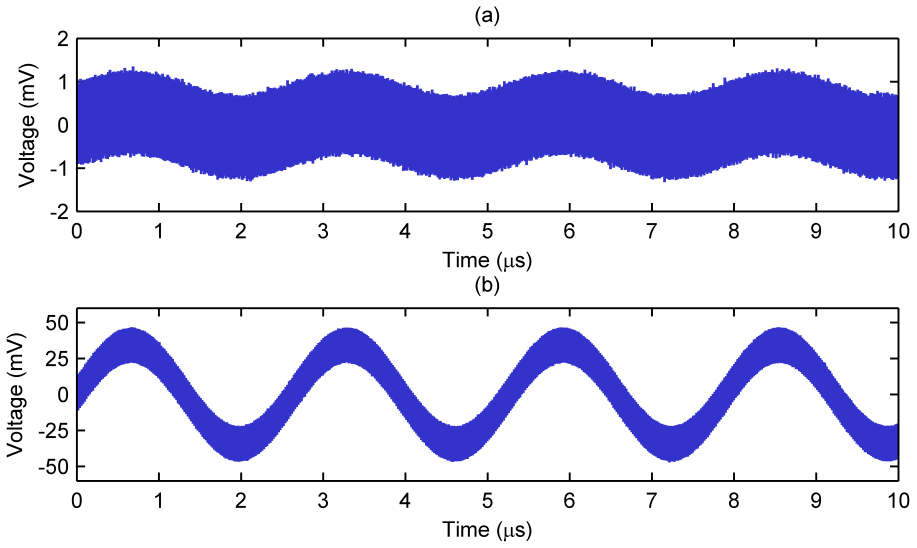

Figure 3.5: 380 kHz ultrasonic signal measured from piezo using oscilloscope using (a) no amplification and (b) differential amplification

To demonstrate the noise reduction achieved by using the designed differential amplifier, the experimental system described in this chapter was used to apply a 20 V peak-to-peak continuous

sine wave excitation to the transmitting piezo of beam P1. The response of the receiving piezo as captured directly by the *Rigol 1074Z* oscilloscope is shown in Figure 3.5(a). The response of the receiving piezo first amplified by the designed differential amplifier before being captured by the same oscilloscope is shown in Figure 3.5(b). The amplified signal shows a great reduction in noise, demonstrating the benefit of differential amplification in an ultrasonic measurement system.

3.3.2 Analog-to-digital convertor

As discussed in Section 3.1.2, it is important to reduce the displayed average noise level (DANL) present in the frequency domain to a level below the amplitude of sideband frequency components. Frequency components present in the signal of an amplitude less than the DANL are not discernible and hence cannot be used for damage detection.

When selecting an appropriate analog-to-digital converter (ADC) for this frequency analysis, the three most prominent factors are sample rate, vertical resolution and memory depth. The sample rate of an ADC determines the maximum frequency that can be analysed; according to the Nyquist limit the sample rate must be at least twice the maximum frequency of interest.

Vertical resolution is the number of discrete levels a measured value can be approximated to. Typical digital oscilloscopes use 8 bits of vertical resolution, which means that the converter splits the measurement range into 256 levels. Memory depth refers to the maximum number of data points that can be captured in one continuous segment. Vertical resolution and memory depth are important for their influence on the DANL of the final spectrum. The theoretical minimum DANL can be calculated by the following expression (Lyons, 2010, pp. 595):

$$\mathrm{DANL}(dBm) = 20\log_{10}\left(\frac{1}{2^n}\right) - 10\log_{10}\left(\frac{m}{2}\right) \tag{3.1}$$

where n is the number of bits of vertical resolution and m is the memory depth. The first term in this expression shows the effect of amplitude accuracy lost by converting an analog signal by n number of digital levels; an ADC with a greater vertical resolution results in a lower DANL. The second term shows the effect of processing gain obtained from having a larger number of data points in the Fourier transform calculation.

The primary obstacle to minimising the DANL is the selection of an ADC with a high bit depth. From equation (3.1), increasing the effective number of bits in the ADC by 1 bit improves the DANL by approximately 6 dB. A similar effect can be obtained by increasing the number of samples in the waveform by four times. For an 8-bit ADC to achieve the same theoretical DANL as a 16-bit ADC, the required increase in data points is 65,526-fold. Acquiring additional

samples to bridge this gap can become impractical due to the increased sample time and requires orders of magnitude more memory depth. It is therefore beneficial to select an ADC that has high vertical resolution as opposed to use of a traditional oscilloscope which is limited to 8 bits, even if the trade-off is for a moderate decrease in memory depth.

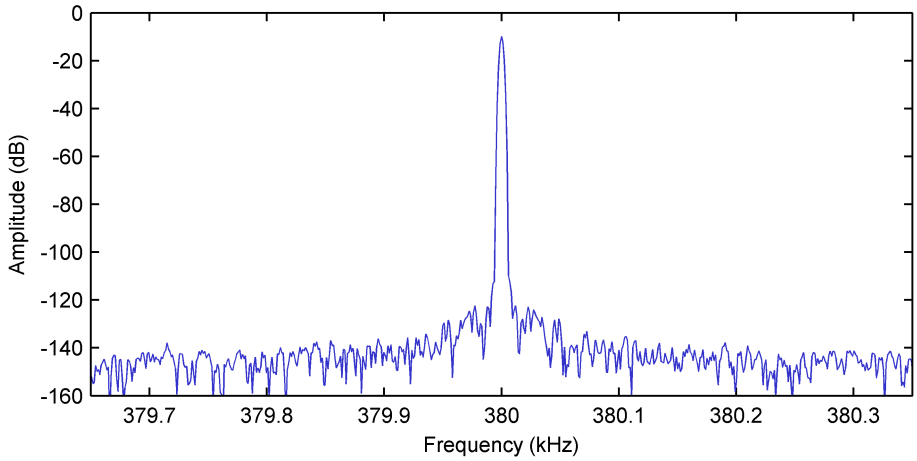

Figure 3.6: Frequency spectrum obtained by AD7760, showing DANL performance of -145 dB

The analog-to-digital interface assembled for this thesis comprises an *Analog Devices AD7760* evaluation board in combination with an *Analog Devices CED1Z* FPGA interface. This arrangement allows sampling of waveforms at 24-bit vertical resolution at 2.5 MSamples/s with a memory depth of 2^{20} samples. Figure 3.6 shows the performance achieved by this ADC when measuring the output of a 1 V peak-to-peak continuous sine wave at 380 kHz, which is an example ultrasonic frequency used in nonlinear vibro-ultrasonic experiments in this thesis. This signal is provided directly to the ADC by the signal generator. The response shown in Figure 3.6 is zoomed to 350 Hz either side of this carrier frequency, to show the region where sideband frequency components relevant to this thesis are generated. At the edge of this region, the DANL performance of the ADC approaches -145 dB. This value is better than the theoretical value of -100 dB calculated from equation (3.1) if an 8-bit digitiser were used, but the ADC does not attain the performance of -200 dB calculated for a 24-bit digitiser due to electronic noise in the measurement system. The lack of any spurious frequencies in this bandwidth is also indicative of good performance of this ADC for the frequency range of interest.

3.4 Signal processing

Further to the discussion of decreasing the displayed average noise level (DANL) of a frequency spectrum are the signal processing topics of windowing and averaging.

3.4.1 Fundamental concepts of spectral analysis

The Fast Fourier Transform (FFT) algorithm converts equally-spaced samples of a signal into an equivalent sampling of the discrete-time Fourier transform of the signal, which is a representation of the original signal as a sum of sinusoids. The FFT therefore provides a representation of the frequency spectrum of the signal sample.

Because the sampling of the original signal in the time-domain is not continuous, the FFT returns a discrete frequency spectrum, where the frequency components are resolved as so-called frequency *bins*. The spacing of these bins, the frequency resolution of the computed spectrum, is inversely proportional to the original sample time T and related to the sampling rate f_s and number of samples N as such:

$$df = \frac{1}{T} = \frac{f_s}{N} \tag{3.2}$$

The sample rate of the signal also controls the maximum frequency which can be resolved f_{max} by Nyquist-Shannon sampling thereom:

$$f_{max} = f_{Nyquist} = \frac{f_s}{2} \tag{3.3}$$

As an example, the instrumentation system used in this thesis and described in Section 3.3 has a maximum sample rate of 2.5 MSamples/s, resulting in a maximum resolvable frequency of 1.25 MHz. It may be desirable to use a lower sample rate however, in order to trade off for a better frequency resolution by equation (3.2), provided that the number of samples N is kept fixed. As discussed in Section 3.3.2, by equation (3.1) it is desirable to use the largest number of samples afforded by instrumentation in order to minimise noise level.

3.4.2 Spectral leakage and windowing functions

The Fast Fourier Transform (FFT) algorithm takes a finite set of data (the sampled data has a finite duration) and assumes it is one period of a continuous, periodic signal. Because the signal is treated as a circular topology, the two endpoints (first and last measurement data point) are treated as being connected. For this reason, spectral information obtained by performing an FFT does not always equate exactly to the actual spectrum of the measured signal.

When the input signal is periodic and there are an integer number of periods contained in the signal, the FFT spectrum matches the actual spectrum of the signal. Figure 3.7(a) shows the spectrum for a measured signal having a single frequency component and an integer number of cycles.

It is likely that an acquisition of data does not contain an integer number of cycles, meaning the first and last data points are discontinuous. Figure 3.7(b) demonstrates the principle known as *spectral leakage*, which gives the appearance of energy in frequencies where it does not exist in the original signal, for a non-integer number of cycles.

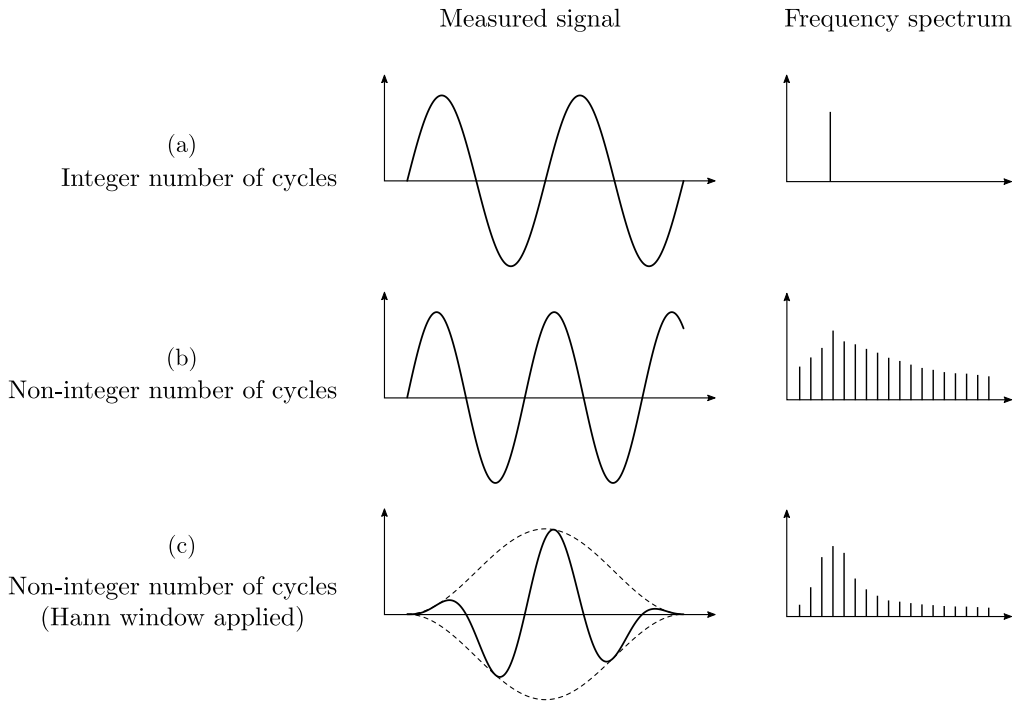

Figure 3.7: Spectral leakage of a periodic signal of a single frequency for various sampling arrangements. The Hann window function is showed as a dotted line.

A practical solution to spectral leakage is *windowing*, where the measured data is multiplied by a window function. A common aim of windowing is to smoothly reduce the amplitude of the signal towards zero at the edges so that the start and end points are continuous, though this is not the case for every window. Figure 3.7(c) shows the effect of a Hann window, given by the

equation

$$w(n) = 0.5\left(1 - cos\left(\frac{2\pi n}{N-1}\right)\right)$$

on the spectral leakage of the same measured signal with a non-integer number of cycles. The dotted line represents the Hann window function itself, with the solid line being the signal which is passed to the FFT algorithm, which is the signal from Figure 3.7(b) multiplied by the Hann window. Compared to the case with no windowing, there is less spectral leakage into frequencies far away from the frequency present in the original signal, and a little more leakage into frequencies very close by.

There are a variety of window functions commonly applied to experimental signals before Fourier analysis, and their effects on the spectrum vary considerably. To choose an appropriate window function, the frequency spectrum of the window function itself can be analysed to determine its characteristics. The spectrum of a typical window function is shown in Figure 3.8 as an illustrative example.

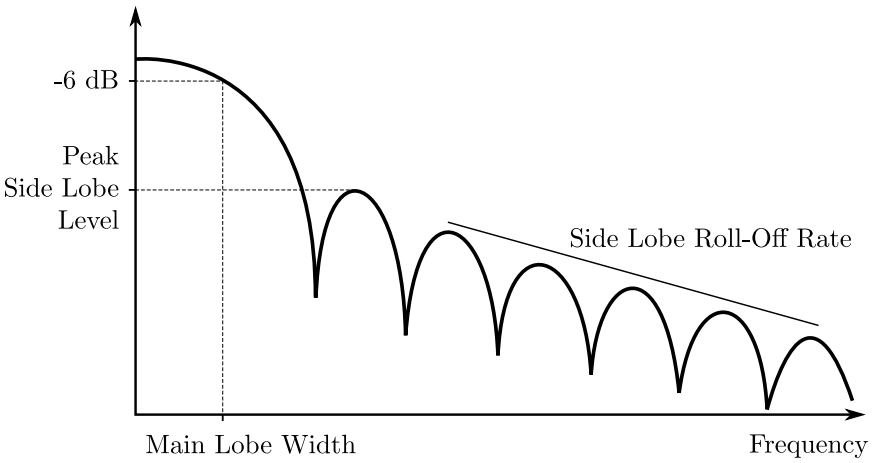

Figure 3.8: Illustration of the frequency spectrum of a typical window function.

Of note in Figure 3.8 are the main lobe and the sidelobes, the width and amplitude of which are important for certain applications. A main lobe occurs for each frequency component in the original signal, and sidelobes occurs on each side of each main lobe. A very wide main lobe limits the frequency resolution in the windowed signal, as the main lobe of one frequency could obscure another frequency component of a similar amplitude through leakage of this main lobe. A very narrow main lobe results in improved spectral resolution, however the trade-off for this is increased energy leakage into sidelobes (Harris, 1978).

Nonlinear vibro-ultrasonics presents a particular challenge, which is the measurement of a probing frequency as well as sideband frequency components which have frequencies very close to the probing frequency but at much smaller amplitudes. In this case, the sidelobes of the centre frequency (probing) component may be large enough so as to obscure the main lobe response of

the sideband components. If this were the case, it would place a limit on the size of sidebands which are discernible and hence a limit on the level of nonlinearity which is measurable. The requirements for a window for nonlinear vibro-ultrasonics are therefore one which minimises the amplitude of sidelobes.

Albrecht (2001) describes a family of cosine-sum windows with minimum sidelobe amplitude appropriate for detection of small signals in highly dynamic spectra, such as sideband frequency components in nonlinear vibro-ultrasonics. Cosine-sum windows are of the form

$$w(n) = \sum_{k=0}^{K} (-1)^k a_k \cos\left(\frac{2\pi kt}{T}\right) \quad \text{for } 0 \leq t \leq T \tag{3.4}$$

For experimental work in this thesis, unless stated otherwise, the 5-term minimum sidelobe solution from Albrecht (2001) is used, the coefficients for which can be found in Table 3.3, along with other commonly used cosine-sum windows.

The spectrum of this window is shown in Figure 3.9. Of note is that the main lobe drops off to a level below that of the first sidelobe approximately 10 bins away from the centre frequency, and that the first sidelobe has an amplitude of roughly -125 dB.

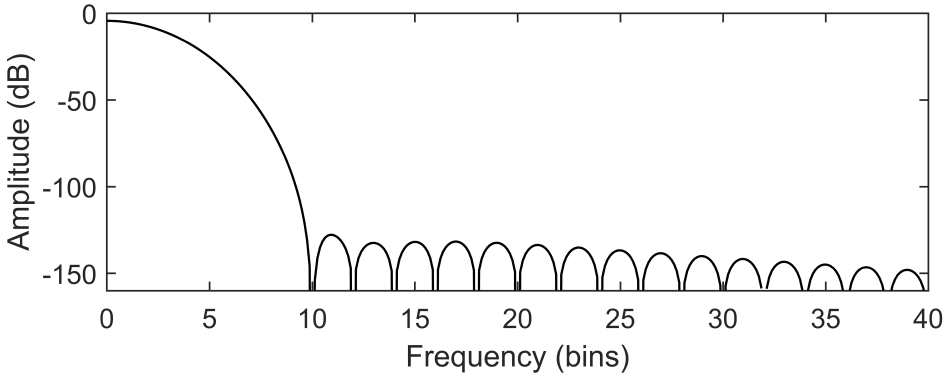

Figure 3.9: Frequency spectrum for the minimal sidelobe window (5-term Albrecht) used in this thesis.

A typical sampling rate of 1.25 MHz and memory depth of 1,048,576 samples used for experimental work in this thesis leads to a bin width of 1.19 Hz. Multiplying this value by 10 (the number of bins where the main lobe drops off, as per Figure 3.9) yields a practical limit on the closeness of sidebands to the central frequency of approximately 12 Hz, in order to have zero overlap with the main lobe. If a sideband frequency component were to be within this range (i.e. if the pumping frequency in a nonlinear vibro-ultrasonics experiment were 12 Hz or less) a modified window can be used with a narrower sidelobe. Albrecht (2010) describes a technique for tailoring a cosine-sum window with these parameters in mind, with which sidelobe level or main lobe width can be arbitrarily chosen.

Figure 3.10 shows frequency spectra from example experimental signals obtained from

Table 3.3: Coefficients for cosine-sum windows

Coefficient	Hamming	Blackman	Nuttall	Flat top	Albrecht (5-term)
a_0	0.54	0.42	0.3635819	0.21557895...	0.32321537 ...
a_1	0.46	0.5	0.4891775	0.41663158...	0.47149214...
a_2	–	0.08	0.1365995	0.27726315...	0.17553412...
a_3	–	–	0.0106411	0.08357894...	0.02849699...
a_4	–	–	–	0.00694736...	0.00126135...

nonlinear vibro-ultrasonic testing, processed with 5 common cosine-sum window functions listed in Table 3.3 as well as with a rectangular window (equivalent to using no window). This signal was obtained using the experimental system described in Section 3.2 and instrumentation described in Section 3.3. A pristine composite laminate beam was excited by a probing frequency of 380 kHz, a vibration pumping frequency of 60 Hz and vibration driving amplitude of 3 V. More details about these experiments are found in Chapter 4.

Due to the very small amplitude of sidebands compared to the centre frequency, the spectra produced using a rectangular window, shown in Figure 3.10(a), does not allow for clear discernment of any sidebands. The Hamming window spectra shown in Figure 3.10(b) reveals the presence of one pair of sidebands, with the sidelobes of this window reaching approximately -80 dB. Figures 3.10(c)-(f) show that the flat top, Blackman, Nuttall and Albrecht windows allow five pairs of sidebands to be discerned. Figure 3.10 also illustrates that for a pumping frequency of 60 Hz, the width of each frequency component is sufficiently narrow to allow clear differentiation.

Experiments were repeated with a 10 Hz pumping vibration, with spectra shown in Figure 3.11. The rectangular and Hamming windows are omitted due to poor performance, similar to that in the previous tests with a 60 Hz pumping frequency. The flat top and Blackman windows do not perform as well as the Nuttall and Albrecht with the lower pumping frequency, with less pairs of sidebands being clearly discernible due to spectral leakage.

Experiments with a 10 Hz pumping vibration were conducted with a lower driving amplitude of 0.1 V, in order to further compare the Nuttall and 5-term Albrecht windows. The results in Figure 3.12 show similar performance of the two windows. Both windows allow for the clear discernment of one pair of sidebands, with further sidebands obscured by the noise floor. The 5-term Albrecht window spectrum in Figure 3.12(b) shows the second and third sideband on the lower frequency (left) side more clearly, though they could easily be mistaken for spurious noise. Viewing of the spectrum in real time shows that the sideband components did not fluctuate as the noise floor did, allowing for confirmation that these peaks were sidebands.

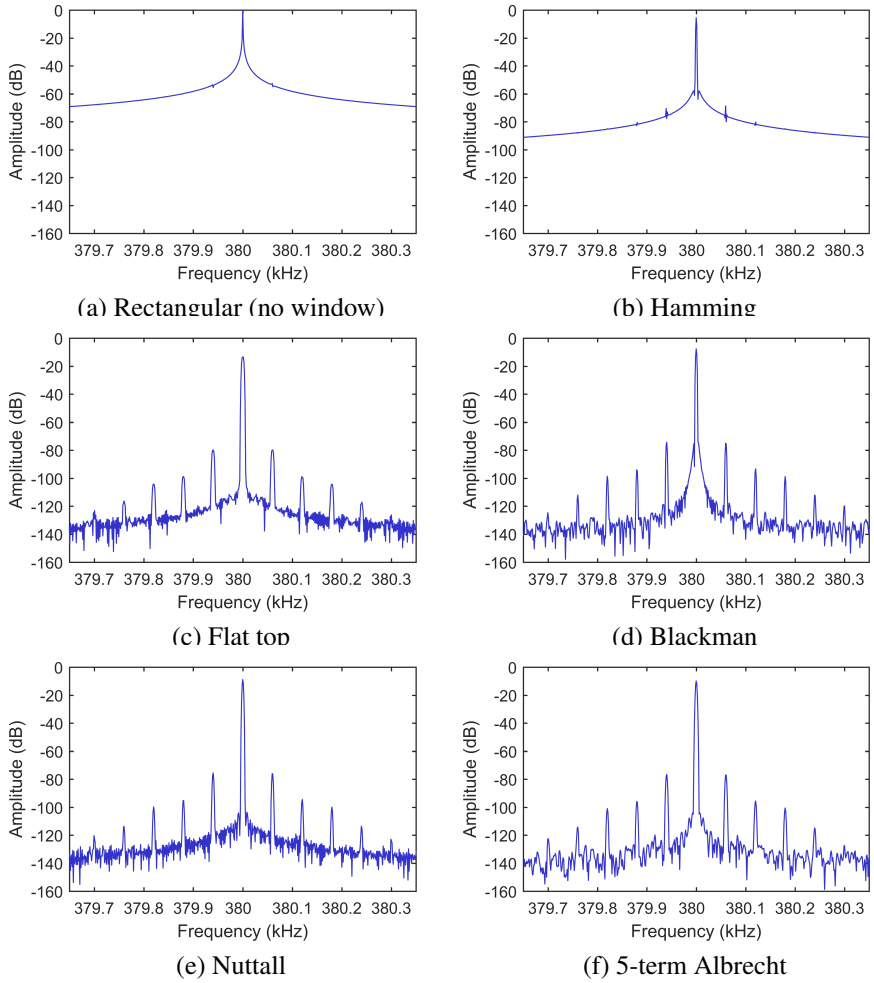

(a) Rectangular (no window) (b) Hamming

(c) Flat top (d) Blackman

(e) Nuttall (f) 5-term Albrecht

Figure 3.10: Comparison of frequency spectra obtained from nonlinear vibro-ultrasonic experiments with six different window functions. Pumping frequency of 60 Hz used.

These results indicate that cosine-sum windows can be useful tools in the signal processing of nonlinear vibro-ultrasonics experiments, with the Nuttall and 5-term Albrecht windows showing particular promise for cases were amplitude and/or frequency spacing of sidebands is low.

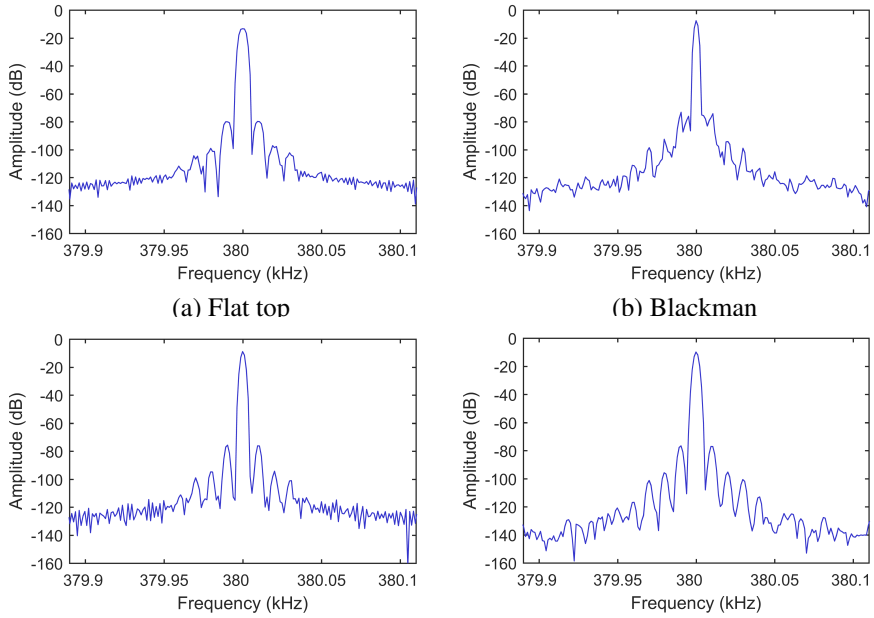

(a) Flat top (b) Blackman

(c) Nuttall (d) 5-term Albrecht

Figure 3.11: Comparison of frequency spectra obtained from nonlinear vibro-ultrasonic experiments with four window functions. Pumping frequency of 10 Hz used

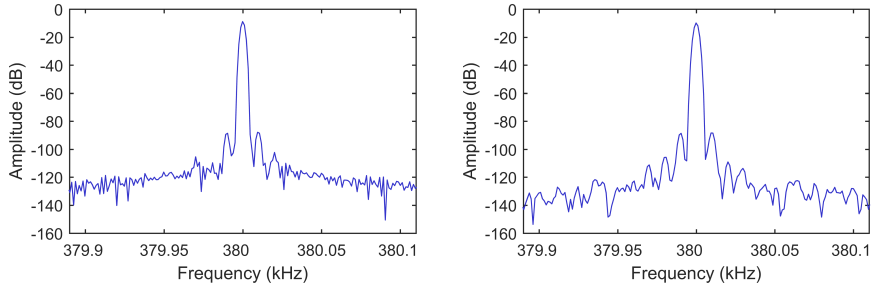

(a) Nuttall (b) 5-term Albrecht

Figure 3.12: Comparison of (a) Nuttall and (b) 5-term Albrecht windows with a 10 Hz pumping frequency of lower amplitude.

3.4.3 Frequency domain averaging

Discernment of sideband frequency components can be further improved through use of averaging, where multiple samples are taken, transformed by FFT and the resulting spectra averaged. Two methods are used to average the spectra: vector averaging and RMS averaging.

RMS averaging is calculated by averaging the energy of the signal across multiple samples. This is computed as follows:

$$X_{rms} = \sqrt{\langle X \cdot X^* \rangle} \tag{3.5}$$

where X is the complex FFT of the signal, X^* is the complex conjugate of X, and $\langle X \rangle$ is the average of X with real and imaginary parts being treated separately.

Figure 3.13 shows frequency spectra from example experimental signals obtained from nonlinear vibro-ultrasonic testing, comparing the case with no averaging to RMS averaging

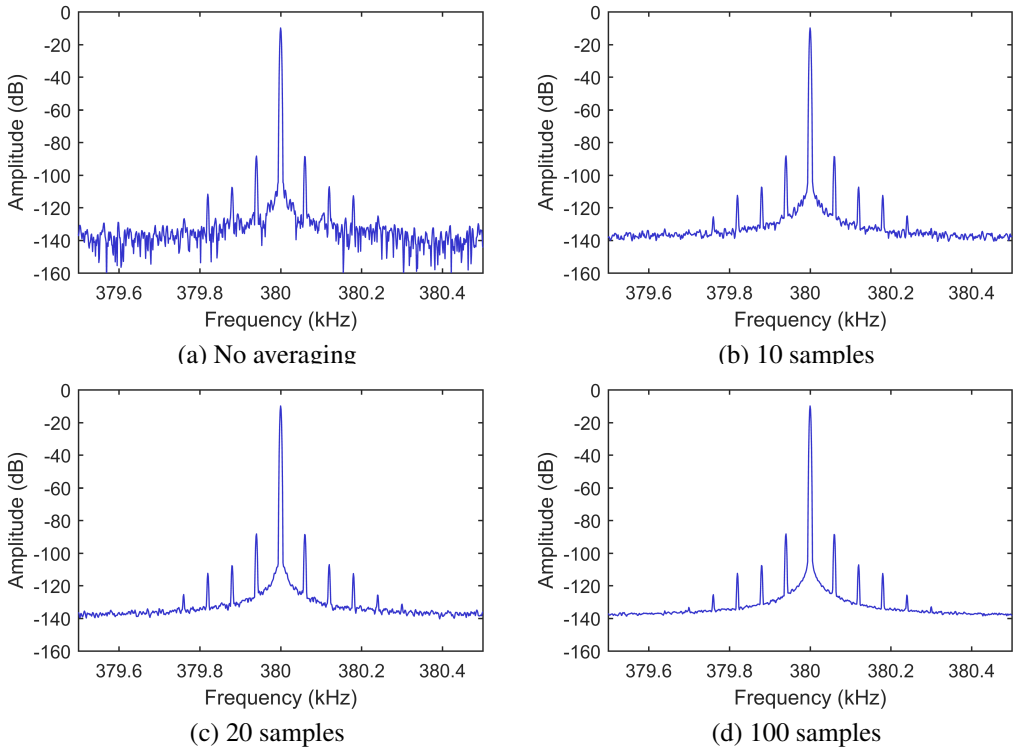

(a) No averaging (b) 10 samples

(c) 20 samples (d) 100 samples

Figure 3.13: Effect of RMS averaging on frequency spectrum from nonlinear vibro-ultrasonic testing.

using 10, 20 and 100 samples. The case with no averaging in Figure 3.13(a) shows a noise floor with significant fluctuations and three clearly visible pairs of sidebands. The 10-sample and 20-sample averages in Figures 3.13(b) and (c) respectively show a smoothing effect on the noise floor, and the appearance of a fourth pair of sidebands. Further smoothing is seen with the 100-sample averaging in Figure 3.13(d), with the feint appearance of a fifth pair of sidebands above the noise floor.

As illustrated by Figure 3.13, RMS averaging reduces fluctuations in the spectrum but does not lower the noise floor. The average power level of the noise components (or *noise power*) of the signal does not decrease by RMS averaging, but the fluctations in the noise power at each frequency reduces (Lyons, 2010, pp. 597). This results in a smoother spectrum, and better approximation to the noise power of the signal.

Vector averaging of the frequency spectra is computed as the following:

$$X_{vector} = \langle X \rangle \tag{3.6}$$

which is the average of X with real and imaginary parts being treated separately. In contrast to RMS averaging, the treatment of the complex output before taking the magnitude means that noise bin values can be positive or negative. For noise with an average value of zero, averaging these values causes the signal bin average to approach its true magnitude (Lyons, 2010, pp. 601).

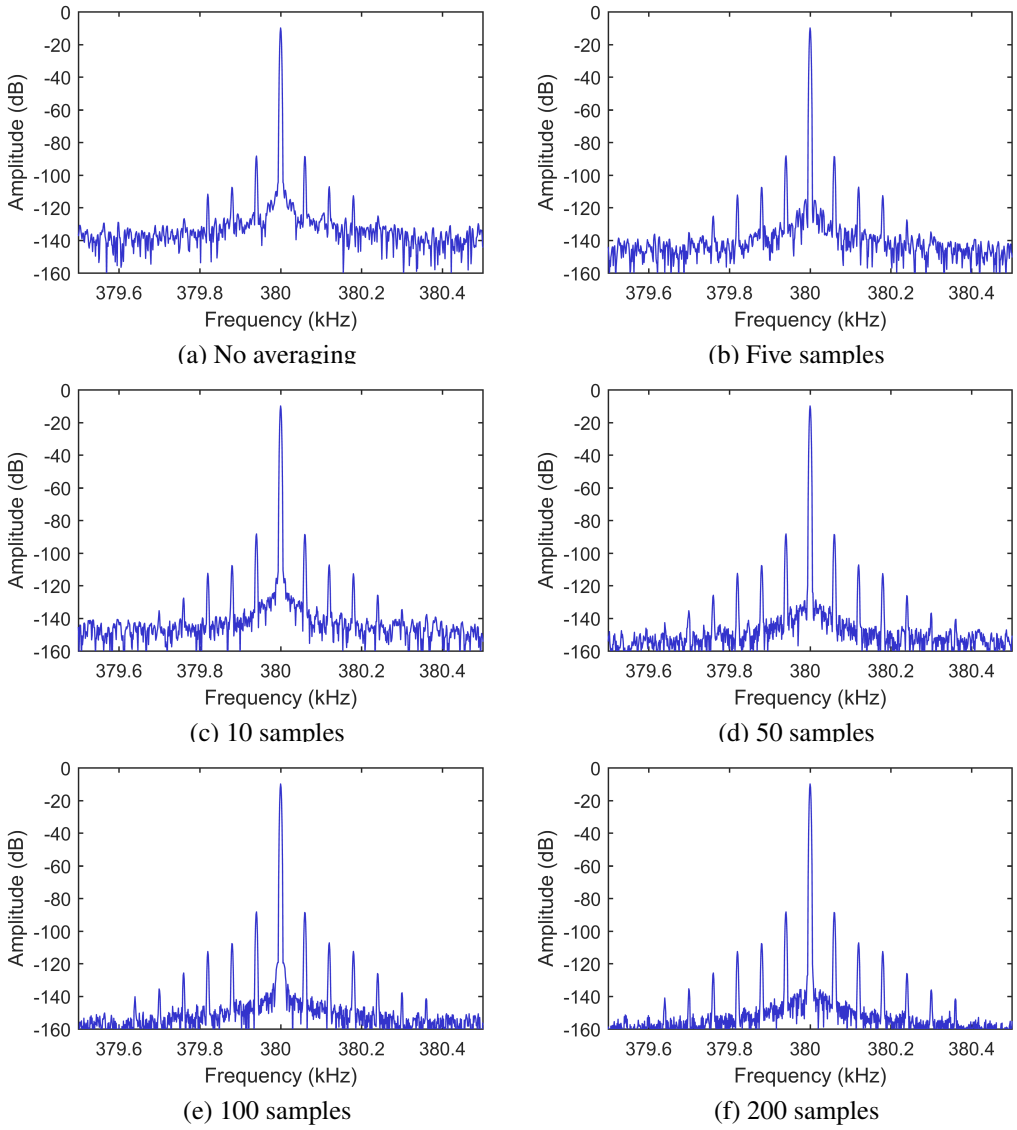

Figure 3.14: Effect of vector averaging on frequency spectrum from nonlinear vibro-ultrasonic testing.

Provided that the noise fluctuations in the signal are not phase coherent, and the measurements are acquired with a phase synchronous trigger, the noise power of the signal is reduced (Lyons, 2010, pp. 602). This is illustrated in Figure 3.14, where frequency spectra are obtained from nonlinear vibro-ultrasonic testing with vector averaging of 5, 10, 50, 100 and 200 samples and compared to the case of no averaging. While for the no averaging case (Figure 3.14(a)) there are three visible pairs of sidebands clearly discernible above the noise floor, this number increases to six pairs once 100 samples are averaged (Figure 3.14(e)).

The reduction in noise floor and hence increase in signal-to-noise ratio of the signal is proportional to the square root of the number of averaged samples N (Lyons, 2010, pp. 595):

$$\mathrm{DANL}_{\mathrm{reduction}} = \mathrm{SNR}_{\mathrm{gain}} = 20\log_{10}(\sqrt{N}) = 10\log_{10}(N) \tag{3.7}$$

This is demonstrated by Figures 3.14(a), 3.14(c) and 3.14(e) showing noise floors of approximately -135 dB, -145 dB and -155 dB for averages of with 1, 10 and 100 samples respectively.

These results clearly show the benefit of using vector averaging for nonlinear vibro-ultrasonics experiments is increased sensitivity to nonlinearity. The threshold for sideband amplitude, and hence level of nonlinearity detectable by a given experimental system, is lowered by vector averaging. The practical trade-off for this increased sensitivity is the requirement that additional samples are taken.

The time period of each 1,048,576 length sample at a sample rate of 1.25 MSamples/s is almost 840 ms, and the time required to acquire each sample approaches 2 s due to real-time processing and instrumentation triggering overhead. The time required to average a large number of samples for a variety of experimental parameters could quickly become prohibitive. Unless specified otherwise, experimental data in this thesis is acquired by RMS averaging of 10 samples, providing consistency of measurements due to low fluctuations while keeping acquisition time of each data point relatively low. Vector averaging is not used by default, as the displayed average noise level in experimental data presented in Chapters 4 and 5 is found to be sufficiently low to measure several pairs of sidebands.

3.5 Experimental analysis

This section describes the experimental analysis that is performed with the experimental system, including the data which is collected and how it is analysed. Included in this section are some examples of specific analyses that are used in Chapters 4 and 5.

3.5.1 Data collection

Data collection is managed by a LabVIEW application. As described in Section 3.3, the LabVIEW application can send instructions to the signal generator through a USB link. In addition to this, the LabVIEW application also instructs the analog-to-digital converter (ADC) when to sample the measurement piezo, and the sound card when to sample the accelerometers. All signal input and output, as well as signal processing and analysis is handled by this application.

The application sends the signal generator instructions for signal type (e.g. continuous sine wave vs. square wave), frequency, amplitude and other special features (e.g. modulation, burst, sweep functions). These instructions cover two output channels, one each for the pumping and the probing wave. The application allows the user to regularly vary an input parameter (amplitude or frequency) from a start to end value, in a user-defined number of increments. The application then performs a loop, where it sends an instruction to the signal generator, waits a defined amount of time, then moves on to send the instruction for the next step of the loop. In this way, a range of parameters can be investigated in an automated manner, for instance

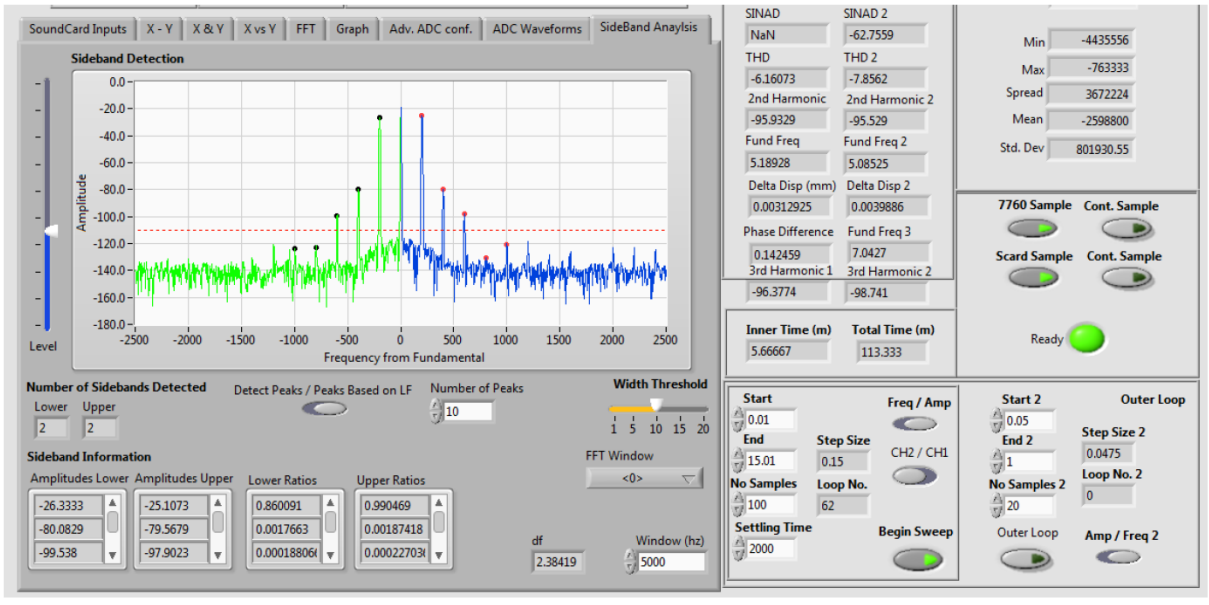

Figure 3.15: Example view of LabVIEW application, for a nonlinear vibro-ultrasonics test where sidebands are present.

increasing the amplitude of the pumping wave in a nonlinear vibro-ultrasonics experiment. Two loops can be run in this manner, so that amplitude and frequency can each be varied.

At each step in the loop, a data acquisition phase is run during the wait time in between parameter switching. During data acquisition, the application takes samples of both accelerometers (using the sound card) and the measurement piezo (using the ADC). The parameters of the ADC sampling are user-defined in the application, and include sample length (up to 1,048,576 samples) and sampling rate (up to 2,500,000 MSamples/s). The signals read into the application are graphed to the user, and a number of useful calculations are performed and displayed. Details of the calculations performed are available in Table 3.4.

For each sample, the input parameters and the calculated output values are recorded for further analysis. This vastly reduces the amount of data storage required, as only important calculated values are stored rather than raw signal data. At 24-bit resolution and 1,048,576 samples, each sample occupies 3 MB of memory. Taking into account averaging of 10 signals, and parameter studies spanning ranges of input values, the amount of data stored quickly becomes impractical - as well as the time required to write this data to disk.

Table 3.4: LabVIEW calculations performed on output signals

Signal	Calculation	Details
Accelerometers (each channel)	Fundamental Frequency	The main frequency present in the signal, used to confirm the structure is vibrating at the desired input frequency.
	SNR	Signal-to-noise ratio of the fundamental frequency, can be compared between experiments to quantify noise.
	Acceleration	Amplitude of the fundamental frequency, which corresponds to the instantaneous peak acceleration.
	Displacement	Peak-to-peak displacement at the measurement location, calculated from acceleration and frequency.
	2^{nd} Harmonic	Amplitude of 2^{nd} harmonic of the fundamental frequency
	3^{rd} Harmonic	Amplitude of 3^{rd} harmonic of the fundamental frequency.
	THD	Total harmonic distortion present in the signal, which is the sum of higher harmonic amplitudes.
Accelerometers (both channels)	Beam Displacement	Beam displacement is calculated by taking the difference of the two channels and measuring the peak acceleration, then converting to displacement. This is a measure of the relative displacement of the two ends of the beam.
	Phase Difference	Difference in phase between the two accelerometer channels, used to determine resonance frequencies.
Measurement piezo	Central Frequency	The main frequency present in the signal, used to confirm the ultrasonic probing wave is being measured.
	Central Amplitude	Amplitude of the probing wave (central frequency), used to quantify throughput of ultrasonic wave from transmitting to measurement piezo.
	SNR	Signal-to-noise ratio used to quantify the noise floor around central frequency.
	Sideband Ratios	The amplitude of sideband frequency components around the central frequency are measured, and divided by the amplitude of the central frequency. More information is provided in Section 3.5.1.1.

3.5.1.1 Sideband amplitude measurements

For each sample, a frequency spectrum is produced in the LabVIEW application using user-defined windowing and averaging. The default setup uses the Albrecht (low sidelobe) window introduced in Section 3.4.2 and RMS averaging of 10 samples. An example of a resulting spectrum (for a composite laminate beam) zoomed in around the probing frequency is shown in Figure 3.16.

For analysis purposes, the amplitude of the probing frequency is labelled A_0 while the first five pairs of sideband amplitudes are labelled A_1 through A_5. A superscript differentiates between sidebands lower (–) and higher (+) than the probing frequency. The amplitudes of each of these frequency components is recorded for each sample, so that further analysis can utilise this data to uncover trends of sideband ampitude with changing system parameters.

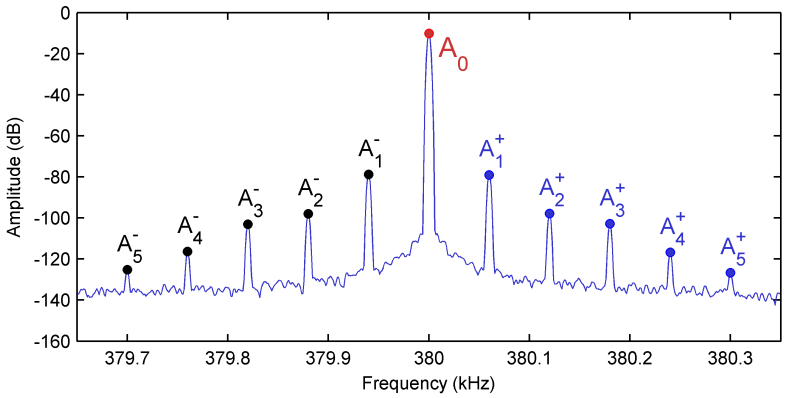

Figure 3.16: Sideband and central frequency labelling used for calculations of sideband ratios and damage indices.

3.5.2 Vibration response analysis

Analysis of specimen response to the low-frequency vibration excitation is performed to understand how the specimen responds to changes in frequency and amplitude. Throughout investigation of nonlinear vibro-ultrasonic testing, vibration amplitude provided by the vibration shaker is varied in order to observe the resulting trend of modulation intensity. It is therefore important to understand how an increase in excitation voltage to the shaker relates to vibration amplitude in the beam.

An example frequency response spectrum is shown in Figure 3.17. This data was obtained for a pristine composite laminate beam (as described in Chapter 4). The beam was excited at frequencies ranging from 40 to 70 Hz, in steps of 0.1 Hz. The input signal was a continuous sine wave with voltage of 3.0 V.

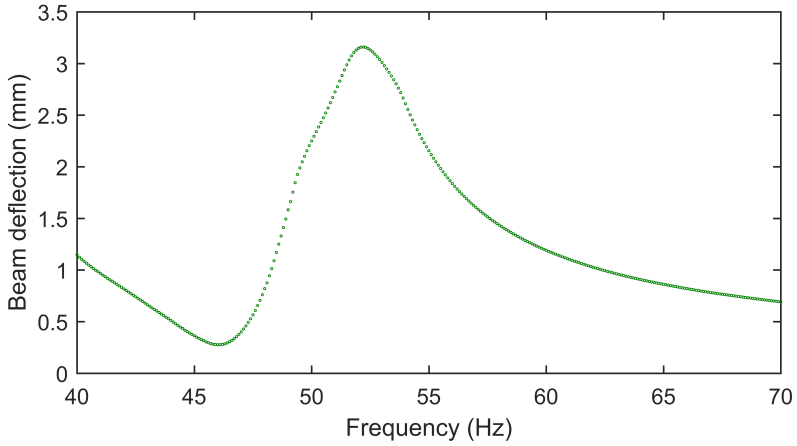

Figure 3.17: Example response of a composite laminate beam to vibration input amplitude of 3.0 V.

At each frequency, the vibration response of the beam was measured using the accelerometers mounted to the shaker clamp and the free end of the beam. The difference between these two acceleration signals was taken, and the amplitude of the resulting signal recorded as a measure of beam deflection amplitude. The results in Figure 3.17 show that the system has a vibrational resonance at approximately 52 Hz, corresponding to the first flexural natural frequency of the beam specimen itself.

Varying the vibration excitation amplitude can provide insight into the amplitude-dependent response behaviour of the specimen. An example analysis was conducted for the same pristine composite laminate beam: frequencies ranging from 40 to 70 Hz, in steps of 0.1 Hz, and at voltage levels of between 0.375 V and 3.0 V. The calculated beam deflection is shown in Figure 3.18 (solid lines).

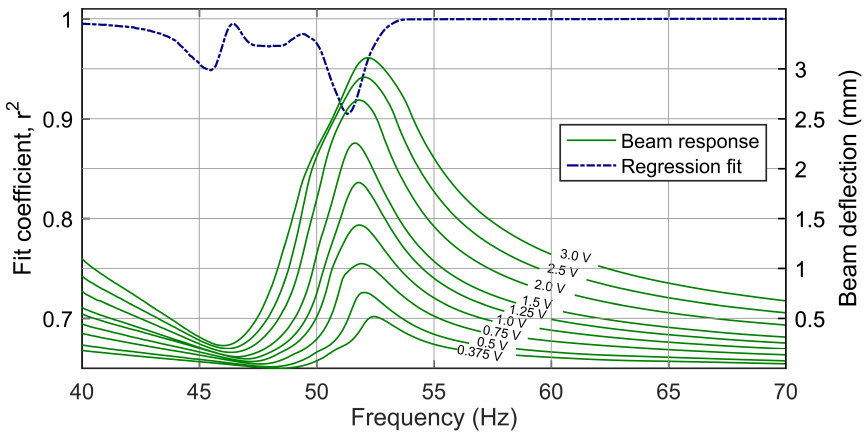

Figure 3.18: Example frequency response of a composite laminate beam at varying input amplitude voltage. Dashed line represents regression fit coefficient at given frequency.

A linear regression can be performed on the voltage-deflection data for each frequency,

and the fit coefficient (r^2) used to quantify the linearity of the relationship between excitation voltage and beam amplitude. The fit coefficient at each frequency is also shown on Figure 4.4 (dashed line). The vibration response of the specimen can help to inform selection of excitation frequency for nonlinear vibro-ultrasonic testing. Deviation from a fit coefficient of 1.0 indicates nonlinear dynamic behaviour of the system.

3.5.3 Vibro-ultrasonic analysis

For investigations into nonlinear vibro-ultrasonic testing, specimens are excited simultaneously by pumping vibration and an ultrasonic probing signal. Both the low- and high- frequency signals used for input are continuous sine waves. Typically, the high-frequency signal is used with an amplitude of 18 V which is the maximum range of the signal generator for which a nonlinearity of less than 1% is guaranteed. The frequency used varies, though typically it is chosen as a frequency at or near a resonant piezo response so that maximum throughput is achieved.

In a typical analysis, the frequency and voltage of the pumping excitation are varied using the LabVIEW application described in Section 3.5.1, with the system allowed to settle for one second between acquisitions. The sideband ratios calculated by the application can be used for further analysis.

A common damage index used in nonlinear vibro-ultrasonic testing is the so-called modulation index (Donskoy et al., 2001; Sutin and Johnson, 2005; Amerini and Meo, 2011):

$$R = \frac{(A_1^- + A_1^+)}{A_0} \tag{3.8}$$

where A_0 is the amplitude at the probing frequency and A_1^- and A_1^+ are the amplitudes of the first sideband pair (see Section 3.5.1.1 for details of sideband labelling). Figure 3.19 shows the result of analysis using the modulation index when both frequency and amplitude are varied, for a set of four composite laminate beams with (D1, D2) and without (P1, P2) damage. Two examples are provided for visualising the data, with modulation index plotted as a function of excitation voltage (Figure 3.19(a)) and beam deflection amplitude (Figure 3.19(b)).

Similar analysis can be performed by calculating the modulation index from other sidebands, for example the second pair of sidebands:

$$R_2 = \frac{(A_2^- + A_2^+)}{A_0} \tag{3.9}$$

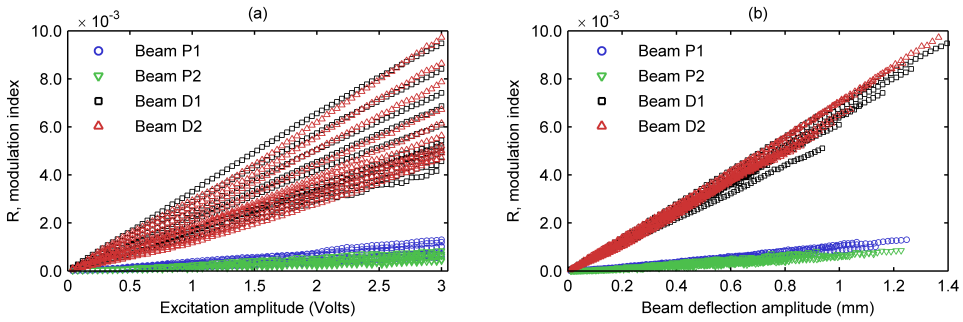

Figure 3.19: Example of modulation index versus (a) shaker amplitude and (b) beam deflection amplitude

With the modulation index established, further analysis on its variation with other system parameters can be performed. For data where modulation index does not have a linear relationship with measured acceleration, R is normalised by the shaker acceleration:

$$\hat{R}_{base} = \frac{R}{a_{base}} = \frac{(A_1^- + A_1^+)}{A_0\, a_{base}} \tag{3.10}$$

where a_{base} is the base excitation acceleration (measured at the shaker). Figure 3.20 shows how this index is typically visualised, plotted as a function of pumping frequency for two aluminium bonded-beam samples with (lighter shade) and without (darker shade) disbond damage at the bondline. This information can provide insight into the relative nonlinear response of beams with a varying pumping frequency.

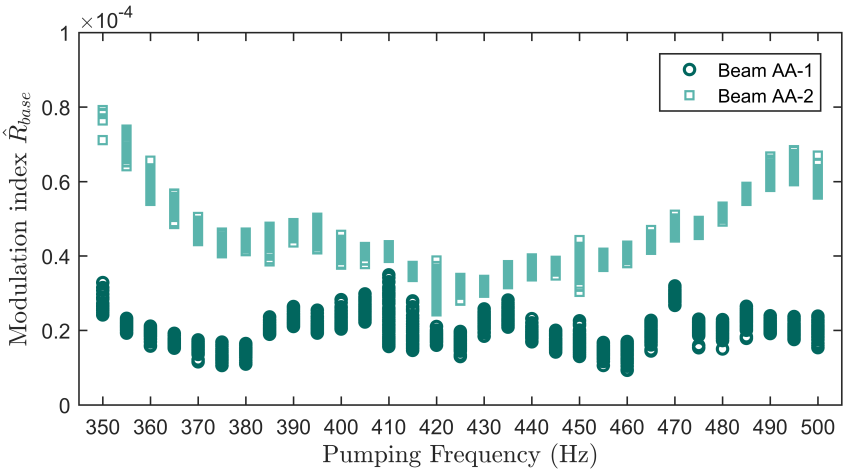

Figure 3.20: Normalised modulation index, $\hat{R}_{base}$, plotted as a function of pumping frequency for samples with (Beam AA-2) and without (Beam AA-1) damage. The frequencies shown here are above the beams' first resonant frequencies of 314 Hz.

Finally, comparisons can be made between amplitudes of different sideband pairs. It may for

example be of interest to determine how the first and second pair of sidebands relate:

$$\bar{R}_{1,2} = \frac{A_1^- + A_1^+}{A_2^- + A_2^+} \tag{3.11}$$

Similarly, it may be of interest to determine how the first pair of sidebands relates to all remaining pairs of sidebands:

$$\bar{R}_{1,2-5} = \frac{A_1^- + A_1^+}{A_2^- + A_2^+ + A_3^- + A_3^+ + A_4^- + A_4^+ + A_5^- + A_5^+} \tag{3.12}$$

An example trend of $\bar{R}_{1,2-5}$ is shown in Figure 3.21 for the same specimens used previously in this section.

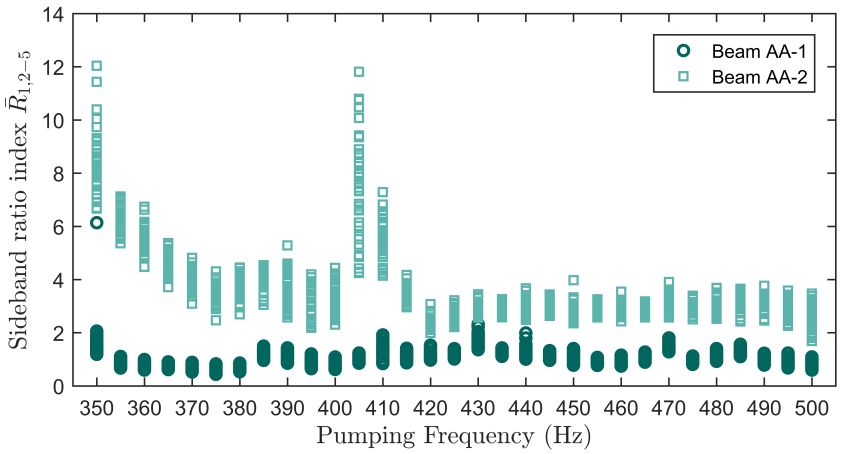

Figure 3.21: Comparative modulation index, $\bar{R}_{1,2-5}$, plotted as a function of pumping frequency for samples with (Beam AA-2) and without (Beam AA-1) damage.

In this section, exemplary data is used to demonstrate the variety of options which exist to present the results of nonlinear vibro-ultrasonic testing, with no discussion made of the particular results. Analysis and discussion of results is found in Chapters 4 and 5 of the thesis.

Chapter 4

Detection of delamination damage in composite laminates

4.1 Introduction

This chapter describes an investigation into the detection of artificial delamination damage in composite beams. Composite laminate beam specimens are studied for their response to vibrations, and an analysis is performed to determine how their response varies by frequency and amplitude of the vibration excitation. This analysis helps to inform the selection of excitation frequencies for nonlinear vibro-ultrasonic testing. Ultimately the beams are studied for how their nonlinear response may lead to detection of delamination damage.

The chapter is organised as follows:

- Section 4.2 provides details of the composite beam specimens used in this study.
- Section 4.3 presents results from a study of the response of the composite laminate beams to vibration excitation, including an analysis of nonlinear vibration behaviour of the beam.
- Section 4.4 presents results from an investigation into the application of nonlinear vibro-ultrasonic testing to the beam specimens.
- Section 4.5 presents results from testing of composite beams which contain delamination damage caused by low-velocity impact, for comparison to the findings presented for artificial delamination damage.
- Section 4.6 summarises the findings of the chapter and highlights extensions of this work to previous studies.

4.2 Composite beam specimens

Four composite laminate beams were used in the investigation, all manufactured from carbon/epoxy unidirectional prepreg plies and measuring 250 mm in length and 25 mm in width. The layup consisted of 16 plies in the stacking sequence of $[0_4/90_4]_s$. The average thickness of the cured laminates was 1.90 mm with a standard deviation of 0.03 mm.

Two of the beams, denoted D1 and D2, were manufactured with a thin Teflon ply between the 5th and 6th plies of prepreg, measuring 25 mm in width and located in the centre of the beam. These Teflon inserts were removed after curing of the beams, resulting in artificial delamination in the laminates shown in Figure 4.1, which extends through the width of the beam. Two beams without damage, denoted P1 and P2, are investigated as pristine references.

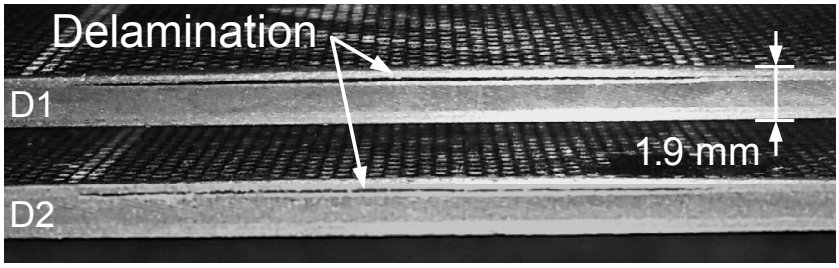

Figure 4.1: Artificial delamination damage in between 5th and 6th ply of beams D1 and D2

Two piezo transducers and two accelerometers were attached to each beam according to the procedures outlined in Section 3.2.1. Figure 4.2 shows a schematic including the placement of piezos and accelerometers and the location of damage.

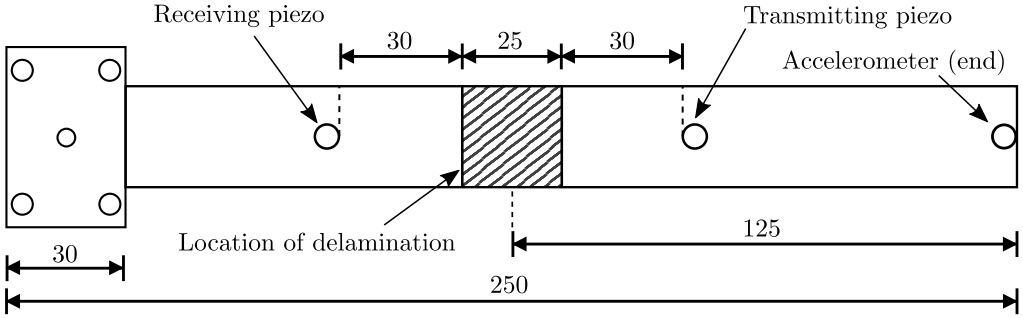

Figure 4.2: Dimensions and details of beam specimens, including placement of piezos and accelerometers in relation to damage.

Figure 4.3 shows beam D1 positioned in the experimental apparatus during testing. The strain relief techniques described in Section 3.2.1 can be seen in this photo, with the piezo wires twisted and secured using sealant tape. It can also be seen that after each secure attachment point, the instrumentation cables attached to the apparatus are not kept in close proximity to the

specimen to avoid unwanted vibration of the wires against the specimens during testing. Also visible in this photo is the vibration shaker clamping assembly to which the beam attaches, described in Section 3.2.2 in more detail.

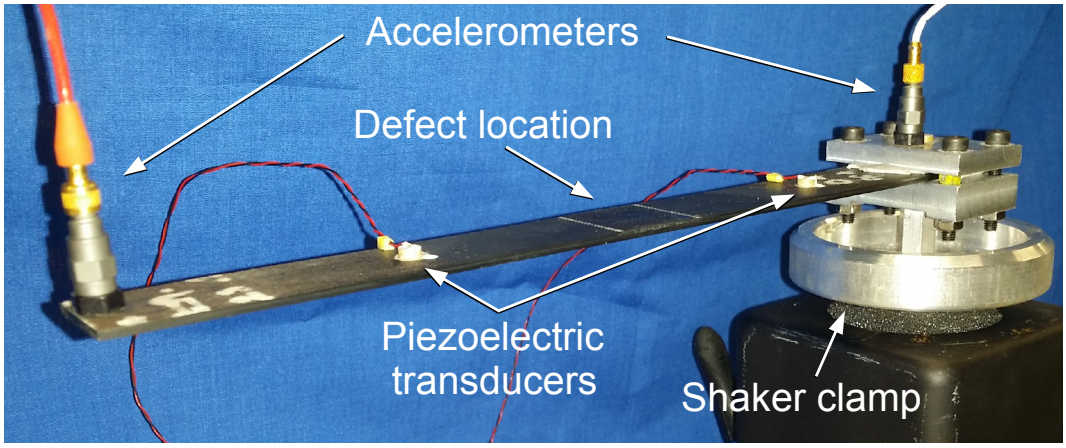

Figure 4.3: Damaged beam specimen in experimental apparatus.

4.3 Response to vibrations

The four beam specimens were analysed for their modal response, following the procedures introduced in Section 3.5.2. The beams were excited at frequencies ranging from 40 to 70 Hz, in steps of 0.1 Hz. The excitation amplitude of the input signal was varied, so that the amplitude-dependent features of the beam response could be determined. The response of the beam is measured as the beam deflection amplitude, calculated from the difference of the two acceleration signals. Figure 4.4 shows the results of this analysis for Beam P1.

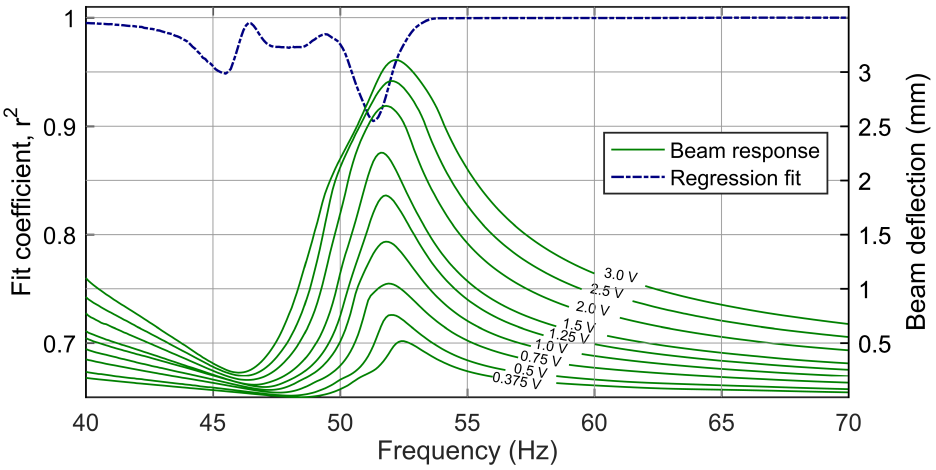

Figure 4.4: Vibration response of Beam P1 at multiple input excitation amplitudes. Dashed line represents regression fit coefficient at given frequency.

The results show that the system has a vibrational resonance at approximately 52 Hz. Using classical lamination theory (Reddy, 1997) to determine an effective flexural stiffness for the beam, it can be confirmed that this corresponds to the first flexural natural frequency of the beam specimen itself (Timoshenko, 1922). Additionally, the results show that the specimen exhibits nonlinear resonance; with an increasing excitation voltage, the resonance peak of the beam shifts, first to lower frequencies and then to higher frequencies.

The nonlinear resonance effect is quantified by the dashed line on Figure 4.4 which represents how well the voltage-deflection data fits a linear regression. For frequencies above approximately 55 Hz, the voltage-deflection data fits a linear regression very well, with r^2 fit coefficient close to 1. Around the resonant frequency shift, this value decreases to a minimum value of 0.905.

The vibrational responses for all four beams are shown in Figure 4.5. In all four cases, a resonant frequency is observed approximately between 52 Hz and 54 Hz, with each of the specimens exhibiting some degree of nonlinear resonance. In order to better compare the fit coefficients of the beam, these are presented together in Figure 4.6.

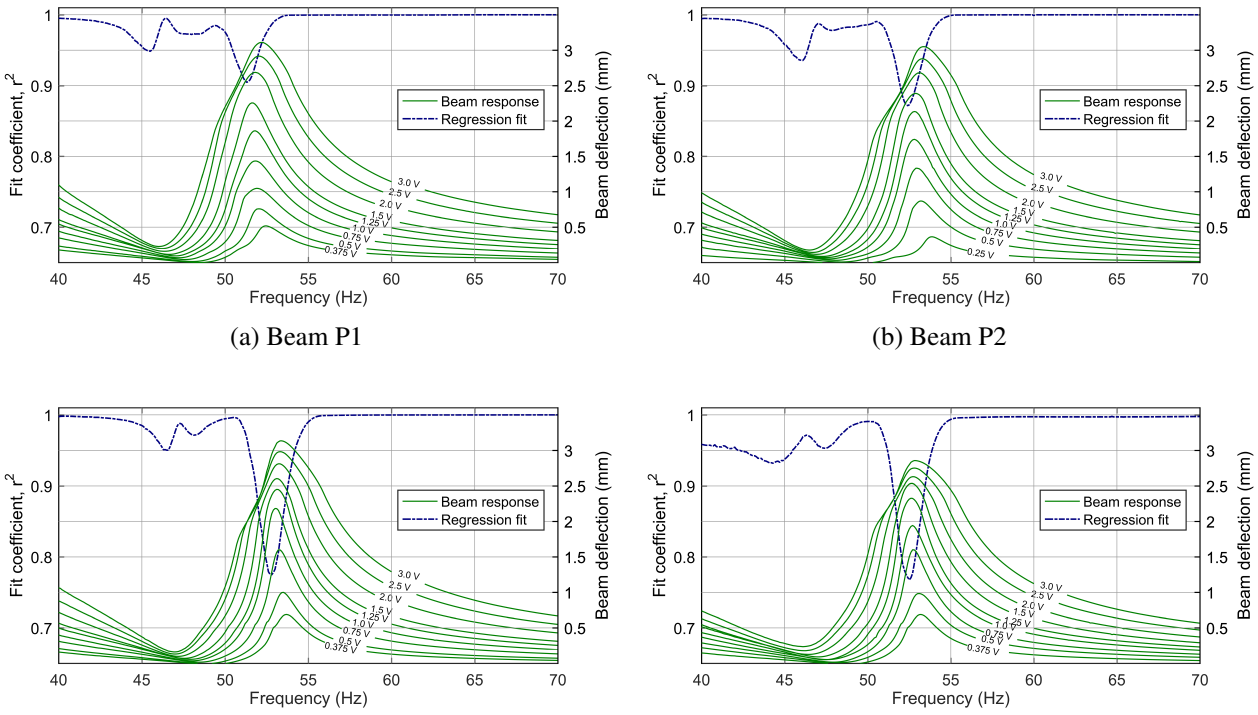

(a) Beam P1

(b) Beam P2

(c) Beam D1

(d) Beam D2

Figure 4.5: Vibration response of four specimens, (a)-(b) pristine beams and (c)-(d) beams with artificial delamination damage. Dashed line represents regression fit coefficient at given frequency.

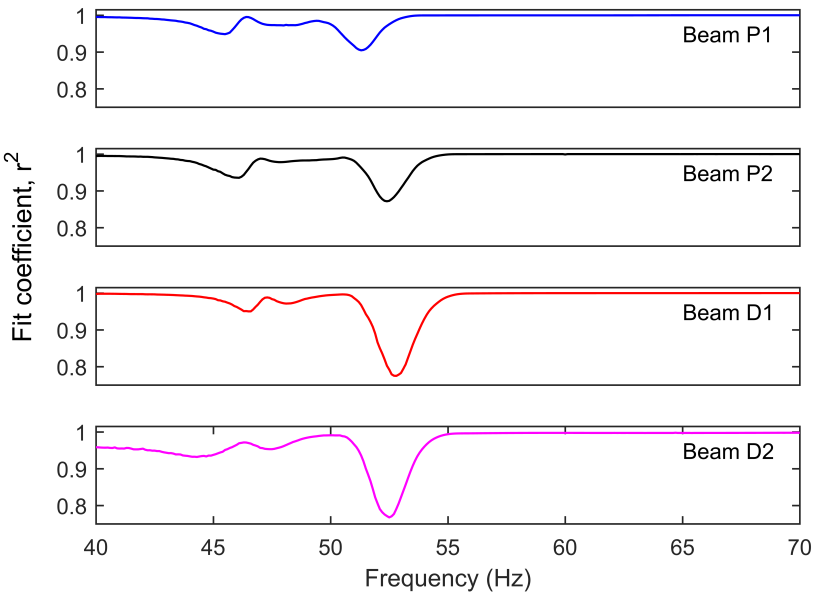

Figure 4.6: Linear regression fit coefficients for the four tested beams.

Of note is that the variation in resonant frequency between the beams is not sufficient to be used as a measure of damage. For example, the resonant frequencies of the beams when using a 0.5 V excitation are 52.0 Hz and 53.2 Hz for the pristine beams P1 and P2, and 53.5 Hz and 53.0 Hz for the damaged beams D1 and D2 respectively. There is larger variation between the two pristine samples than between the pristine and damaged sample, likely due to slight variations in thickness during manufacture.

Figure 4.6 shows that all four beams exhibit very linear voltage-deflection behaviour for frequencies tested above approximately 55 Hz, indicated by the r^2 fit coefficient of approximately 1.0. Around resonance, a drop in linearity is observed for all four beams. Notably, beams D1 and D2 having artifical delamination damage exhibit a greater degree of nonlinearity, with minimum r^2 values of 0.7749 and 0.7676, respectively, compared to minimum values of 0.8717 and 0.9046 respectively for beams P1 and P2.

The shifting resonance peak and the regression fit coefficient (r^2) data clearly shows that even for a pristine composite laminate specimen, an increase in excitation voltage does not produce the same proportional increase in beam deflection at all frequencies. The source of this nonlinearity is likely a combination of inherent material nonlinearity, nonlinearities of the mechanical system including clamp and vibration shaker assembly, and nonlinear dynamics of the beams - particularly given the deflection amplitude reaches levels in excess of 3mm, more than 1.5 times their thickness. An analysis of the nonlinear bending of the beam can be found in Section 4.3.1

While previous studies have generally used pumping frequencies equal to resonant frequencies (e.g. Aymerich and Staszewski 2010a; Klepka et al. 2014), this analysis shows that the dynamic nonlinearity of the system is likely to be maximal at resonance. Hence, the results of this study suggest that for optimised sensitivity and robustness of nonlinear vibro-ultrasonic experiments, pumping frequencies should be selected such that inherent nonlinearities associated with vibration behaviour of the system are minimal.

4.3.1 Nonlinear beam deflection

The strain-displacement relation for small strains based on Euler-Bernoulli beam theory is given by:

$$\varepsilon_{xx} = \frac{\partial u_x}{\partial x} = y\frac{\partial \varphi}{\partial x} = y\frac{\partial^2 w}{\partial x^2} \tag{4.1}$$

where ε_{xx} is the strain in the beam in the x-direction (along the length of the beam), u_x is the component of the displacement vector in the x-direction, y is the coordinate through the

thickness of the beam, φ is the angle of rotation of the normal to the mid-surface of the beam, and w is the deflection of the beam.

The first mode of flexural vibration for a cantilever beam is described by the following deflection curve (Graff, 1975):

$$w(x) = \frac{w_{max}}{2}\left[cosh(\beta Lx) - cos(\beta Lx) - \sigma sinh(\beta Lx) + \sigma sin(\beta Lx)\right] = \frac{w_{max}}{2}\,Y(x) \tag{4.2}$$

where $\beta = 1.875$ and $\sigma = 0.7341$. The deflection of the beam is thus the curve $Y(x)$ scaled by a factor $\frac{w_{max}}{2}$ where w_{max} is the deflection at the free end of the beam. Differentiating twice and combining with equation (4.1) yields the following expression for axial strain:

$$\varepsilon_{xx} = y\left(\frac{w_{max}}{2}\right)Y''(x) \tag{4.3}$$

This shows that the strain in the beam is proportional to the deflection at the free end of the beam, provided displacements and rotations are sufficiently small.

In order to derive the mode shape in equation (4.2), the following approximation was made to the beam curvature equation:

$$\kappa = \frac{\dfrac{\partial^2 w}{\partial x^2}}{\left[1 + \left(\dfrac{\partial w}{\partial x}\right)^2\right]^{\frac{3}{2}}} \approx \frac{\partial^2 w}{\partial x^2} \tag{4.4}$$

This is a reasonable approximation provided displacements and rotations are small such that the denominator term is close to unity. For larger amplitudes of deflection this approximation becomes less accurate, given the presence of the $\dfrac{\partial w}{\partial x}$ term in the denominator. In this case, axial strain in the beam due to bending is not linearly proportional to the amplitude of deflection.

This amplitude-dependent term also appears in the expression for axial finite (i.e. not infinitesimally small) strain in an Euler-Bernoulli beam (Wierzbicki, 2013):

$$\varepsilon_{xx} = \frac{\partial u_x}{\partial x} + \frac{1}{2}\left(\frac{\partial w}{\partial x}\right) \tag{4.5}$$

If analysis is extended to a nonlinear Timoshenko beam formulation, the expression for axial finite strain contains more amplitude-dependent terms (Wierzbicki, 2013):

$$\varepsilon_{xx} = (1 - w\frac{\partial \varphi}{\partial x})cos\varphi + \frac{\partial w}{\partial x}sin\varphi - y\frac{\partial \varphi}{\partial x} - 1 \tag{4.6}$$

Figure 4.7 shows the formulations for axial strain from equations (4.3), (4.5) and (4.6) applied to a beam model with parameters matching the specimens introduced in Section 4.2. For a given deflection amplitude at the tip of the cantilever, the maximum axial strain amplitude at the mid-point of the beam ($x = \frac{L}{2}$) was calculated.

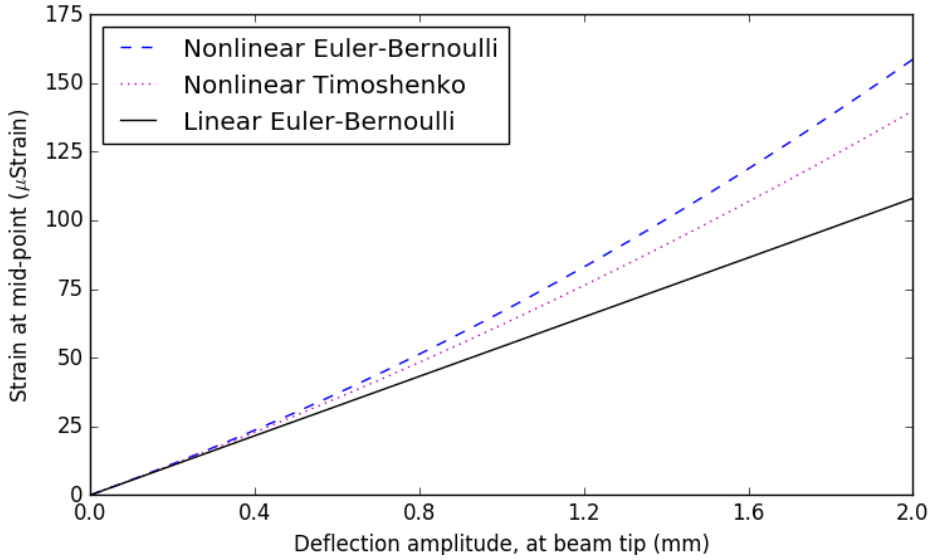

Figure 4.7: Maximum strain at the mid-point of the beam as a function of deflection amplitude at beam tip, calculated from three different strain formulations.

This analysis helps to explain the findings from Section 4.3, where the linearity of the relationship between excitation voltage and beam deflection amplitude was observed to decrease around resonance, where beam deflection amplitude exceeds 1 mm. At an amplitude of 1 mm, the deviation between linear and nonlinear strain-displacement relationship is approximately 10 μStrain, or approximately 20%. The findings of this analysis highlight the importance of nonlinear dynamics on the response of the beam at resonance, due to increased vibration amplitude.

4.4 Response to vibro-ultrasonic testing

Nonlinear vibro-ultrasonic testing was performed on the beam specimens according to the procedures introduced in Section 3.5.3.

A frequency sweep was performed in order to determine a suitable frequency for the ultrasonic excitation signal. The sweep was performed using the apparatus described in Section 3.2, with all vibro-ultrasonic testing instrumentation attached to the beam. This is done so that the response is measured during conditions matching those of vibro-ultrasonic testing. A continuous sine wave signal of peak-to-peak amplitude of 18 V was generated with frequencies ranging from 325 kHz to 425 kHz in steps of 0.25 kHz. The excitation signal was applied to the piezo closest to the free end of the beam. The response amplitude of the receiving piezo was measured at each frequency.

The response curves for beams P1 and D1 are shown in Figure 4.8. From the response of the four beams, an excitation frequency of 380 kHz was selected because it was at or near a peak in piezo response for all beams. For the two pristine beams, this corresponds to a response amplitude at 380 kHz of approximately -10 dB, while for the damaged beams the response is

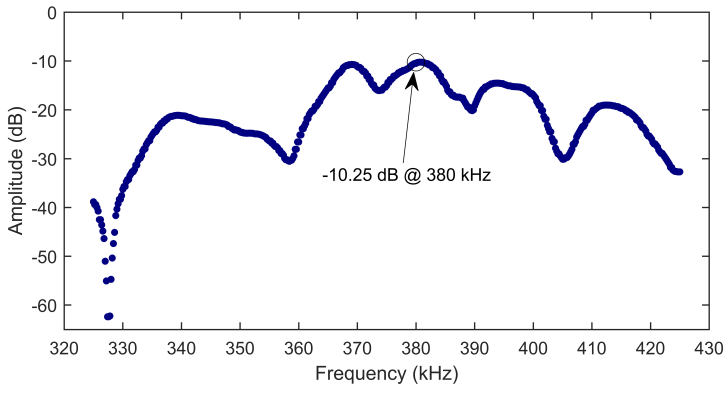

(a)

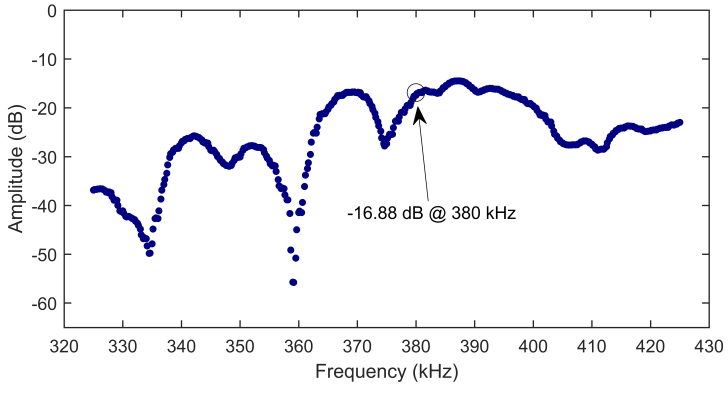

(b)

Figure 4.8: High frequency response curves for (a) beam P1 and (b) beam D1

approximately -17 dB. The lower amplitude measured for the damaged beams demonstrates that the energy of the ultrasonic wave energy does not transmit as efficiently as in the pristine samples, likely due to reflection and damping caused by the delamination.

The beams were next excited simultaneously by pumping vibration and an ultrasonic probing signal. Both the low- and high-frequency signals used for input were continuous sine waves. Based on the analysis of the frequency response of the beams, the ultrasonic signal had a frequency of 380 kHz and a peak-to-peak amplitude of 18 V. A frequency range of 60 to 70 Hz was selected for vibration excitation, based on analysis performed in Section 4.3 determining that all beams exhibited a linear relationship between excitation voltage and beam deflection amplitude in this range.

The low-frequency excitation voltage was varied from 0.04 V to 3.0 V in steps of 0.04 V, and for each step the system was allowed to settle for one second before acquisition was made at the receiving transducer. This was performed using the data collection procedures and LabVIEW application described in Section 3.5.1, and repeated for low frequencies from 60 to 70 Hz, in steps of 1 Hz, for all four beams.

Frequency data was obtained using the Albrecht window and RMS averaging of 10 samples. Figure 4.9 shows the resulting frequency spectrum obtained from testing of beam P1, with a vibration excitation of 60 Hz at 3.0 V. The spectrum is zoomed around the central frequency of 380 kHz.

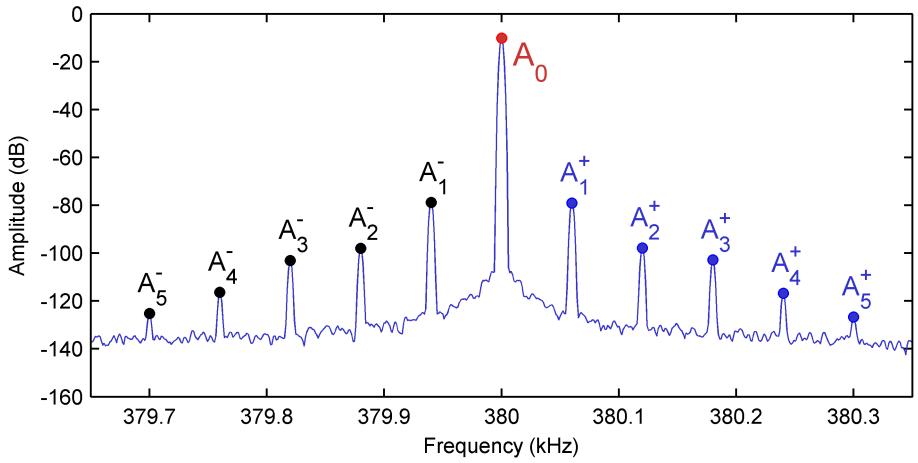

Figure 4.9: Resulting frequency spectrum measured from beam P1, with a pumping excitation of 60 Hz at 3.0 V. The labelling of amplitudes used for further analysis is also shown.

The spectrum in Figure 4.9 contains five pairs of sidebands visible above the noise floor. This is an outstanding result which highlights the effectiveness of the experimental and measurement system in reducing the noise floor around the frequency of interest.

Labels on Figure 4.9 indicate amplitudes of interest - the amplitude of the probing frequency A_0 and of each individual sideband, A_1 through A_5, with a superscript differentiating between sidebands lower $(-)$ and higher $(+)$ than the probing frequency.

4.4.1 Effect of increasing excitation amplitude

From sideband amplitude data, a modulation index, $R = (A_1^- + A_1^+)/A_0$, was calculated for each sample. Figures 4.10(a) and 4.10(b) show this modulation index versus increasing excitation voltage of the vibration shaker for beams P1 and D1 respectively. The artificially delaminated beam D1 exhibits a greater degree of modulation than the pristine beam P1, with a maximum modulation index of 1.5×10^{-3} and 10×10^{-3} respectively.

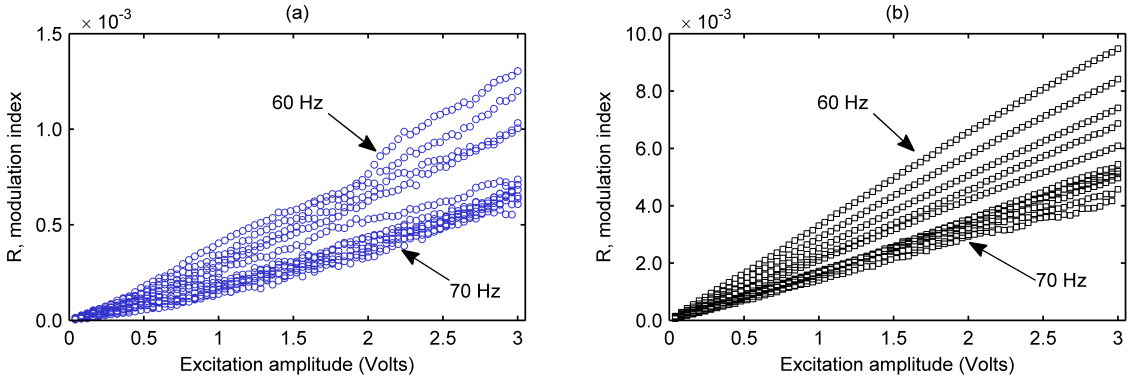

Figure 4.10: Modulation index versus shaker voltage input for (a) beam P1 and (b) beam D1

While this data shows that the modulation index for a certain frequency increases with increasing shaker voltage, it also shows that the modulation index for a particular shaker voltage varies depending on the frequency of excitation, with 60 Hz producing the greatest degree of modulation for all beams. As frequency increases to 70 Hz, the modulation index decreases. These observations are as expected, since the low-frequency response curves from Section 4.3 show an approximate halving of amplitude in beam deflection when moving from 60 to 70 Hz, reflected in an approximate halving of the gradient of the modulation index-voltage curve between these frequencies.

Figure 4.11(a) shows data for all four beams superimposed, illustrating the large spread of modulation index for different frequencies; while there is a clear difference in modulation index between pristine and damaged beams, the spread in modulation index for a damaged beam is larger than this difference. Figure 4.11(b) instead shows modulation index plotted against measured beam deflection amplitude during excitation. In this case, the data points collapse into two clear regions, with all data showing a very clear linear relationship between vibration amplitude and modulation index. At the highest beam deflection amplitudes, the difference in

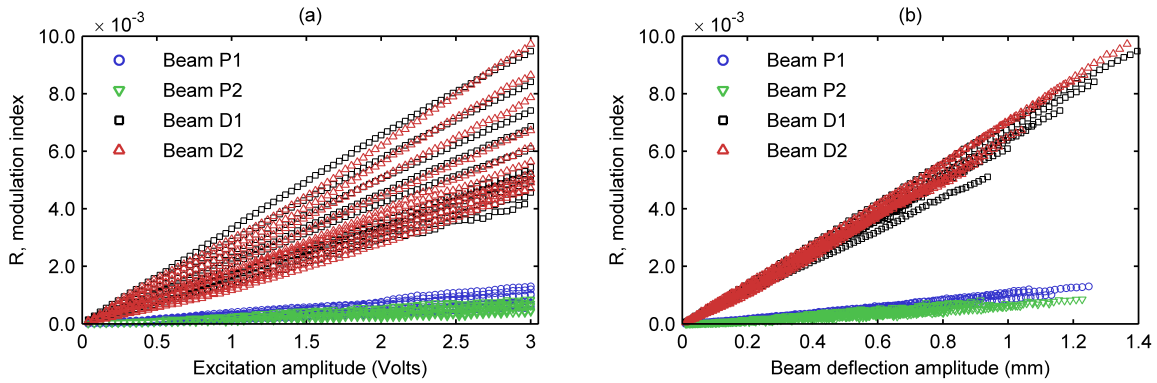

Figure 4.11: Modulation index versus (a) shaker amplitude and (b) beam deflection amplitude

modulation index between the pristine and damaged beams is approximately 9×10^{-3}.

These findings show a strong dependence of nonlinear wave interaction on the amplitude of the pumping wave in the presence of nonlinearity, a dependence which is observable only due to the amount of data available here compared to other studies.

As shown in Section 4.3.1, the measured deflection of the beam is proportional to the strain within the beam, and hence the measured modulation index increases approximately linearly with strain amplitude in all four beams. The relationship between excitation voltage and modulation index studied elsewhere in literature is hence only meaningful when excitation voltage is a predictor of strain amplitude, which is generally not the case due to frequency dependence and variations between specimens. In this study, the measure of beam deflection is proportional to strain; granted all beams investigated are of approximately identical geometry and material, the relationship between beam deflection and strain is very similar for all beams.

The data in Figure 4.11(b) indicate a higher modulation index for the beams with artificial delamination damage compared to pristine beams for the same deflection. This is attributed to the delamination causing a larger degree of nonlinear wave interaction than surrounding material for a given strain amplitude. That duplicate samples for both the damaged and the pristine cases closely agree with one another is significant, and further supports the notion that the presence of the delamination is the cause of greater measured nonlinear frequency mixing.

Repeat experiments were performed after removing and reattaching specimens to the experimental apparatus and reconnecting all instrumentation to the system. A complete set of results including additional data from repeat experiments can be found in Appendix A. The results from repeated experiments are consistent with the findings presented in this chapter. This is an indication that the minute differences in system boundary conditions (i.e. tension/weight from instrumentation cables, position and deformation of rubber in the clamp assembly) did not cause a significant effect between specimen tests.

4.5 Low-velocity impact induced delamination damage

This section presents data collected from nonlinear vibro-ultrasonic testing of composite laminate samples containing delamination damage due to low-velocity impact.

4.5.1 Specimen manufacture

Four composite laminate panels measuring 300 mm x 300 mm were manufactured using 8 plies of *Hexply* M18/1 woven fabric carbon/epoxy prepreg. The average thickness of the cured laminates was approximately 1.82 mm.

Low-velocity impact tests were conducted using a drop-weight test frame, built in-house, which includes a rebound braking system to avoid multiple impacts. The test frame is shown in Figure 4.12. A falling weight of 3.0223 kg is guided by rails from an adjustable height onto the test sample. Attached to the falling weight is a hemispherical steel head with a diameter of 25.4 mm and a *Dytran 1050V6* load cell, in turn connected to a *Tektronix TDS 420A* oscilloscope. The height from which the weight is dropped from determines the energy level, with the impact velocity measured by two-gate laser measurements immediately prior to impact.

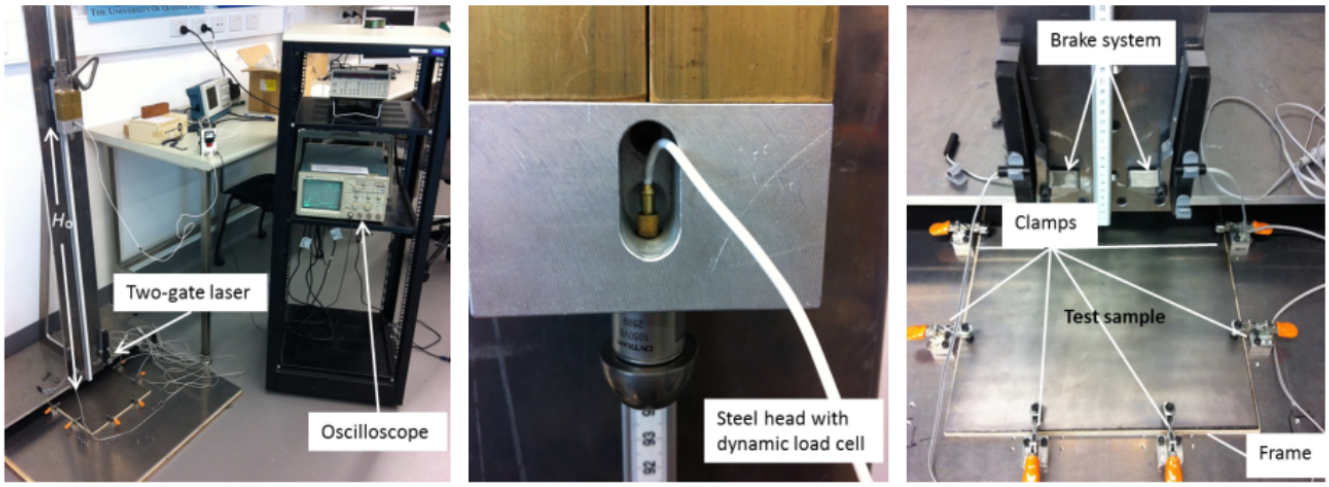

Figure 4.12: Low-velocity drop-weight test frame setup, adapted from Reiner (2016).

During the impact events, the steel head of the falling weight impacted the centre of the panels. Two of the composite laminate panels were struck with 20 J of impact energy, with the remaining two panels struck with 30 J. This value of impact energy is calculated from the gravitational potential formula:

$$E_{pot} = mgh \tag{4.7}$$

where m is mass, h is drop height and g is gravitational acceleration.

The impact events caused visible damage to the panels; damage to the underside of the panels is shown in Figure 4.13. The extent of visible damage is larger for the 30 J tests than for the 20 J tests.

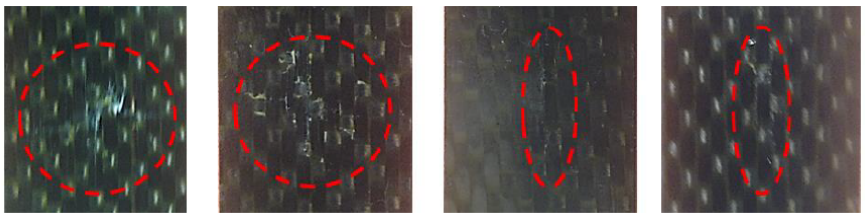

(a) 30 J impact (b) 20 J impact

Figure 4.13: Damage viewed from the bottom surface of the panels after impact testing.

Force-time data collected from the load cell is integrated to find absorbed energy $E_a(t)$ at time t according to:

$$E_a(t) = \frac{m(v_i^2 - v(t)^2)}{2} + mg\delta(t) \tag{4.8}$$

where $v_i = \sqrt{2gh}$ is the initial velocity. Velocity at time t is given by

$$v(t) = v_i + gt - \int_0^t \frac{F(t)}{m} dt \tag{4.9}$$

where $F(t)$ is the force measured at the load cell, and finally the impactor displacement $\delta(t)$ at time t is given by

$$\delta(t) = v_i t + \frac{gt^2}{2} - \int_0^t \left(\int_0^t \frac{F(t)}{m} dt \right) \tag{4.10}$$

The force-time data for one each of a 20 J and 30 J impact event are shown in Figure 4.14,

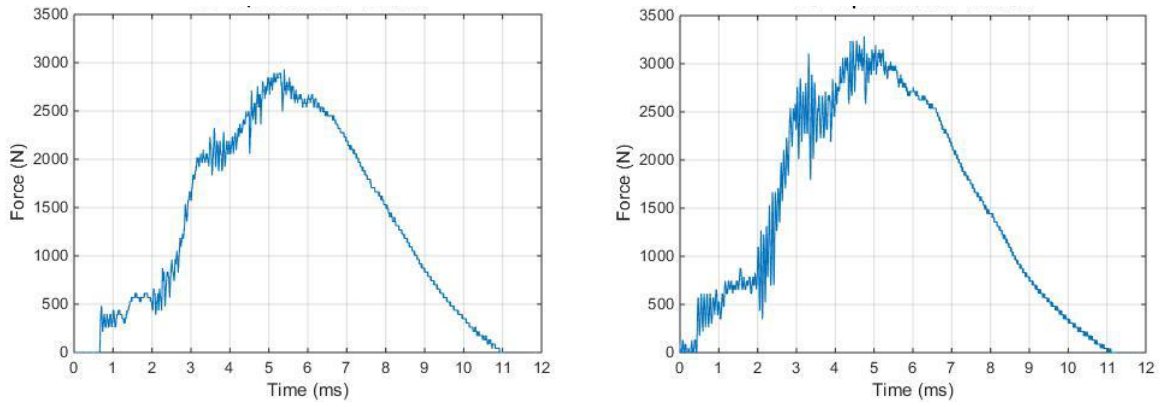

(a) 20 J impact (b) 30 J impact

Figure 4.14: Impact force vs time during impact testing of composite laminate panels.

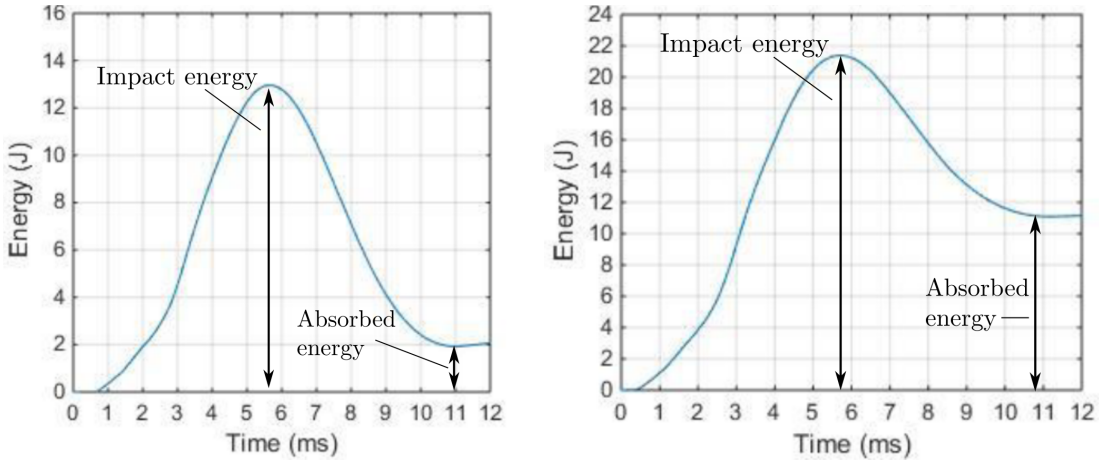

(a) 20 J impact (b) 30 J impact

Figure 4.15: Absorbed energy, E_a, vs time during impact testing of composite laminate panels.

and the absorbed energy data calculated from Equation (4.8) are shown in Figure 4.15. The final, constant value of absorbed energy in Figure 4.15 is used as a measure of total energy absorbed by the panel during testing. The peak value on these plots is the actual impact energy, which is lower than that predicted by the potential energy prior to impact.

These force-time and energy-time histories are very similar to results in literature for low-velocity impacts of fibre-reinforced composite laminate panels (e.g. Belingardi and Vadori, 2002; Liu and Liaw, 2010; Reiner et al., 2016), giving confidence in their use for quantifying the relative energy absorbed by the composite laminates. For the remainder of this section, the impact events will be referred to as 20 J or 30 J impact events, even though the measured impact and absorbed energy is lower.

From each of the four panels, a 25 mm wide beam was cut from the centre of the panel which included the damage zone caused by impact testing. These four beams are the test specimens for nonlinear vibro-ultrasonic testing performed in this section. In addition to these four specimens, two additional beams were cut from a pristine part of the panels, representing pristine comparison specimens. Table 4.1 lists the specimen designations used for these beams,

Table 4.1: Composite beam specimen designations for impact damage testing

Specimen designation	Description	Impact energy (J)	Absorbed energy (J)
IP1, IP2	Pristine	–	–
ID20-1	20 J impact damage zone	12.95	2.05
ID20-2	20 J impact damage zone	14.78	2.61
ID30-1	30 J impact damage zone	21.38	11.14
ID30-2	30 J impact damage zone	21.83	12.13

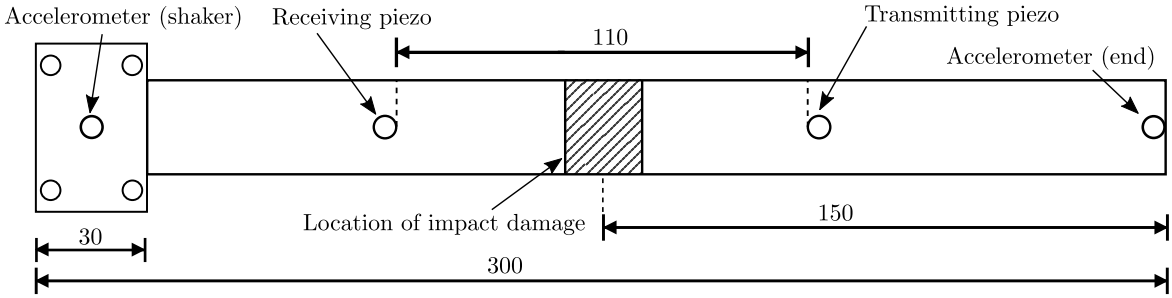

Figure 4.16: Dimensions and details of impact beam specimens, including placement of piezos and accelerometers in relation to the impact locations.

including for each beam the measured impact and absorbed energies from the analysis presented in Equation (4.8) and Figure 4.15.

Each beam specimen was instrumented with two piezo transducers according to the procedures outlined in Section 3.2.1. Figure 4.16 shows a schematic including the placement of piezos and accelerometers during experimentation for the beam specimens with impact damage.

4.5.2 Response to vibration

The six beams were analysed for their modal response, following the procedures introduced in Section 3.5.2. The results of this analysis for a pristine specimen (Beam IP1) and a damaged specimen (Beam ID30-1) are shown in Figures 4.17(a) and 4.17(b) respectively.

The modal analysis was conducted for all six beams; the results shown for the pristine and damaged specimens are a good representation of the larger set of results for both pristine beams and all damaged beams. For all beams, a vibrational resonance is observed at approximately 43 Hz, corresponding to the first flexural natural frequency of the beam itself. Nonlinear resonance

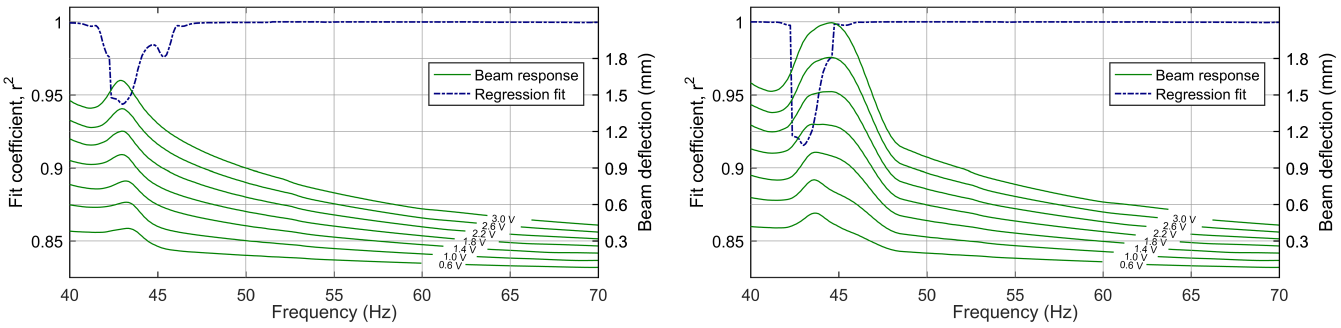

(a) Pristine specimen

(b) 30 J impact

Figure 4.17: Vibration response of (a) Beam IP1 and (b) Beam ID30-1. Dashed line represents regression fit coefficient at given frequency.

is exhibited; for increasing excitation voltages, the resonance peak shifts to lower frequencies.

The dashed line on each of Figures 4.17(a) and 4.17(b) is a measure of how well the voltage-deflection data fits a linear regression; a dip in this measure around resonance confirms nonlinear resonance. The degree of nonlinear resonance in all six beams is less than those studied in Section 4.3; consider the pristine specimens beams P1 and P2 with minimum r^2 values of 0.8717 and 0.9046 respectively, while the minimum r^2 value exhibited by the six beams examined here was 0.9154 (Beam ID30-1). This can be explained by the lower deflection amplitudes in the response of these beams, and by the analysis of Section 4.3.1 that predicts a more nonlinear displacement-strain relationship at larger deflection amplitudes.

4.5.3 Response to vibro-ultrasonics

Nonlinear vibro-ultrasonic testing was performed on the beam specimens according to the procedures introduced in Section 3.5.3. As described in Section 4.4, a frequency sweep was performed in order to determine suitable ultrasonic excitation frequencies. A frequency of 343 kHz was selected as it was at or near a peak in piezo response for all six beams.

The beams were excited simultaneously by pumping vibation and ultrasonic probing signal. A frequency range of 50 to 55 Hz was selected for vibration excitation, based on analysis in the previous section which determined that all beams exhibited a linear relationship between

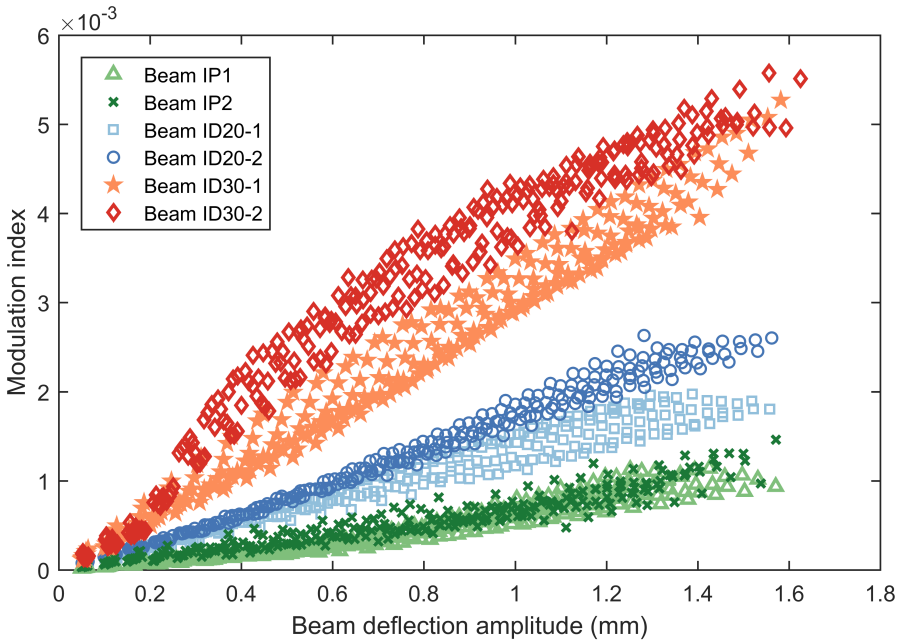

Figure 4.18: Modulation index versus beam deflection amplitude for pristine composite laminate beam specimens and those with impact damage.

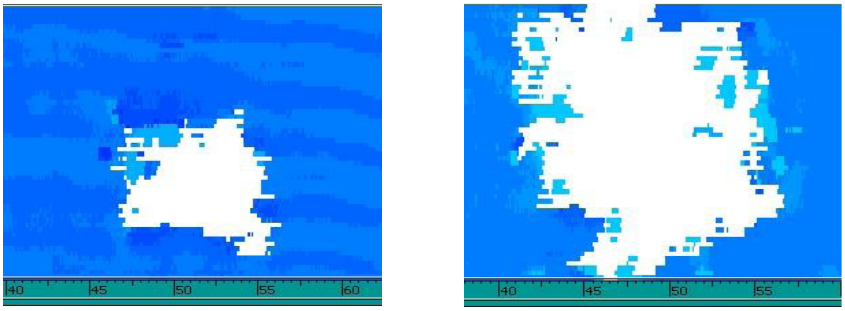

(a) 20 J impact (b) 30 J impact

Figure 4.19: Ultrasonic C-scan images of the damage zones of impacted composite laminate samples (Beams ID20-1 and ID30-1), white indicates no backwall reflection. Scales are in mm.

excitation voltage and beam deflection amplitude in this range. The procedure to collect sideband data for this parameter space is the same as used in Section 4.4.

Results for vibro-ultrasonic testing of the specimens are presented in Figure 4.18, with modulation index, $R = (A_1^- + A_1^+)/A_0$ shown versus increasing beam deflection amplitude.

The data in Figure 4.18 indicate a higher modulation index for the beams with impact damage compared to pristine beams, for the same amplitude of beam deflection. This is an indication that, like artificial delamination damage, a larger degree of nonlinear wave interaction occurs in the damaged region than surrounding material for a given strain amplitude.

Significantly, the specimens impacted with a 30 J strike (ID30-1 and ID30-2) exhibited a greater modulation index than those impacted with a 20 J strike (ID20-1 and ID20-2). This result suggests that the 30 J strikes resulted in damage within the composite laminates that caused more nonlinear wave interaction than the 20 J strikes. The visible damage shown in Figure 4.13 supports this notion; the extent of visible damage is larger for the 30 J strikes.

To better quantify the level of damage present within each specimen, ultrasonic C-scan imaging was performed. The images in Figure 4.19 show that the 20 J impacts resulted in a damage area approximately 10 mm in diameter, while for 30 J impacts the area is approximately 25 mm in diameter. Aymerich and Staszewski (2010a) provided X-ray imaging of their specimens that showed a 10 mm diameter damage area for a peak impact energy of 2.04 J, and approximately 25 mm diameter damage area for an impact energy of 10 J. Recalling that the 20 J and 30 J impact events resulted in impact energies of approximately 2 J and 12 J respectively, these damage zone sizes indicated from C-scan imaging are consistent with literature for these energy levels.

These findings show that the degree of nonlinearity is dependent on the area of the damage zone; more micro-cracks and delaminations within the composite laminate allow for more

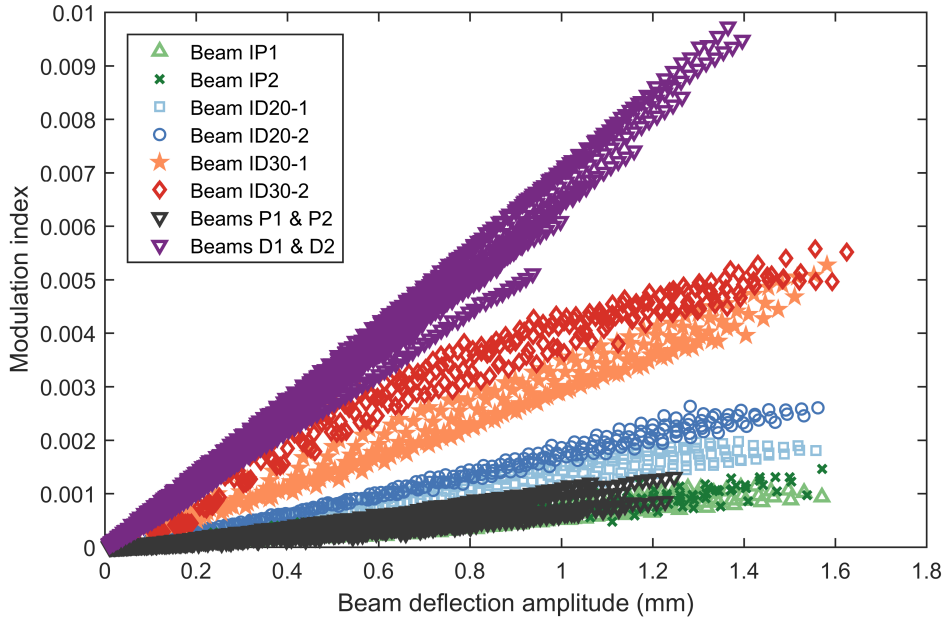

Figure 4.20: Comparison of modulation index versus beam deflection amplitude for artificial delamination damage and low-velocity impact induced damage.

nonlinear wave interaction to occur. Close agreement between duplicate samples for both impact energy levels suggests (and pristine specimens) reinforce this finding.

Figure 4.20 shows the data in Figure 4.18 superimposed with modulation index data for the beam specimens studied in Section 4.4. Beams P1 and P2 are shown to exhibit a similar degree of nonlinearity to IP1 and IP2; the inherent nonlinearity in all four pristine specimens match closely. The modulation index measured for beams with impact-induced damage is however less than that of artificial delamination damage; even for beams ID30-1 and ID30-2 where the damage area measured by C-scan is comparable to the artificial delamination (25 mm diameter), the degree of nonlinearity is different by a factor of 2.

These findings confirm that nonlinear vibro-ultrasonic inspection of laminar damage induced by impact loading of composite laminates is able to distinguish the damage through an increase in measured nonlinearity. The results reinforce the findings earlier in the chapter, where it was shown for artificial delamination damage that there is a strong dependence of nonlinear wave interaction on the amplitude of the pumping wave in the presence of damage.

4.6 Summary of findings

The work presented in this chapter demonstrates that the current study into detection of delamination damage in composite laminate beams confirms results from studies which have been introduced in the literature review (Chapter 2). These include:

- Gross laminar defects in composite laminates causes an increase in nonlinearity to such a degree as to cause an observable shift in the resonance frequency through the nonlinear resonance phenomenon.
- Nonlinearity due to laminar damage in composite laminates causes the modulation index obtained from nonlinear vibro-ultrasonic testing to be much larger than for pristine specimens.
- The effect of increasing excitation amplitude on nonlinear vibro-ultrasonic testing of composite laminates is a monotonic increase in modulation index.

This work also includes the following extensions to previous studies in the literature:

- Analysis of the relationship between excitation voltage and vibration amplitude and presentation of a method for determining frequencies where this relationship is linear, to inform frequency selection for nonlinear vibro-ultrasonic experiments.
- Highlighting that dynamic nonlinearity of the system is likely to be maximal at resonance, and that for maximised sensitivity and robustness of nonlinear vibro-ultrasonic experiments, the pumping frequency should be selected close to resonance but at frequencies for which a linear relationship exists between excitation input voltage and displacement amplitude.
- Demonstration of how the deliberate selection of experimental instrumentation and signal processing techniques which increase discernibility of sideband frequency components generated in nonlinear vibro-ultrasonic testing leads to a very low noise floor and clearly defined sideband peaks.
- The automated data collection procedure used in this work leads to a large amount of data points per nonlinear vibro-ultrasonic test, covering a much larger parameter space than previous studies with data more closely spaced. This in turn enables demonstration of a strong dependence of nonlinear wave interaction on the amplitude of the pumping wave in the presence of nonlinearity.

Chapter 5

Detection of bondline damage in adhesively bonded beams

5.1 Introduction

This chapter describes the application of nonlinear vibro-ultrasonics to detect bondline damage in adhesively bonded structures. The chapter is organised as follows:

- Section 5.2 describes an investigation into the detection of bondline damage in bonded composite laminate beams. This is first done using the methodology established in Chapter 4, with extensions to the method used to investigate the results further. Results from Chapter 4 are also revisited for comparison.
- Section 5.3 presents the results of nonlinear vibro-ultrasonic testing of bonded aluminium beams with and without bondline damage. Rather than using the typical methodology established in Chapter 4, the pumping frequency is varied over a large range and advanced analysis techniques are performed using measurements of the resulting sideband frequency components.
- Section 5.4 summarises the findings of the investigations and the importance of these findings on the use of nonlinear vibro-ultrasonic testing for detection of damage in adhesively bonded structures.

5.2 Bonded composite laminate beams

5.2.1 Specimen manufacture

Composite laminate panels measuring 300 mm x 100 mm were manufactured using 6 plies of *Hexply* M18/1 woven fabric carbon/epoxy prepreg. The average thickness of the cured laminates was approximately 1.45 mm. These panels were then bonded together using *Cytec* FM 300NK adhesive film. The bonded panels were then cut into the final beam specimens of 300 mm length and 25 mm width, having an average thickness of approximately 3.05 mm.

Two of the specimens, designated beams B1 and B2, were manufactured as described, with seven additional specimens manufactured with an inclusion at the bondline during curing to simulate bondline damage. Two of these specimens, designated RF1 and RF2, included a 60 mm wide strip of Airtech Wrightlon 5200 release film, folded onto itself twice into as ”S” configuration, and flattened to produce a 20 mm wide strip. The remaining five specimens included a folded strip of DuPont Kapton polyimide film, with final width ranging from 10 mm to 40 mm. A complete list of beam specimens is found in Table 5.1. Of note are beams K10-2 and K20-2, whose Kapton film inclusion was removed after curing.

Each beam specimen was instrumented with two piezo transducers according to the procedures outlined in Section 3.2.1. Figure 5.1 shows a schematic including the placement of piezos and accelerometers during experimentation for the beam specimens with a 20 mm width inclusion. Note that for beams with a differently sized inclusion, the distance between piezos was kept fixed while keeping the defect centred.

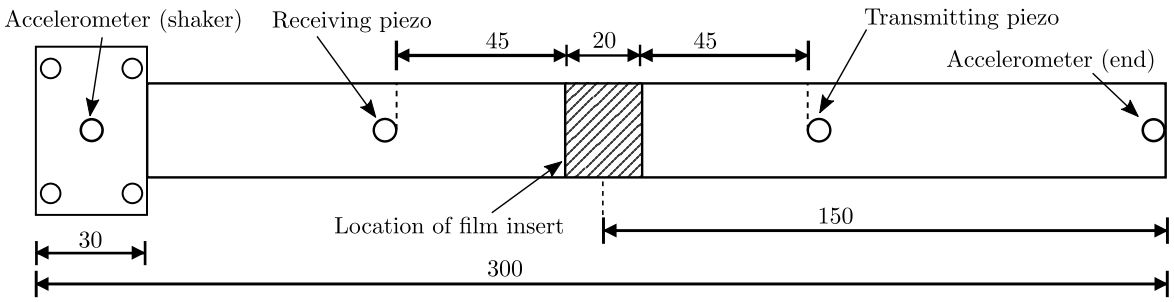

Figure 5.1: Dimensions and details of bonded beam specimens, including placement of piezos and accelerometers in relation to a 20 mm inclusion defect.

Table 5.1: Bonded composite beam specimen designations

Specimen designation	Inclusion type	Inclusion size
B1, B2	None	–
RF1, RF2	Wrightlon 5200 release film	20 mm
K10-1	Kapton HN film	10 mm
K10-2	Kapton HN film (removed)	10 mm
K20-1	Kapton HN film	20 mm
K20-2	Kapton HN film (removed)	20 mm
K40	Kapton HN film	40mm

5.2.2 Response to vibration

The beam specimens were analysed for their modal response, following the procedures introduced in Section 3.5.2. The beams were each excited with a frequency sweep from 40 to 80 Hz in steps of 0.1 Hz with an excitation amplitude of 1.0 V to establish the vibration resonance of each beam. Table 5.2 lists the resonant frequencies found for each beam.

Table 5.2: First resonant frequency measured for bonded composite beam specimens

Specimen	B1	B2	RF1	RF2	K10-1	K10-2	K20-1	K20-2	K40
Resonant Frequency (Hz) (1.0 V excitation)	56.9	57.3	56.4	55.8	57.0	56.6	56.2	57.6	56.5

The expected effect of damage at the bondline of the beams is a reduction in stiffness and a corresponding reduction in resonant frequency. These results indicate that the variation in resonant frequency between the beams is not an apparent indicator of the inclusion of damage in some specimens. In fact, beam K20-2 which has a 20 mm section of the bondline not cured to the top adherend was found to have the largest resonant frequency.

Analysing the bonded beam as a layered plate and using classical lamination theory (Reddy, 1997) to determine an effective flexural stiffness, it can be confirmed that the frequencies presented here correspond to the first flexural natural frequency of the specimens. Furthermore, the variation from the lowest resonant frequency (55.8 Hz) to the highest (57.6 Hz) can be explained by a variation of 0.1 mm in the average thickness of the bonded beam specimen (Graff, 1975).

Four of the specimens were investigated in more detail for their amplitude-dependent vibration response. Beams B1, RF1, K20-2 and K40 were each excited at frequencies ranging from 45 Hz to 75 Hz, in steps of 0.1 Hz, for excitation amplitude ranging from 0.5 V to 3.0

V. Figure 5.2 shows the results of these analyses, including the beam response curves for the different excitation amplitudes (solid line) and the linearity of the voltage-displacement relationship (dashed line).

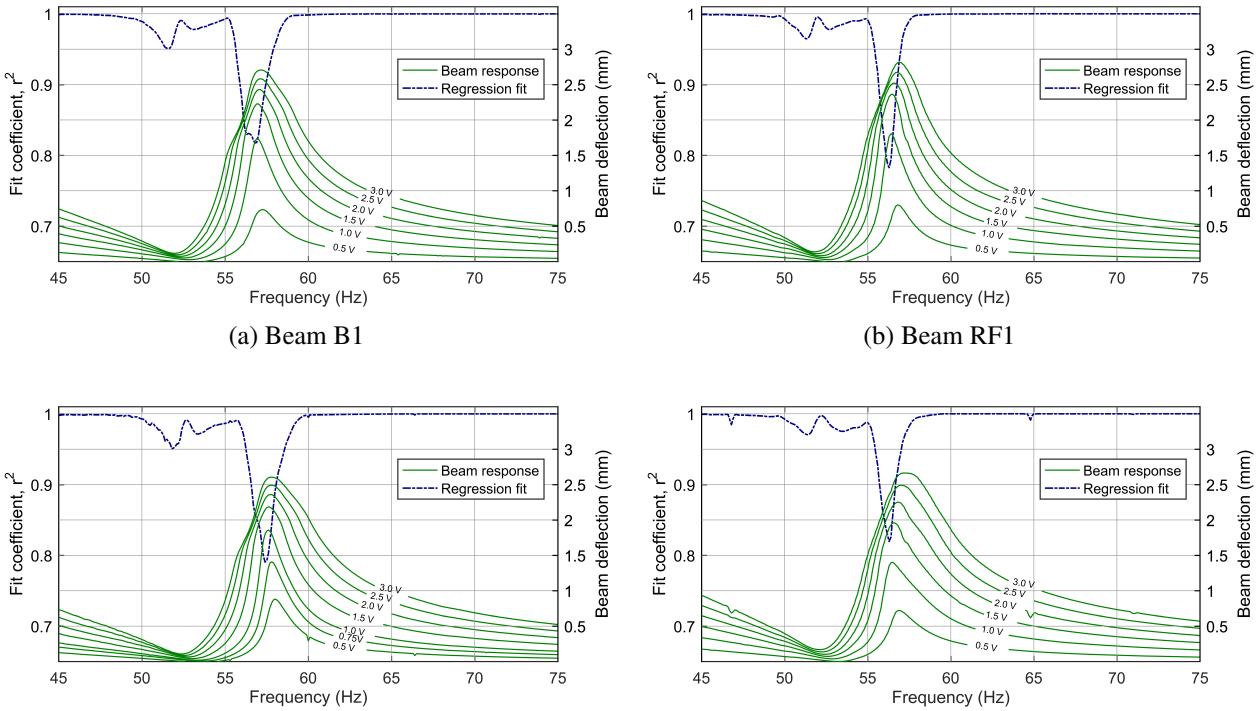

(a) Beam B1

(b) Beam RF1

(c) Beam K20-2

(d) Beam K40

Figure 5.2: Vibration response of four bonded composite specimens with (a) intact bondline, (b) 20 mm release film, (c) 20 mm Kapton film, removed post-cure, (d) 40 mm Kapton film.

For the four beams tested, some degree of the nonlinear resonance phenomenon is observed; with an increasing excitation voltage, the resonance peak of each specimen shifts, first to lower frequencies and then to higher frequencies.

Quantifying the nonlinear resonance shift by how well the voltage-deflection data fits a linear regression (dashed line, Figure 5.2) reveals a similar measure of nonlinearity between beams. All four specimens show a dip in linearity at resonance, with the minimum linearity (r^2 value) ranging from 0.8195 for beam K40 to 0.7827 for beam RF1. These results suggest that the inherent nonlinearity in a bonded composite beam structure, as measured by nonlinear resonance shift, is not greatly affected by the inclusion of damage at the bondline. This is unlike the findings for delamination damage in Chapter 4, where the specimens with damage exhibited a greater degree of nonlinearity as measured by minimum r^2 value (for example a minimum linearity of 0.8717 for a pristine sample compared to 0.7676 for a sample with delamination).

The results here also show that all four beams exhibit linear voltage-deflection behaviour for frequencies between approximately 60 Hz and 75 Hz, indicated by the r^2 fit coefficient not

deviating from 1.0. For the studies in the following section, it will be these frequencies selected as the pumping frequency for nonlinear vibro-ultrasonic testing, so that inherent nonlinearities associated with the vibration behaviour of the system are minimised.

5.2.3 Response to vibro-ultrasonics

Proceeding with the methodology established in Chapter 4, a frequency sweep was performed in order to determine a suitable frequency for the ultrasonic excitation signal. The sweep was performed using the apparatus described in Section 3.2, with all vibro-ultrasonic testing instrumentation attached to the beam. A continuous sine wave signal of peak-to-peak amplitude of 18 V was generated with frequencies ranging from 350 kHz to 450 kHz in steps of 0.25 kHz. The excitation signal was applied to the piezo closest to the free end of the beam, and the response amplitude of the receiving piezo was measured for each frequency.

The response curves for beams B1, B2, RF1 and RF2 are shown in Figures 5.3 and 5.4. From the frequency response curves, a frequency of 400 kHz was selected to perform nonlinear vibro-ultrasonic testing on beams B1 and RF1, as these beams both had a strong response at this frequency: -31 dB for beam B1, and -28 dB for beam RF1.

The nonlinear vibro-ultrasonic testing on beams B1 and RF1 was performed by simultaneous excitation by pumping vibration and the ultrasonic probing signal. Both the low- and high-frequency used for input were continuous sine waves. Based on the analysis of the high frequency response of the beams, the ultrasonic signal had a frequency of 400 kHz and a peak-to-peak amplitude of 18 V. A frequency range of 65 to 70 Hz was selected for the vibration excitation, based on analysis performed in Section 5.2.2 determining that the beams exhibited a linear relationship between excitation voltage and beam deflection amplitude in this range.

The low-frequency excitation voltage was varied from 0.05 V to 5.0 V in steps of 0.05 V,

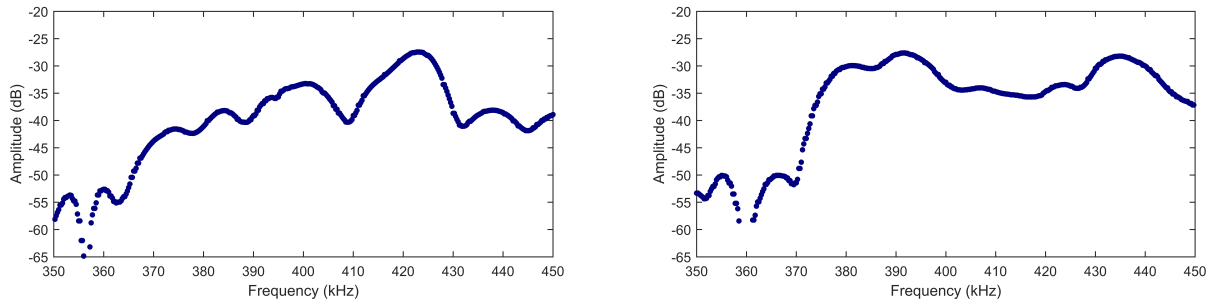

(a) Beam B1 (b) Beam B2

Figure 5.3: High frequency response curves for bonded beam specimens with an intact bondline.

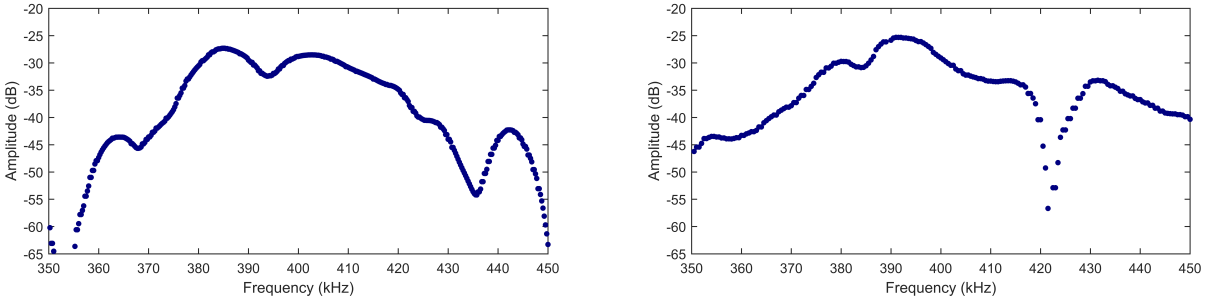

(a) Beam RF1 (b) Beam RF2

Figure 5.4: High frequency response curves for bonded beam specimens with 20 mm release film.

using the data collection procedures described in Section 3.5.1 and Chapter 4. The modulation index introduced in Chapter 4, $R = (A_1^- + A_1^+)/A_0$, was calculated for each sample. Figure 5.5 shows this modulation index plotted against measured beam deflection amplitude during excitation.

The data in Figure 5.5 indicate a higher modulation index for beam RF1 which has a 20 mm wide section of release film at the bondline, when compared to beam B1 with no bondline damage. This can be interpreted as the bondline inclusion causing a larger degree of nonlinear wave interaction than surrounding material for a given strain amplitude, since the modulation index is a measure of nonlinear wave interaction due to nonlinear frequency mixing phenomena.

Repeat experiments were performed, this time with the high frequency selection changed to 390 kHz, with all other parameters were kept fixed. The results from this analysis are shown in Figure 5.6.

Contrary to expectations, when a frequency of 390 kHz was chosen as a probing frequency,

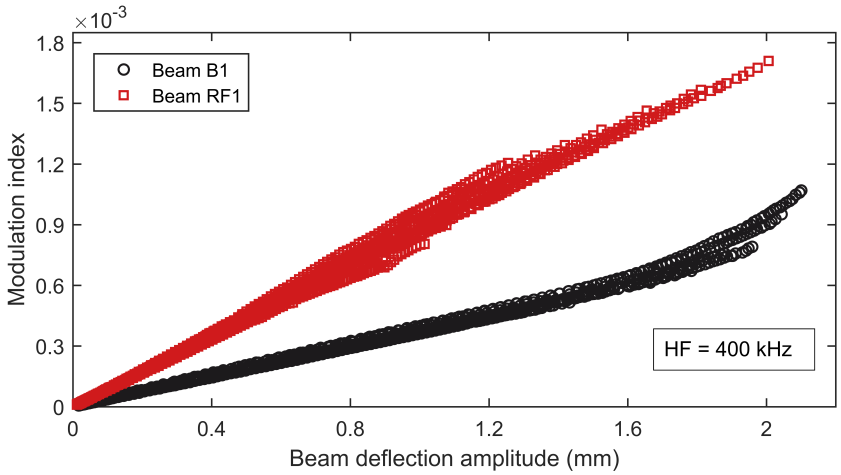

Figure 5.5: Modulation index versus beam deflection amplitude for beams B1 and RF1, excitation high frequency of 400 kHz, low frequency range 65 to 70 Hz.

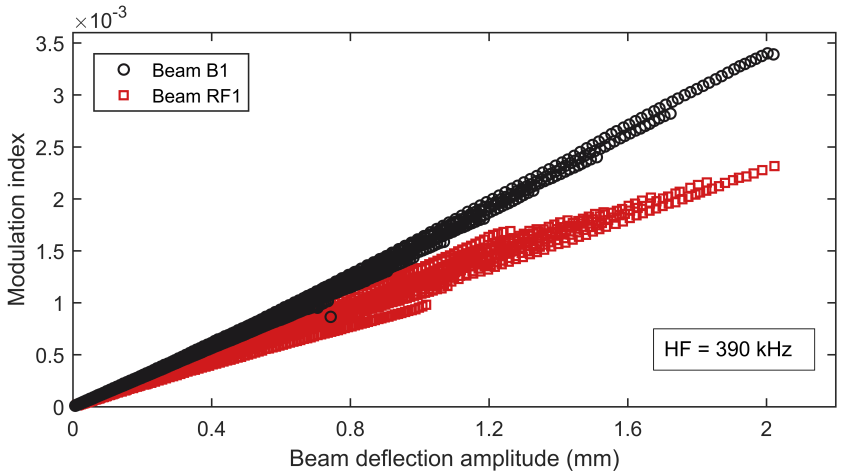

Figure 5.6: Modulation index versus beam deflection amplitude for beams B1 and RF1, excitation high frequency of 400 kHz, low frequency range 65 to 70 Hz.

beam B1 with an intact bondline exhibits a larger degree of frequency mixing, as measured by modulation index), than beam RF1 with a release film inclusion. This is the opposite to what was observed in Figure 5.5 where a frequency of 400 kHz was used for the probing wave. These results have revealed that the nonlinearity measured by nonlinear vibro-ultrasonic testing may be dependent on the frequency of the probing wave.

These findings call into question the results of nonlinear vibro-ultrasonic testing using a single probing frequency, such as those presented in Chapter 4. In order to investigate this further, the specimens from Chapter 4 are revisited for further analysis.

5.2.4 Effect of varying probing frequency on modulation index

Nonlinear vibro-ultrasonic testing was performed on beams P1 and D1, as per the established methodology. In contrast to previous tests introduced in this thesis, the pumping frequency and amplitude were not varied, being kept fixed at 60 Hz and 1.0 V, respectively. Instead, the high frequency was varied from 325 kHz to 425 kHz in steps of 0.25 kHz. For each sample, the modulation index, $R = (A_1^- + A_1^+)/A_0$, was calculated. The results from this analysis are presented in Figure 5.7.

There are two main observations present from Figure 5.7: that the modulation index varies significantly with different probing frequencies (by as much as 40 dB for beam D1, which is a 100-fold difference), and that the modulation index is higher for beam D1 than for beam P1 at every tested probing frequency.

The modulation indices presented in literature, including the one used here, normalise the amplitude of the sideband frequency components by the amplitude of the probing frequency.

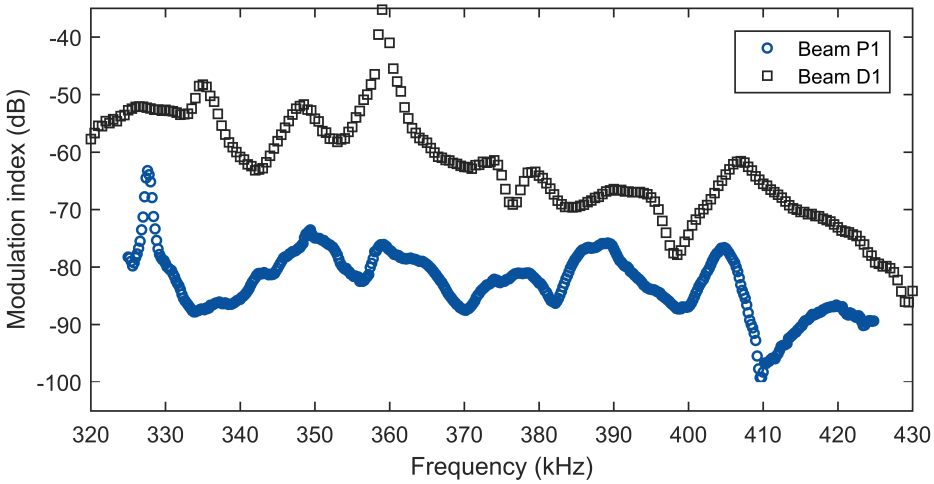

Figure 5.7: Modulation index versus frequency of probing wave for beam P1 and D1.

This idea relates back to nonlinear frequency mixing theory introduced in Section 2.3.4.1 which states that the amplitude of the sideband components is proportional to $\beta A_1 A_2$ where β is a nonlinearity parameter, and A_1 and A_2 are amplitudes of the two excitations. For this reason, the finding that modulation index varies so significantly with probing frequency is an unexpected result.

That the modulation index is always higher for beam D1 no matter the probing frequency is an indication that the artificial delamination damage increases the nonlinear response of the beam compared to the pristine beam P1. However the variation in just how more nonlinear the response is measured to be indicates a probing-frequency dependence not accounted for by the modulation index. For these two samples depending on the choice of high frequency the relative modulation index can be as low as double (6 dB difference at 386 kHz probing frequency) and as high as 100-fold (40 dB difference at 335 kHz and 359 kHz probing frequencies). These findings appear to indicate that the relative value of modulation index alone cannot be used to characterise the extent of artificial delamination damage in composite laminates.

Previous studies (e.g. Sohn et al., 2013) have shown for a damaged specimen that the magnitude of the first pair of sidebands can vary with probing frequency, though there is no consensus as to the mechanism. As the present study is able to discern very small sidebands, it is possible to observe that this trend is present for the pristine beams as well. This indicates that at least part of the probing frequency-dependence of the modulation index is not related to the defect but to something inherent to the specimens and/or system.

Nonlinear vibro-ultrasonic testing was next performed on the bonded composite beam specimens using the same procedure described above for varying the high frequency. The pumping frequency and amplitude were kept fixed at 70 Hz and 1.0 V, respectively, while the

high frequency was varied from 350 kHz to 450 kHz in steps of 0.25 kHz. For each sample, the modulation index, $R = (A_1^- + A_1^+)/A_0$, was calculated.

The results of this analysis for beams B1 and B2 having no inclusion and beams RF1 and RF2 having a 20 mm release film inclusion are presented in Figure 5.8. These results show at a glance that the addition of a release film inclusion does not greatly differentiate a bonded composite beam from one without a bondline inclusion. Depending on the probing frequency selected, one of these beams may appear to be more nonlinear than another to nonlinear vibro-ultrasonic testing. It is not possible even from this analysis – which is one step further advanced than the single-frequency nonlinear vibro-ultrasonics methodology presented in Chapter 4 and in literature – to confidently distinguish the beams with release film inclusions from those with an intact bondline.

Consider in the context of these results, the findings of other studies where only a single probing frequency was used, or for example Klepka et al. (2014), where results were compared for two probing frequencies. The data presented in those studies represents only a fraction of the story that Figure 5.8 tells. In order to confidently determine that one specimen is more nonlinear than another, one must show that this holds true for a range of probing frequencies, as was shown for the beams with artificial delamination damage (Figure 5.7).

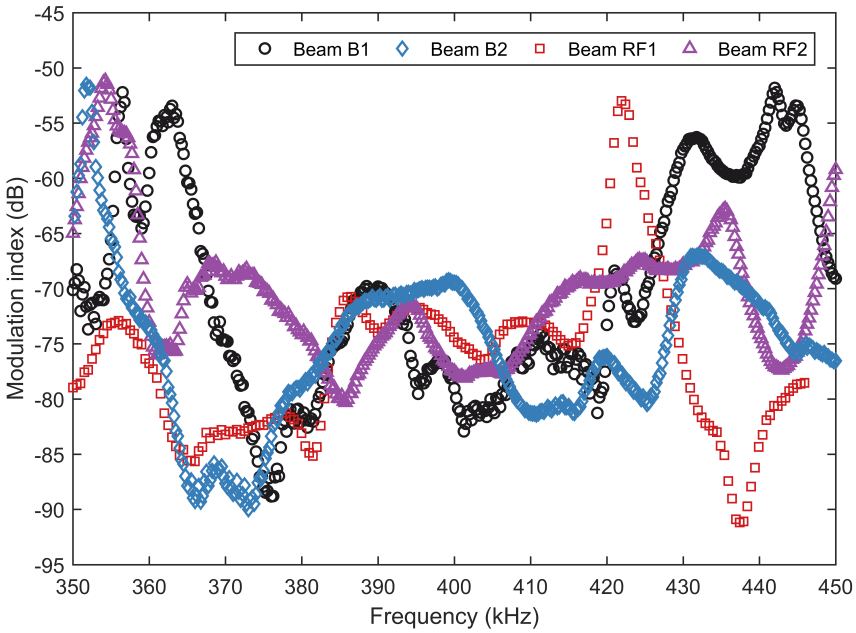

Figure 5.8: Modulation index versus frequency of probing wave for beams B1 & B2 (no defect) and RF1 & RF2 (release film inclusion).

The results of this analysis for the remaining bonded composite beams are presented in Figure 5.9. These results show much the same as Figure 5.8, that the beams are not able to be confidently distinguished from one another either by calculation of modulation index at a single probing frequency or over a range of probing frequencies.

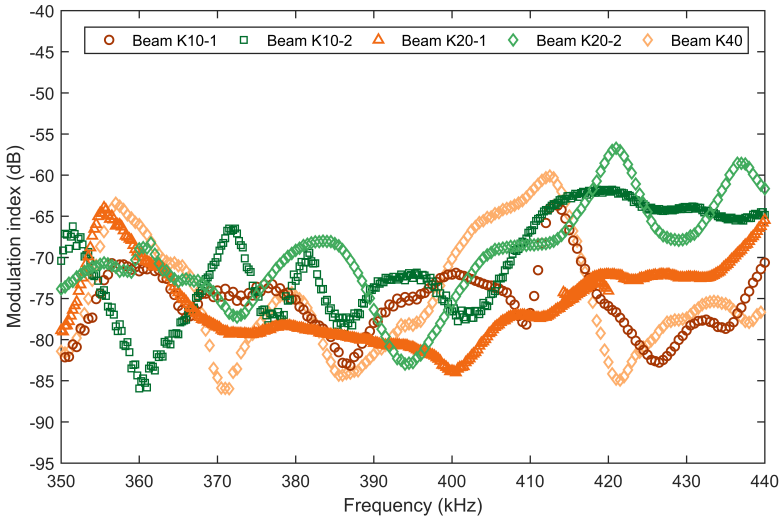

Figure 5.9: Modulation index versus probing frequency for beams K10-1 & K10-2, K20-1 & K20-2 and K40.

Figure 5.10 shows the results of this analysis only for the bonded composite beams which have a Kapton inclusion at the bondline (not removed). Beam K10-1 has an inclusion 10 mm in length, beam K20-1 an inclusion 20 mm in length, and beam K40 an inclusion 40 mm in length. Also shown is data from an extra specimen, K20-3, which was manufactured in the same way as beam K20-1, and has an inclusion 20 mm in length. These results do not clearly show any evidence for the bondlines with differently sized inclusions exhibiting different degrees of nonlinearity, nor of the two samples with the same sized inclusions sharing common features in their response.

Similarly, Figure 5.11 shows the results of this analysis only for the bonded composite beams which have had a Kapton inclusion at the bondline removed. As before, data for an extra specimen with a 20 mm inclusion is provided (beam K20-4). As for the specimens with the Kapton inclusion, no clear differentiating features are obtained from this analysis for beams with differently sized damage. One potential reason for a larger damage not causing an increase in nonlinearity, is that the nonlinear wave interaction is dominated by local effects at the crack tip – in this case, at the edges of the disbonds or inclusions. As the defect is increased in length, these edges remain the same size allowing for the same degree of contact between surfaces, i.e. rubbing or clapping of the crack.

The data for all bonded composite beams shows an inability to confidently distinguish

the beams with bondline defects from those with an intact bondline using a fixed pumping frequency and varying probing frequency. One explanation for this finding could be that the specific defect considered here is not sensitive to the pumping frequency of 70 Hz used for all tests; as described in the literature review, pumping frequency selection can affect measurement of nonlinearity (e.g. Lim et al., 2014a, where for some pumping frequencies the defect did not exhibit more nonlinearity than the control).

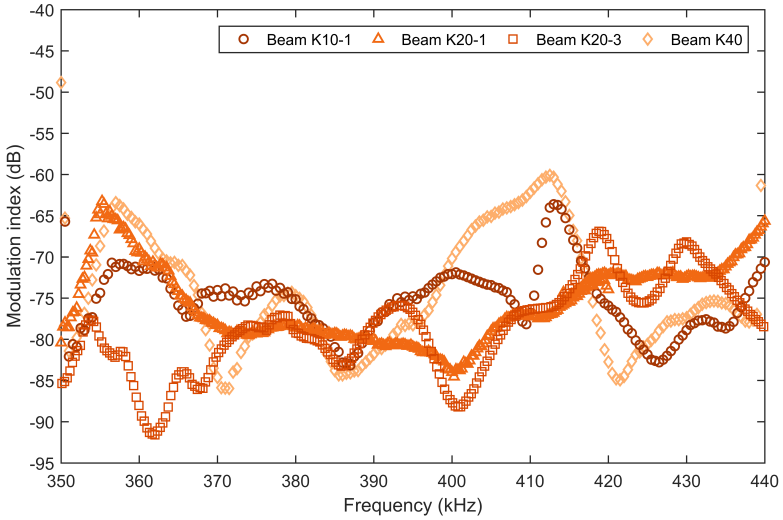

Figure 5.10: Modulation index versus probing frequency for beams K10-1, K20-1, K20-3 and K40. These beams have an inclusion of Kapton film in their bondline.

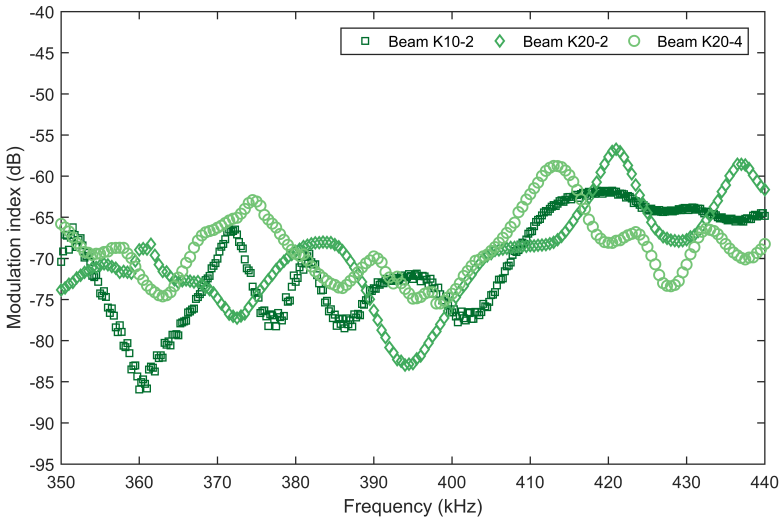

Figure 5.11: Modulation index versus probing frequency for beams K10-2, K20-2 and K20-4. These beams had an inclusion of Kapton film in their bondline that has been removed prior to testing.

5.3 Bonded aluminium beams

5.3.1 Specimen manufacture

Bonded beam specimens were manufactured by bonding aluminium beams together using Cytec FM 300NK adhesive film. The beams measured 300 mm in length and 25 mm in width.

Two of the bonded beams, designated AS-1 and AS-2, were manufactured with both aluminium adherends having a thickness of approximately 2 mm. The remaining two beams, AA-1 and AA-2 were manufactured by bonding a 2 mm beam with a 1 mm beam. The result is that the bondlines of AS-1 and AS-2 are at a plane of symmetry through the thickness of the beam, while AA-1 and AA-2 are not.

The beam specimens AS-2 and AA-2 were manufactured with a folded strip of DuPont Kapton polyimide film of 20 mm width at the centre of the beam. This film was removed after curing, leaving the portion of the bondline at this location such that the adhesive was not cured to one adherend. The adherend to which the adhesive is not cured in this location is referred to as the ”top” member of the beam, and it is this top member of the beam to which all instumentation is attached during experimentation.

Each beam specimen was instrumented with two piezo transducers according to the procedures outlined in Section 3.2.1. Figure 5.12 shows a schematic including the placement of piezos and accelerometers during experimentation for the bonded aluminium beam specimens. Note that the experiments performed with these specimens were in a configuration with a second clamp at the previously free end, so that the second accelerometer is now placed in the middle of the beam.

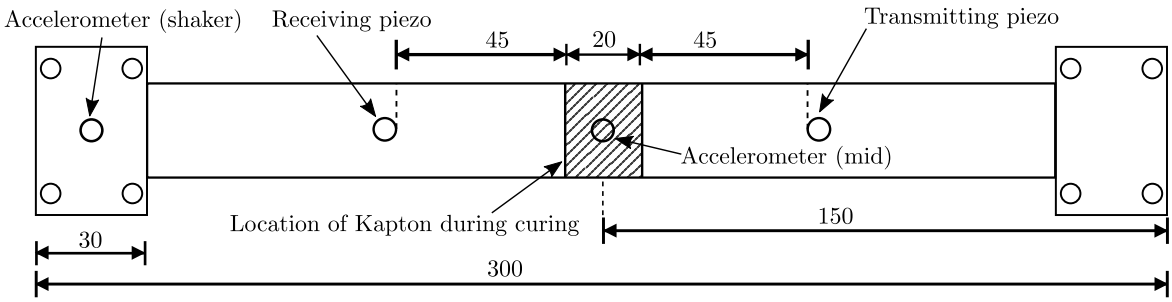

Figure 5.12: Dimensions and details of aluminium bonded beam specimens, including placement of piezos and accelerometers in relation to the 20 mm bondline defect.

5.3.2 Experimental methodology

The four aluminium bonded beam specimens were analysed for their modal response, following the procedures introduced in Section 3.5.2. The beams were each excited with a frequency sweep from 20 to 500 Hz in steps of 1 Hz with an excitation amplitude of 1.0 V to establish the vibration resonance of each beam. Table 5.3 lists the resonant frequencies found for each beam.

Table 5.3: First resonant frequency measured for bonded aluminium beam specimens

Specimen	AS-1	AS-2	AA-1	AA-2
Resonant Frequency (Hz) (1.0 V excitation)	324	316	259	252

Based on previous analysis presented in Chapters 4 and 5, a frequency range well-above the resonant frequencies of the beams was selected for use in nonlinear vibro-ultrasonics experiments: 350 Hz to 500 Hz.

One probing frequency was selected for each beam, determined by sweeping with an input amplitude of 18.0 V, frequencies from 250 kHz to 500 kHz in steps of 0.25 kHz, and measuring the amplitude of throughput to the receiving piezo. For each beam, the frequency which resulted in the greatest throughput was selected. The selected probing frequency for each specimen, as well as the received amplitude, are listed in Table 5.4.

Table 5.4: Selected probing frequency inputs for bonded aluminium beam specimens

Specimen	AS-1	AS-2	AA-1	AA-2
Probing Frequency (Hz)	407250	402500	392000	385000
Received Amplitude (dB)	-27.72	-28.69	-19.76	-20.12

Experiments were performed to determine the effect of the pumping frequency selection on the modulation index obtained from nonlinear vibro-ultrasonic testing. Each specimen was simultaneously excited at its selected probing frequency and at pumping vibration frequencies of 350 Hz to 500 Hz in steps of 5 Hz. For each of these pumping frequencies, the low-frequency excitation voltage was varied from 1.0 V to 4.0 V in steps of 0.05 V, using the data collection procedures described in Section 3.5.1.

Sideband amplitudes were measured for each sample, according to the procedure outlined in Section 3.5.1.1, so that further analysis of trends with varying pumping frequency could be carried out.

5.3.3 Results and analysis

Figure 5.13 shows the results from nonlinear vibro-ultrasonic testing of the symmetric bonded aluminium beams, AS-1 and AS-2. Here the modulation index R introduced in Section 3.5.3 is normalised by a_{base}, which is the acceleration amplitude measured at the base (vibration shaker) during excitation, as per equation (5.1).

$$\hat{R}_{base} = \frac{R}{a_{base}} = \frac{(A_1^- + A_1^+)}{A_0\, a_{base}} \tag{5.1}$$

The results in Figure 5.13 somewhat reflect the results for composite bonded beams from Section 5.2; as the excitation frequency is changed, in this case the pumping frequency, the relative nonlinearity of the two beams (as measured by the modulation index) changes. Selection of a different frequency can change which specimen appears more nonlinear. Studies

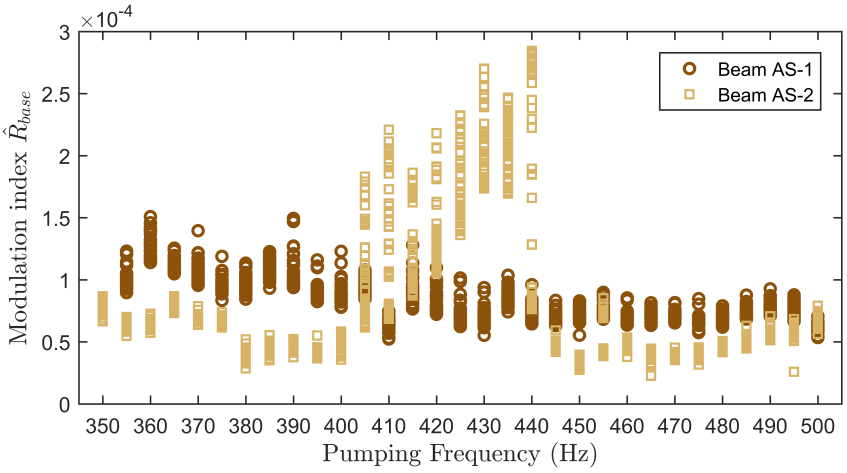

Figure 5.13: Modulation index $\hat{R}_{base}$ versus pumping frequency for AS-1 and AS-2.

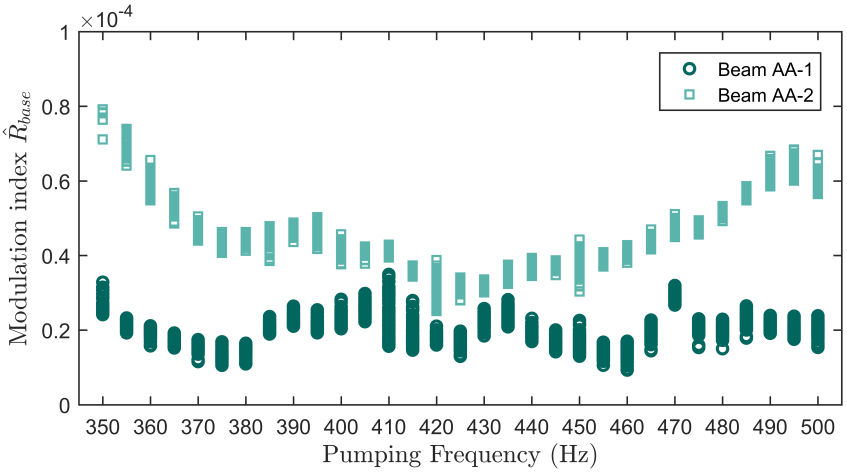

Figure 5.14: Modulation index $\hat{R}_{base}$ versus pumping frequency for beams AA-1 and AA-2.

in literature which have investigated the effect of pumping frequency selection have shown limited results where the degree of measured nonlinearity is affected by pumping frequency selection, for example Chrysochoidis et al. (2011a) show this phenomenon for artificial delamination damage. What is significant about the results shown in Figure 5.13 is that other studies have not provided data of this nature, where the pumping frequency changes which specimen appears more nonlinear.

There is a notable region between approximately 400 Hz and 440 Hz where beam AS-2 having bondline damage has a local increase in nonlinearity. This phenomenon is not exhibited by the intact beam AS-1, which has a relatively stable value of $\hat{R}_{base}$ across all investigated pumping frequencies. Given that the two beams have similar resonant frequencies (which are below 350 Hz) and identical geometry, this band could represent frequencies for which more nonlinear wave interaction occurs. Similarly, Lim et al. (2014a) found that when pumping frequency was varied during vibro-ultrasonic inspection of aluminium components containing fatigue cracks, there was a large amount of variation in measure of nonlinearity; very little variation was found for identical pristine samples, supporting the findings of this study. This suggests that the defect responds to certain pumping frequencies in such a way as to cause an increased degree of nonlinear wave interaction.

The results of the same analysis for the asymmetric beams AA-1 and AA-2 is presented in Figure 5.14. Beam AA-2 with bondline damage was measured to have a greater degree of nonlinearity than the intact beam AA-1 at all investigated pumping frequencies. For both beams, variation in the value of $\hat{R}_{base}$ is observed across the investigated pumping frequencies.

The amplitudes of the second pair of sidebands, A_2^- and A_2^+, are used to calculate an

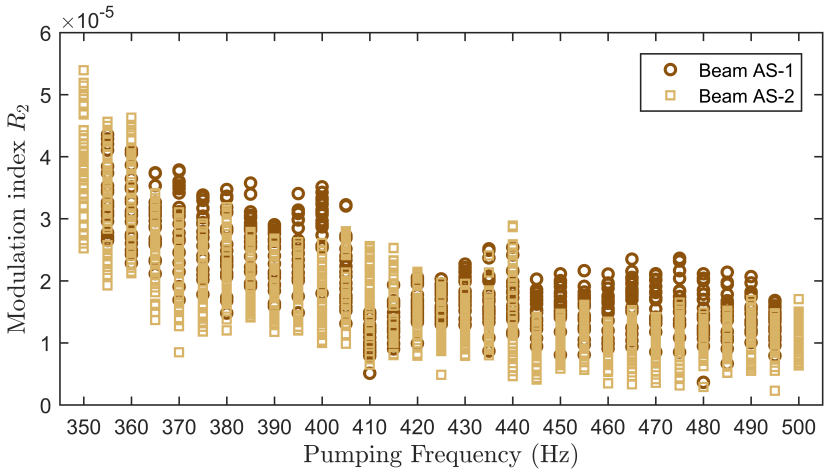

Figure 5.15: Modulation index $\hat{R}_{2,base}$, calculated from the amplitude of the second pair of sidebands, versus pumping frequency for bonded aluminium beams AS-1 and AS-2.

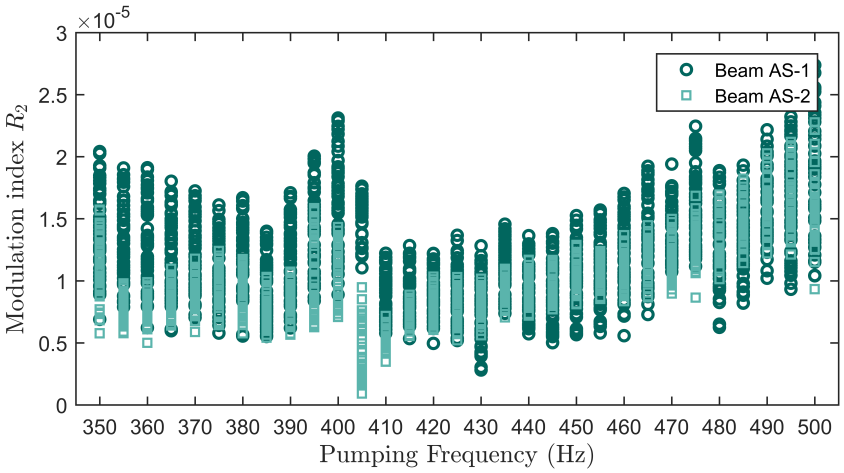

Figure 5.16: Modulation index $\hat{R}_{2,base}$, calculated from the amplitude of the second pair of sidebands, versus pumping frequency for bonded aluminium beams AA-1 and AA-2.

alternative modulation index:

$$\hat{R}_{2,base} = \frac{R_2}{a_{base}} = \frac{(A_2^- + A_2^+)}{A_0\, a_{base}} \tag{5.2}$$

Figure 5.15 shows the results for $\hat{R}_{2,base}$ for the symmetric beams AS-1 and AS-2. There is little difference in the value of $\hat{R}_{2,base}$ between beams AS-1 and AS-2, and only a slight, downward variation in the value as pumping frequency increases. This is in contrast to the value of $\hat{R}_{base}$ shown in 5.13 which exhibited a sharp increase for beam AS-1 over a narrow band of frequencies.

The results using modulation index $\hat{R}_{2,base}$ for tests on the asymmetric beams AA-1 and AA-2 are presented in Figure 5.16. As for the other pair of beams, there is little difference in the value of this modulation index between beams AA-1 and AA-2. These findings suggest that the second pair of sideband amplitudes is not sensitive to the addition of gross damage at the adhesive interface of the bonded aluminium beams.

In order to further investigate the relative sensitivity of the first pair of sideband amplitudes compared with higher pairs, an alternative modulation index $\bar{R}_{1,2-5}$ is calculated as per equation (5.3). This modulation index

$$\bar{R}_{1,2-5} = \frac{A_1^- + A_1^+}{A_2^- + A_2^+ + A_3^- + A_3^+ + A_4^- + A_4^+ + A_5^- + A_5^+} \tag{5.3}$$

The results for $\bar{R}_{1,2-5}$ calculated for beams AS-1 and AS-2 are shown in Figure 5.17. Much the same as for the value of $\hat{R}_{base}$, these results show that beam AS-2 having interface damage exhibits a sharp increase in modulation index at a band of frequencies from approximation 400

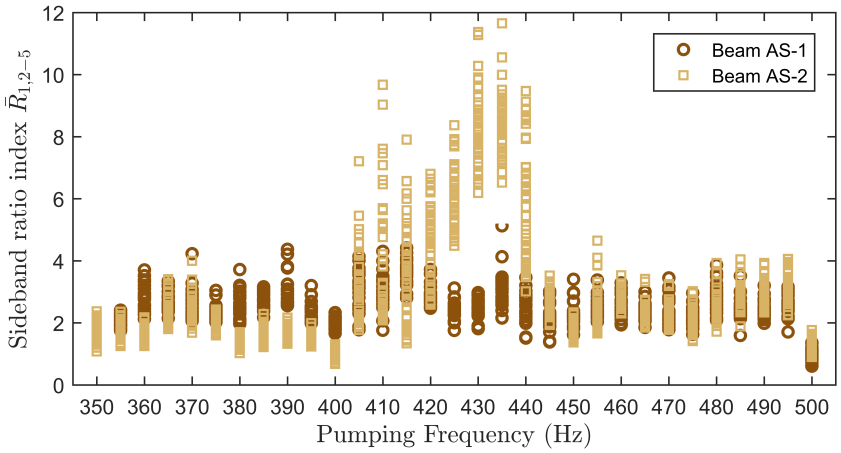

Figure 5.17: Modulation index $\bar{R}_{1,2-5}$, a relative measure of the first pair of sidebands compared to remaining sidebands, versus pumping frequency for beams AS-1 and AS-2.

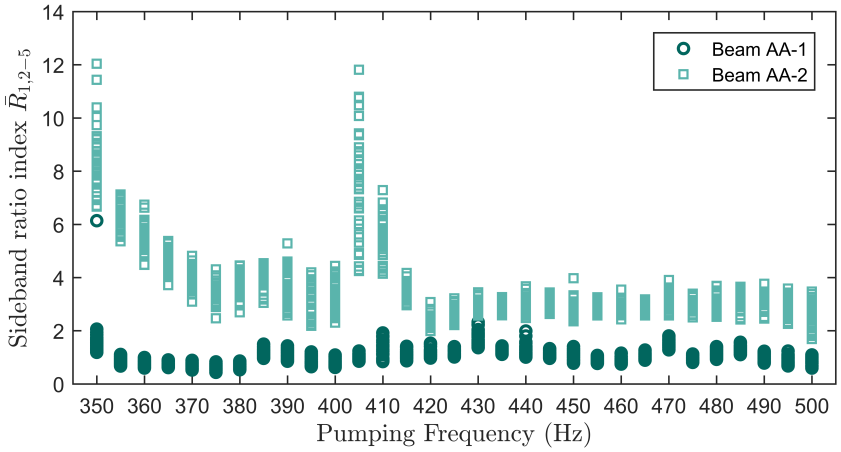

Figure 5.18: Modulation index $\bar{R}_{1,2-5}$, a relative measure of the first pair of sidebands compared to remaining sidebands, versus pumping frequency for beams AA-1 and AA-2.

Hz to 440 Hz, with no similar effect seen for beam AS-1. Significantly, the values of $\bar{R}_{1,2-5}$ for tests performed at pumping frequencies outside of this range varies very little between beams AS-1 and AS-2, which is in contrast to the results using $\hat{R}_{base}$.

The results for the same analysis of beams AA-1 and AA-2 are shown in Figure 5.18. It is observed that the modulation index $\bar{R}_{1,2-5}$ calculated for AA-2 shows very little variation in value for pumping frequencies above approximation 420 Hz, in contrast to the values of $\hat{R}_{base}$ which varied significantly across this range of frequencies (see Figure 5.14). Additionally, while the value of $\bar{R}_{1,2-5}$ is larger for beam AA-2 than beam AA-1 for all investigated pumping frequencies, this effect is maximised at pumping frequencies below approximately 370 Hz and between 400 Hz and 420 Hz.

The findings from calculation of the alternative modulation index $\bar{R}_{1,2-5}$ show that

normalising the amplitude of the first pair of sidebands by all remaining pairs of sidebands – determining how large the first pair of sidebands is relative to the remaining – highlights a measurable difference between the beams with and without bondline damage. While beams AS-1 and AA-1 without an interface defect exhibit a relatively stable value of $\bar{R}_{1,2-5}$ across all testing pumping frequencies and maximum values of approximately 4 and 2 respectively, beams AS-2 and AA-2 both contain ranges of pumping frequencies where the value of $\bar{R}_{1,2-5}$ increases significantly, to as high as 12 for both beams.

These findings also suggest that the first pair of sideband amplitudes is more sensitive to the presence of the interface than the remaining pairs. This is similar to the findings of Aymerich and Staszewski (2010a) where it was shown that for a set of impact-induced damage in composite laminates, the second pair of sidebands experienced the largest growth for increasing pumping amplitudes. Compared to studies from literature however, the present study presents data for a large parameter space, for a range of pumping frequencies and for a range of pumping excitation amplitudes. This helps to highlight that the sensitivity of the first pair of sidebands to the damage is dependent on the pumping frequency used for testing. which could be an explanation for why the analysis presented in Section 5.2.4 for a varying probing frequency (but for a single pumping frequency) was unable to distinguish between pristine and damaged samples.

5.4 Summary of findings

The experimental results and analyses presented in this chapter demonstrate the following important findings relevant to the use of nonlinear vibro-ultrasonic testing as a means of detecting damage in adhesively bonded beams:

- The typical methodology of selecting a single probing frequency and a single vibration excitation frequency is unable to confidently differentiate intact interfaces in bonded composite beams from those with gross bondline defects. Instead, the relative nonlinearity measured between specimens depends on the ultrasonic probing frequency used; selection of a different frequency can change which specimen appears more nonlinear.

- No concrete evidence is found that nonlinear vibro-ultrasonic testing conducted in the typical manner, or with trials over a range of probing frequencies, is sensitive to gross bondline defects. This is in contrast to artifical delamination damage in composite laminates investigated in Chapter 4 of this thesis, for which a measured increase in nonlinearity is observed for all tested probing frequencies using the same methodology.

- Normalising the amplitude of the first pair of sidebands by all remaining pairs of sidebands results in a modulation index which is able to highlight selections of pumping frequency which lead to a measured increase in nonlinearity in the aluminium bonded beams with interface damage. The pumping frequencies which exhibit this increase in nonlinearity are found in narrow bands, and the phenomenon does not exist for the beams without damage. This result highlights that advanced data analysis techniques and specific combinations of system parameters may be required to highlight differences between specimens with and without bondline damage in adhesively bonded structures.

Chapter 6

Conclusions and future work

6.1 Summary of findings

The work undertaken in this thesis was focused on understanding the influence of system parameters on the generation and detection of sideband frequency components in nonlinear vibro-ultrasonic testing of fibre-reinforced composite structures.

The majority of studies published in the area of nonlinear vibro-ultrasonics report spectra for pristine specimens containing no sideband frequency components. Granted that nonlinear frequency mixing (which produces sidebands) occurs at every stage of experimentation, even in the electrical systems used for measurement of the resultant signal, a spectra without sidebands is indicative of a noise floor limiting effective measurement of nonlinearity. Chapter 3 of this thesis provides an in-depth, quantitative analysis of the experimental system and methodology used in this work with regard to the ability to discern sidebands. The result of this analysis is the selection of system components, experimental procedures, analyses and signal processing parameters which minimise the displayed average noise level.

Very limited examples exist in literature of nonlinear vibro-ultrasonic tests performed with frequencies that do not correspond to a structural resonance of the test specimen. In response to this, work was carried out in Chapter 4 to determine the effect that a structural resonance has on the relationship between excitation input voltage and displacement amplitude within the composite laminate beam samples. It is shown that the dynamic nonlinearity of the system is likely to be maximal at resonance; it is recommended then that for maximised sensitivty and robustness of nonlinear vibro-ultrasonic experiments, the pumping frequency should be selected close to resonance but at frequencies for which a linear relationship exists between excitation input voltage and displacement amplitude.

In order to investigate the influence of system parameters over a large parameter space and with sufficiently close spacing of data points, an experimental system was developed which is capable of automating data collection across ranges of input parameters. This capability enabled the demonstration of a strong dependence of nonlinear wave interaction on the amplitude of the pumping wave in the presence of nonlinearity, with the large number of data points collected for composite laminate beam specimens in Chapter 4 across a range of frequencies occupying clear regions per specimen, and all data showing a very clear relationship between vibration amplitude and modulation index. These results confirm findings of previous studies that the nonlinearity due to laminar damage in composite laminates, both artificial and that caused by impact, causes the modulation index to be much larger than for pristine specimens, and that the effect of increasing exctiation amplitude is a monotonic increase in modulation index.

Chapter 5 describes an investigation into the detection of bondline damage in adhesively bonded composite laminate beams. It is shown that the methodology established in Chapter 4 using a single probing frequency and limited band of vibration excitation frequencies provides an unexpected assessment of the beams with and without bondline damage – depending on the probing frequency selected, the beams with bondline damage may appear more nonlinear or less nonlinear. An extension to the method involving a sweep of the probing frequency across a large range of values is used to investigate the results further. This extension shows that while the samples with laminar damage investigated in Chapter 4 show a consistently higher level of nonlinearity than pristine beams no matter the probing frequency, no such clear differentiation is possible for the adhesively bonded composite beams. It is possible that this effect is caused by the selection of pumping frequency due to an inherent sensitivity of the defect to particular frequencies.

In order to investigate the effect of bondline damage in isolation, without the added complexity of fibre-reinforcement of the composite laminates, a study was performed on adhesively bonded aluminium beams with and without bondline damage. Rather than selecting a narrow band of pumping frequencies as for previous tests, the pumping frequency was varied over a large range. By normalising the amplitude of the first pair of sidebands by all remaining pairs of sidebands, a modulation index is established which is able to highlight specific selections of pumping frequency which lead to a measured increase in nonlinearity in the beams with interface damage. The pumping frequencies for which this behaviour is exhibited are found in narrow bands, and the phenomenon is not shown to exist for beams without damage.

Overall, results from these investigations into adhesively bonded beams indicate that it is not trivial to develop a methodology for inspection using nonlinear vibro-ultrasonics that can

confidently determine the integrity of a bondline. The findings of this thesis suggest that careful selection of experimental parameters as well as data analysis procedures is required to differentiate a beam with bondline damage from a pristine sample, and that to be confident in an assessment may require testing at a range of input frequencies.

6.2 Major contributions of the thesis

To summarise, this thesis makes the following important contributions towards the successful use of nonlinear vibro-ultrasonics for detection of damage and weak bonds in composite structures:

- A quantitative analysis of the influence of experimental instrumentation and signal processing parameter selection on discernibility of sideband frequency components was presented in Chapter 3. The results presented in Chapter 4 highlight that the deliberate selection of these parameters for sideband discernibility leads to many visible pairs of sidebands due to a very low noise floor and clearly defined sideband peaks.
- Results presented in Chapter 4 for beams with artificial and impact-induced delamination damage show that nonlinear vibro-ultrasonic inspection is able to confidently identify a beam with laminar damage from a pristine specimen. The results also show the strong dependence of nonlinear wave interaction on the amplitude of the pumping wave in the presence of damage. It is therefore shown to be necessary to study trends with respect to a predictor variable that is always proportional to wave amplitude, rather than (for example) excitation input voltage.
- Results presented in Chapter 5 for adhesively bonded composite beams provide evidence that typical nonlinear vibro-ultrasonic methodology using a single probing frequency and single vibration excitation frequency is insufficient to characterise one specimen as more nonlinear than another. The finding that selection of different system parameters can change this relation necessitates a methodology which investigates a range of input parameters.
- Comparison of different damage indices calculated for experimental data presented in Chapter 5 for adhesively bonded aluminium beams show that advanced data analysis techniques are able to highlight specific combinations of system parameters that lead to a difference in measurement between undamaged and damaged bondlines. This informs future work by showing that a range of parameters must be investigated in order to make a confident assessment of damage in structures.

6.3 Recommendations for future work

Based on the findings and contributions of this thesis, the following recommendations for future work are presented:

- The findings of this thesis should be confirmed for other types of damage both in metal and composite structures. The systematic evaluation of an experimental parameter space presented in this thesis should be applied to investigations of, for example, fatigue crack growth in metals and impact damage in composite laminates. These damage types have significant presence in existing literature, however many studies have not considered the sideband discernibility issues discussed in this work and have not explored a large space of closely spaced experimental parameters. Confirming for instance that these types of damage show clear differentiation of a damaged sample from a pristine one over a range of probing frequencies would improve confidence in the use of methodologies which select only a single probing frequency.

- The insight gained from the work in this thesis (and from revisiting other types of damage, as recommended) should be used to gain an understanding of the underlying physical mechanisms which are the sources of nonlinear wave interaction. These mechanisms must be properly understood so that inspection methodologies can be designed which can confidently determine the integrity of a bondline.

- The use of different wave modes should be investigated, to determine if all wave modes share the same limitations with respect to detecting bondline damage in adhesively bonded structures.

- A practical limitation of the application of nonlinear vibro-ultrasonics is the use of a vibration shaker to generate the low frequency pumping wave. While a vibration shaker allows for a range of vibration amplitudes and frequencies (particularly low frequencies) to be investigated, it is challenging to incorporate into an inspection strategy for a real engineering structure. It is therefore important to extend this work on nonlinear vibro-ultrasonics to dual-ultrasonic applications, where the pumping wave is provided by an ultrasonic transducer.

Appendix A

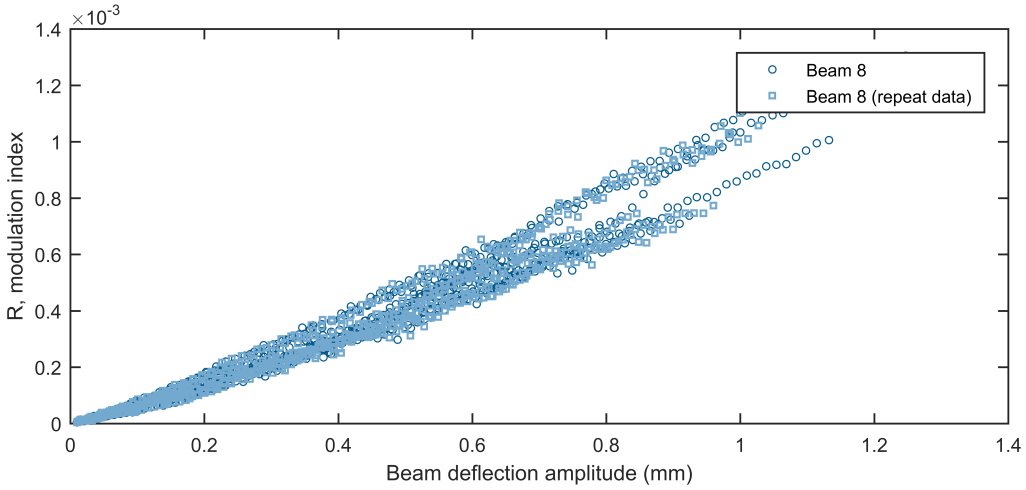

Figure A.1: Modulation index for Beam P1, repeat trials.

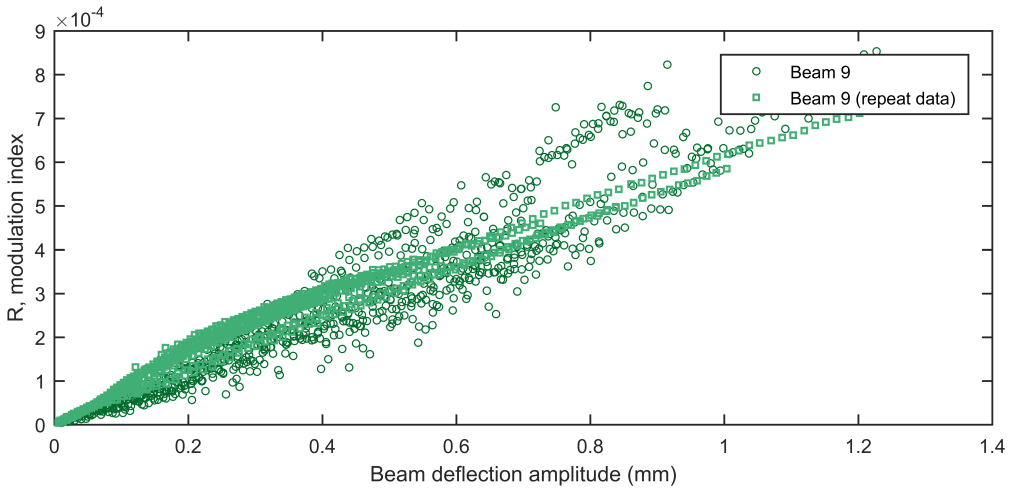

Figure A.2: Modulation index for Beam P2, repeat trials.

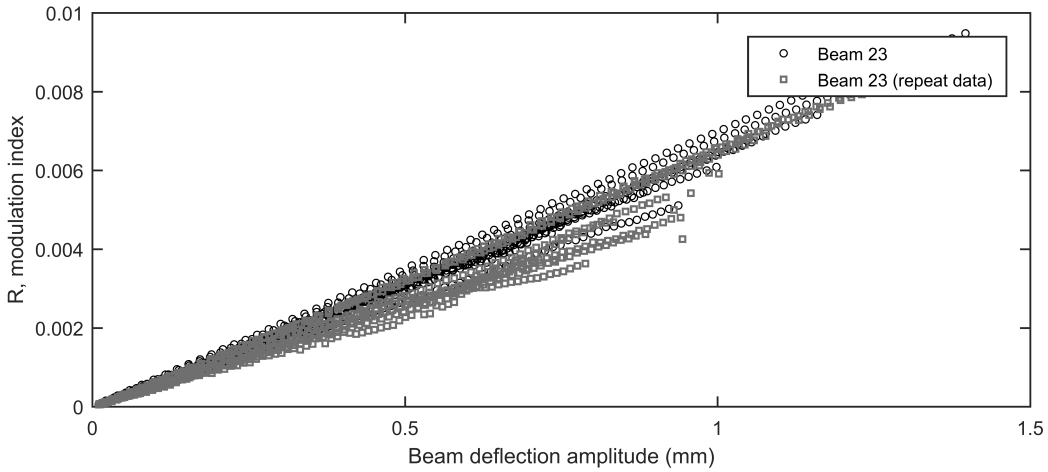

Figure A.3: Modulation index for Beam D1, repeat trials.

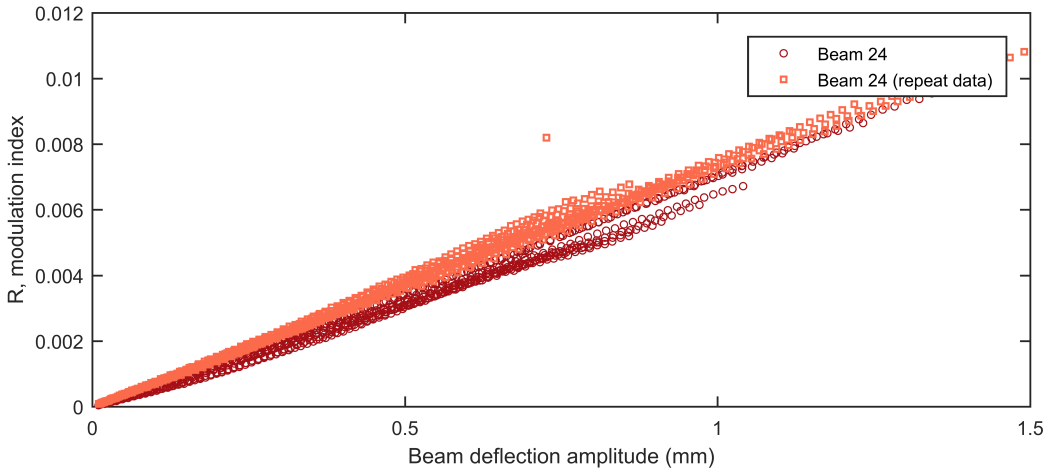

Figure A.4: Modulation index for Beam D2, repeat trials.

References

Achenbach, J.D. (1973). *Wave Propagation in Elastic Solids*. Applied Mathematics and Mechanics Series. North-Holland Publishing Company. ISBN: 9780444104656.

Adams, R.D. and Cawley, P. (1988). "A review of defect types and nondestructive testing techniques for composites and bonded joints". *NDT International* 21.4, pp. 208–222.

Adler, L. and Nagy, P.B. (1991). "Second order nonlinearities and their application in NDE". *Review of Progress in Quantitative Nondestructive Evaluation* 10B, pp. 1813–1820.

Albrecht, H. H. (2001). "A family of cosine-sum windows for high-resolution measurements". In: *2001 IEEE International Conference on Acoustics, Speech, and Signal Processing. Proceedings (Cat. No.01CH37221)*. Vol. 5, 3081–3084 vol.5.

Albrecht, H. H. (2010). "Tailoring of Minimum Sidelobe Cosine-Sum Windows for High-Resolution Measurements". *The Open Signal Processing Journal* 3, pp. 20–29.

Amerini, F. and Meo, M. (2011). "Structural health monitoring of bolted joints using linear and nonlinear acoustic/ultrasound methods". *Structural Health Monitoring* 10.6, pp. 659–672.

Aymerich, F. and Staszewski, W. J. (2010a). "Impact damage detection in composite laminates using nonlinear acoustics". *Composites Part A: Applied Science and Manufacturing* 41.9, pp. 1084–1092.

Aymerich, F. and Staszewski, W.J. (2010b). "Experimental Study of Impact-Damage Detection in Composite Laminates using a Cross-Modulation Vibro-Acoustic Technique". *Structural Health Monitoring* 9.6, pp. 541–553.

Baby, S., Nagaraja Kowmudi, B., Omprakash, C.M., Satyanarayana, D.V.V., Balasubramaniam, K. and Kumar, V. (2008). "Creep damage assessment in titanium alloy using a nonlinear ultrasonic technique". *Scripta Materialia* 59.8, pp. 818–821.

Belingardi, Giovanni and Vadori, Roberto (2002). "Low velocity impact tests of laminate glass-fiber-epoxy matrix composite material plates". *International Journal of Impact Engineering* 27.2, pp. 213–229. ISSN: 0734-743X.

Blanloeuil, P., Rose, L.R.F., Guinto, J.A., Veidt, M. and Wang, C.H. (2016a). "Closed crack imaging using time reversal method based on fundamental and second harmonic scattering". *Wave Motion* 66, pp. 156–176.

Blanloeuil, P., Rose, L.R.F., Guinto, J.A., Veidt, M. and Wang, C.H. (2016b). "Modified time reversal imaging of a closed crack based on nonlinear scattering". In: vol. 9804.

Cantrell, J.H. and Yost, W.T. (1994). "Acoustic harmonic generation from fatigue-induced dislocation dipoles". *Philosophical Magazine A: Physics of Condensed Matter, Structure, Defects and Mechanical Properties* 69.2, pp. 315–326.

Cantrell, J.H. and Yost, W.T. (2001). "Nonlinear ultrasonic characterization of fatigue microstructures". *International Journal of Fatigue* 23.SUPPL. 1.

Chan, E., Rose, L.R.F., Veidt, M. and Wang, C.H. (2014). "Characterisation of laminar damage in a composite panel by diffraction tomography based imaging method using Lamb waves". In: *Proc. 8th Australasian Congress on Applied Mechanics*, pp. 364–371.

Chan, E., Rose, L.R.F. and Wang, C.H. (2016). "A comparison and extensions of algorithms for quantitative imaging of laminar damage in plates. II. Non-monopole scattering and noise tolerance". *Wave Motion* 66, pp. 220–237.

Chrysochoidis, N.A., Barouni, A.K. and Saravanos, D.A. (2011a). "Delamination detection in composites using wave modulation spectroscopy with a novel active nonlinear acousto-ultrasonic piezoelectric sensor". *Journal of Intelligent Material Systems and Structures* 22.18, pp. 2193–2206.

Chrysochoidis, N.A., Toulitsis, A.K. and Saravanos, D.A. (2011b). "Impact damage detection in composites using an active nonlinear acousto-ultrasonic piezoceramic sensor". In: *Proceedings of SPIE - The International Society for Optical Engineering*. Vol. 7981.

Chrysochoidis, Nikolaos A, Assimakopoulou, Theoni T and Saravanos, Dimitris A (2015). "Nonlinear wave structural health monitoring method using an active nonlinear piezoceramic sensor for matrix cracking detection in composites". *Journal of Intelligent Material Systems and Structures* 26.15, pp. 2108–2120.

Croxford, A.J., Wilcox, P.D., Drinkwater, B.W. and Konstantinidis, G. (2007). "Strategies for guided-wave structural health monitoring". *Proceedings of the Royal Society A: Mathematical, Physical and Engineering Sciences* 463.2087, pp. 2961–2981.

Dieulesaint, E. and Royer, D. (1980). *Elastic waves in solids : applications to signal processing*. English. Chichester [Eng.] ; New York : J. Wiley. ISBN: 047127836X.

Donskoy, D., Sutin, A. and Ekimov, A. (2001). "Nonlinear acoustic interaction on contact interfaces and its use for nondestructive testing". *NDT and E International* 34.4, pp. 231–238.

Donskoy, D, Zagrai, A, Chudnovsky, A, Golovin, E and Agarwala, V (2006). "Nonlinear Vibro-acoustic Modulation Technique for Life Prediction of Aging Aircraft Components". In: *Structural Health Monitoring 2006: Proceedings of the Third European Workshop*, pp. 251–258.

Drinkwater, BW and Wilcox, PD (2006). "Ultrasonic arrays for non-destructive evaluation: A review". *NDT & E International* 39.7, pp. 525–541. ISSN: 0963-8695.

Graff, K.F. (1975). *Wave Motion in Elastic Solids*. Dover Books on Physics. Dover Publications. ISBN: 9780486667454.

Gresil, M., Yu, L. and Giurgiutiu, V. (2011). "Fatigue crack detection in thick steel structures with piezoelectric wafer active sensors". In: *Proceedings of SPIE*. Vol. 7983,

Harris, F. J. (1978). "On the use of windows for harmonic analysis with the discrete Fourier transform". *Proceedings of the IEEE* 66.1, pp. 51–83. ISSN: 0018-9219.

Holmes, Caroline, Drinkwater, Bruce W. and Wilcox, Paul D. (2008). "Advanced post-processing for scanned ultrasonic arrays: Application to defect detection and classification in non-destructive evaluation". *Ultrasonics* 48.6–7. Selected Papers from {ICU} 2007, pp. 636–642. ISSN: 0041-624X.

Hopkins, D, Neau, G and Le Ber, L (2011). "Advanced phased-array technologies for ultrasonic inspection of complex composite parts". In: *Proc. Smart Materials, Structures & NDT in Aerospace Conference*.

Huthwaite, P. (2014). "Evaluation of inversion approaches for guided wave thickness mapping". *Proceedings of the Royal Society A: Mathematical, Physical and Engineering Sciences* 470.2166.

Huthwaite, P. and Simonetti, F. (2013). "High-resolution guided wave tomography". *Wave Motion* 50.5, pp. 979–993.

Jhang, Kyung-Young (2009). "Nonlinear ultrasonic techniques for nondestructive assessment of micro damage in material: A review". *International Journal of Precision Engineering and Manufacturing* 10.1, pp. 123–135. ISSN: 2005-4602.

Kazakov, V.V., Sutin, A. and Johnson, P.A. (2002). "Sensitive imaging of an elastic nonlinear wave-scattering source in a solid". *Applied Physics Letters* 81.4, pp. 646–648.

Kessler, S.S., Spearing, S.M. and Soutis, C. (2002). "Damage detection in composite materials using Lamb wave methods". *Smart Materials and Structures* 11.2, pp. 269–278.

Kim, J.-Y., Jacobs, L.J., Qu, J. and Littles, J.W. (2006). "Experimental characterization of fatigue damage in a nickel-base superalloy using nonlinear ultrasonic waves". *Journal of the Acoustical Society of America* 120.3, pp. 1266–1273.

Kim, J.-Y., Yakovlev, V.A. and Rokhlin, S.I. (2003). "Parametric modulation mechanism of surface acoustic wave on a partially closed crack". *Applied Physics Letters* 82.19, pp. 3203–3205.

Kim, J.-Y., Yakovlev, V.A. and Rokhlin, S.I. (2004). "Surface acoustic wave modulation on a partially closed fatigue crack". *Journal of the Acoustical Society of America* 115.5 I, pp. 1961–1972.

Kino, Gordon S (1987). *Acoustic waves : devices, imaging, and analog signal processing*. English. Englewood Cliffs, N.J. : Prentice-Hall. ISBN: 0130030473.

Klepka, A. (2013). "Nonlinear Acoustics". In: *Advanced Structural Damage Detection*. Ed. by T. Stepinski, T. Uhl and W. Staszewski. John Wiley & Sons, Ltd, pp. 73–107.

Klepka, A., Pieczonka, L., Staszewski, W.J. and Aymerich, F. (2014). "Impact damage detection in laminated composites by non-linear vibro-acoustic wave modulations". *Composites Part B: Engineering* 65, pp. 99–108.

Klepka, A., Staszewski, W.J., Di Maio, D. and Scarpa, F. (2013). "Impact damage detection in composite chiral sandwich panels using nonlinear vibro-acoustic modulations". *Smart Materials and Structures* 22.8.

Klepka, A, Staszewski, WJ, Jenal, RB, Szwedo, M, Iwaniec, J and Uhl, T (2012). "Nonlinear acoustics for fatigue crack detection – experimental investigations of vibro-acoustic wave modulations". *Structural Health Monitoring* 11.2, pp. 197–211.

Kolsky, H. (1963). *Stress Waves in Solids*. Dover Books on Physics. Dover Publications.

Korotkov, A.S., Slavinskij, M.M. and Sutin, A.M. (1994). "Variations of acoustic nonlinear parameters with the concentration of defects in steel". *Akusticheskij Zhurnal* 40.1, pp. 84–87.

Kulkarni, S.S. and Achenbach, J.D. (2008). "Structural health monitoring and damage prognosis in fatigue". *Structural Health Monitoring* 7.1, pp. 37–49.

Li, W., Cho, Y. and Achenbach, J.D. (2012). "Detection of thermal fatigue in composites by second harmonic Lamb waves". *Smart Materials and Structures* 21.8.

Lim, Hyung Jin, Sohn, Hoon, DeSimio, Martin P. and Brown, Kevin (2014a). "Reference-free fatigue crack detection using nonlinear ultrasonic modulation under various temperature and loading conditions". *Mechanical Systems and Signal Processing* 45.2, pp. 468–478.

Lim, Hyung Jin, Song, Byeongju, Park, Byeongjin, Liu, Peipei and Sohn, Hoon (2014b). "Non-contact visualization of nonlinear ultrasonic modulation for reference-free fatigue crack detection". In: *SPIE Proceedings*. Vol. 9061,

Lissenden, C.J., Liu, Y. and Rose, J.L. (2015). "Use of non-linear ultrasonic guided waves for early damage detection". *Insight: Non-Destructive Testing and Condition Monitoring* 57.4, pp. 206–211.

Liu, Yanxiong and Liaw, Benjamin (2010). "Effects of Constituents and Lay-up Configuration on Drop-Weight Tests of Fiber-Metal Laminates". eng. *Applied Composite Materials* 17.1, pp. 43–62. ISSN: 0929-189X.

Lyons, R.G. (2010). *Understanding Digital Signal Processing*. Pearson Education. ISBN: 9780137028528.

Mahaut, Steve, Roy, Olivier, Beroni, Claude and Rotter, Bernhard (2002). "Development of phased array techniques to improve characterization of defect located in a component of complex geometry". *Ultrasonics* 40.1–8, pp. 165–169. ISSN: 0041-624X.

Mattei, C. and Marty, P. (2003). "Imaging of Fatigue Damage in CFRP Composite Laminates Using Nonlinear Harmonic Generation". *AIP Conference Proceedings* 657.1, pp. 989–995.

Meo, M., Polimeno, U. and Zumpano, G. (2008). "Detecting damage in composite material using nonlinear elastic wave spectroscopy methods". *Applied Composite Materials* 15.3, pp. 115–126.

Meo, M. and Zumpano, G. (2005). "Nonlinear elastic wave spectroscopy identification of impact damage on a sandwich plate". *Composite Structures* 71.3–4, pp. 469–474.

Muller, M., Mitton, D., Talmant, M., Johnson, P. and Laugier, P. (2008). "Nonlinear ultrasound can detect accumulated damage in human bone". English. *Journal of Biomechanics* 41.5, pp. 1062–1068.

Muller, M., Sutin, A., Guyer, R., Talmant, M., Laugier, P. and Johnson, P.A. (2005). "Nonlinear resonant ultrasound spectroscopy (NRUS) applied to damage assessment in bone". *The Journal of the Acoustical Society of America* 118.6, pp. 3946–3952.

Nagy, P.B. (1998). "Fatigue damage assessment by nonlinear ultrasonic materials characterization". *Ultrasonics* 36.1-5, pp. 375–381.

Nagy, P.B. and Adler, L. (1992). "Acoustic nonlinearity in plastics". *Review of Progress in Quantitative Nondestructive Evaluation* 11B, pp. 2025–2032.

National Instruments (2010). *Fundamentals of Ultrasonic Imaging and Flaw Detection*. URL: `http://www.ni.com/white-paper/3368/en/` (visited on 10/02/2017).

Ng, C.T. and Veidt, M. (2009). "A Lamb-wave-based technique for damage detection in composite laminates". *Smart Materials and Structures* 18.7.

Nucera, C. and Lanza Di Scalea, F. (2014). "Nonlinear wave propagation in constrained solids subjected to thermal loads". *Journal of Sound and Vibration* 333.2, pp. 541–554.

Parsons, Z. and Staszewski, W.J. (2006). "Nonlinear acoustics with low-profile piezoceramic excitation for crack detection in metallic structures". *Smart Materials and Structures* 15.4, pp. 1110–1118.

Pieczonka, L., Ukowski, P., Klepka, A., Staszewski, W.J., Uhl, T. and Aymerich, F. (2014). "Impact damage detection in light composite sandwich panels using piezo-based nonlinear vibro-acoustic modulations". *Smart Materials and Structures* 23.10.

Polimeno, U. and Meo, M. (2008). "Understanding the effect of boundary conditions on damage identification process when using non-linear elastic wave spectroscopy methods". *International Journal of Non-Linear Mechanics* 43.3, pp. 187–193.

Pruell, C., Kim, J.-Y., Qu, J. and Jacobs, L.J. (2009). "A nonlinear-guided wave technique for evaluating plasticity-driven material damage in a metal plate". *NDT and E International* 42.3, pp. 199–203.

Rauter, N. and Lammering, R. (2014). "Experimental investigation of fatigue damage in composite structures considering second harmonic Lamb waves". In: *Proc. 7th European Workshop on Structural Health Monitoring*, pp. 1647–1654.

Rauter, N. and Lammering, R. (2015). "Impact damage detection in composite structures considering nonlinear lamb wave propagation". *Mechanics of Advanced Materials and Structures* 22.1-2, pp. 44–51.

Rauter, N., Lammering, R. and Kühnrich, T. (2016). "On the detection of fatigue damage in composites by use of second harmonic guided waves". *Composite Structures* 152, pp. 247–258.

Reddy, J. N. (1997). *Mechanics of laminated composite plates: theory and analysis*.

Reiner, Johannes (2016). *A computational investigation of failure modes in hybrid titanium composite laminates*. PhD Thesis, School of Mechanical and Mining Engineering. The University of Queensland.

Reiner, Johannes, Torres, Juan Pablo, Veidt, Martin and Heitzmann, Michael (2016). "Experimental and numerical analysis of drop-weight low-velocity impact tests on hybrid titanium composite laminates". *Journal of Composite Materials* 50.26, pp. 3605–3617.

Reynolds, W.N. (1984). "Nondestructive testing (NDT) of fibre-reinforced composite materials". *Materials and Design* 5.6, pp. 256–270.

Rose, J.L. (1999). *Ultrasonic Waves in Solid Media*. Cambridge University Press. ISBN: 9780521640435.

Rose, J.L. (2002). "A baseline and vision of ultrasonic guided wave inspection potential". *Journal of Pressure Vessel Technology, Transactions of the ASME* 124.3, pp. 273–282.

Rose, L.R.F., Chan, E. and Wang, C.H. (2015). "A comparison and extensions of algorithms for quantitative imaging of laminar damage in plates. I. Point spread functions and near field imaging". *Wave Motion* 58, pp. 222–243.

Scott, I.G. and Scala, C.M. (1982). "A review of non-destructive testing of composite materials". *NDT International* 15.2, pp. 75–86.

Sohn, Hoon, Lim, Hyung Jin, DeSimio, Martin P., Brown, Kevin and Derriso, Mark (2013). "Fatigue crack detection using guided waves nonlinear modulation". In: *SPIE Proceedings*. Vol. 8695,

Solodov, I., Krohn, N. and Busse, G. (2010). "Nonlinear ultrasonic NDT for Early defect recognition and imaging". *Proceedings of the 10th European Conference on Non-Destructive Testing*.

Solodov, I., Pfleiderer, K., Gerhard, H. and Busse, G. (2004). "Nonlinear acoustic approach to material characterisation of polymers and composites in tensile tests". *Ultrasonics* 42.1-9, pp. 1011–1015.

Solodov, I.Yu. (1998). "Ultrasonics of non-linear contacts: Propagation, reflection and NDE-applications". *Ultrasonics* 36.1-5, pp. 383–390.

Strutt (3rd Baron Rayleigh), J. W. (1896). *The Theory of Sound*. second. Vol. II. Macmillan and Co., Ltd.

Su, Z., Ye, L. and Lu, Y. (2006). "Guided Lamb waves for identification of damage in composite structures: A review". *Journal of Sound and Vibration* 295.3-5, pp. 753–780.

Sutin, A.M. and Donskoy, D.M. (1998). "Vibro-acoustic modulation nondestructive evaluation technique". In: *Proceedings of SPIE - The International Society for Optical Engineering*. Vol. 3397, pp. 226–237.

Sutin, A.M. and Johnson, P.A. (2005). "Nonlinear elastic wave NDE II. Nonlinear wave modulation spectroscopy and nonlinear time reversed acoustics". In: *AIP Conference Proceedings*. Vol. 760, pp. 385–392.

Sutin, A.M. and Nazarov, V.E. (1995). "Nonlinear acoustic methods of crack diagnostics". *Radiophysics and Quantum Electronics* 38.3, pp. 109–120.

Timoshenko, S.P. (1922). "On the transverse vibrations of bars of uniform cross-section". *Philosophical Magazine Series 6* 43.253, pp. 125–131.

Van Damme, Bart and Van Den Abeele, Koen (2014). "The Application of Nonlinear Reverberation Spectroscopy for the Detection of Localized Fatigue Damage". *Journal of Nondestructive Evaluation* 33.2, pp. 263–268. ISSN: 1573-4862.

Van Den Abeele, K., Carmeliet, J. and Van de Velde, K. (2001a). "Inferring the degradation of pultruded composites from dynamic nonlinear resonance measurements". *Polymer Composites* 22.4, pp. 555–567.

Van Den Abeele, K., Le Bas, P. Y., Van Damme, B. and Katkowski, Tomasz (2009). "Quantification of material nonlinearity in relation to microdamage density using nonlinear reverberation spectroscopy: Experimental and theoretical study". *The Journal of the Acoustical Society of America* 126.3, pp. 963–972.

Van Den Abeele, K. and Van de Velde, K. (2000). "Correlation between dynamic nonlinearity and static mechanical properties of corroded E-glass reinforced polyester composites". *AIP Conference Proceedings* 509.1, pp. 1359–1365.

Van Den Abeele, K.E.-A., Johnson, P.A. and Sutin, A. (2000). "Nonlinear Elastic Wave Spectroscopy (NEWS) techniques to discern material damage, Part I: nonlinear wave modulation spectroscopy (NWMS)". *Research in Nondestructive Evaluation* 12.1, pp. 17–30.

Van Den Abeele, K.E.-A., Sutin, A., Carmeliet, J. and Johnson, P.A. (2001b). "Micro-damage diagnostics using nonlinear elastic wave spectroscopy (NEWS)". *NDT and E International* 34.4, pp. 239–248.

Vary, A. (1990). "Acousto-Ultrasonics". In: *Non-Destructive Testing of Fibre-Reinforced Plastics Composites*. Ed. by J. Summerscales. Vol. 2. Elsevier Science Publishers. ISBN: 9781851664689.

Veidt, M., Ng, C.T., Hames, S. and Wattinger, T. (2008). "Imaging laminar damage in plates using Lamb wave beamforming". *Advanced Materials Research* 47-50 PART 1, pp. 666–669.

Wierzbicki, T. (2013). *2.080J/1.573J Structural Mechanics, Fall 2013 (Massachusetts Institute of Technology: MIT OpenCourseWare)*. URL: https://ocw.mit.edu/courses/mechanical-engineering/2-080j-structural-mechanics-fall-2013/course-notes/MIT2_080JF13_Lecture6.pdf (visited on 04/28/2017).

Woolfries, S. (1998). "The effects of friction between crack faces on nonlinear wave propagation in microcracked media". *Journal of the Mechanics and Physics of Solids* 46.4, pp. 621–644.

Xiang, Y., Deng, M., Xuan, F.-Z. and Liu, C.-J. (2012). "Effect of precipitate-dislocation interactions on generation of nonlinear Lamb waves in creep-damaged metallic alloys". *Journal of Applied Physics* 111.10.

Yeum, C.M., Sohn, H., Ihn, J.B. and Lim, H.J. (2012). "Instantaneous delamination detection in a composite plate using a dual piezoelectric transducer network". *Composite Structures* 94.12, pp. 3490–3499.

Zagrai, A., Donskoy, D., Chudnovsky, A. and Golovin, E. (2008). "Micro-and macroscale damage detection using the nonlinear acoustic vibro-modulation technique". *Research in Nondestructive Evaluation* 19.2, pp. 104–128.

Zaitsev, V. Yu, Gusev, V. and Castagnède, B. (2002). "Observation of the "Luxemburg–Gorky effect" for elastic waves". *Ultrasonics* 40.1–8, pp. 627–631.

Zaitsev, V. and Sas, P. (2000). "Nonlinear response of a weakly damaged metal sample: A dissipative modulation mechanism of vibro-acoustic interaction". *JVC/Journal of Vibration and Control* 6.6, pp. 803–822.

Zaitsev, Vladimir, Nazarov, Veniamin, Gusev, Vitaly and Castagnede, Bernard (2006). "Novel nonlinear-modulation acoustic technique for crack detection". *NDT E International* 39.3, pp. 184–194.